THE UNIVERSITY OF SUSSEX

DEVELOPMENT OF CODED MODULATION TECHNIQUES FOR THE MOBILE RADIO ENVIRONMENT

Reyat Yilmaz

Submitted for the degree of D. Phil.

November, 1993

VARIABLE PRINT QUALITY

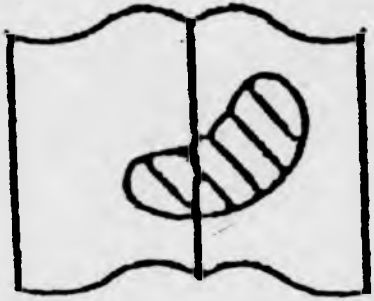

CONTENTS

LIST OF FIGURES

LIST OF TABLES

THE UNIVERSITY OF SUSSEX

DEVELOPMENT OF CODED MODULATION TECHNIQUES FOR THE MOBILE RADIO ENVIRONMENT

Submitted for the degree of D. Phil.

November, 1993

Reyat Yilmaz

ABSTRACT

The search for improving the power efficiency is addressed in this thesis for some modulation schemes in the mobile radio environment. This topic has been the focus of attention for the past several years and modulation techniques such as trellis coded modulation (TCM) and continuous phase modulation (CPM) with convolutional codes have evolved.

In this thesis, the advantages that can be obtained with specific coded modulations as compared to their uncoded cases are examined. Two kind of coding techniques, namely trellis coded modulation (TCM) combined with PSK and the combination of convolutional coding with partial response digital phase modulation (DPM), are examined.

While TCM undoubtedly achieves real coding gains under Gaussian noise channels, it is still an open question how it performs under other channel impairments. This is addressed in this thesis concerning time invariant intersymbol interference (ISI) and frequency selective Rayleigh fading channels. The type of coding examined with PSK is the trellis coding. In particular, Ungerboeck's trellis coded 8-PSK scheme (rate of 2/3 with 4-states) is emphasized. To recover this kind of signal corrupted by time invariant ISI or frequency selective Rayleigh fading channels, receiver structures based on maximum likelihood sequence estimation (MLSE) are introduced. Their performances are evaluated by computer simulations. The results show that this detection algorithm has superior performance when compared with conventional hard-decision demodulation.

Partial response digital phase modulation (DPM) is a constant amplitude modulation scheme with attractive spectral characteristics. Its advantages over CPM motivated a consideration of this modulation scheme in mobile radio transmission. In this thesis the case of rate 1/2 convolutional coding in partial response binary and 4-level DPM is emphasized. The main interest of this study is to find the best combinations of 1/2 rate convolutional encoder, mapping rule and partial response DPM modulator (binary and 4-level) for given memory length and modulation index. The error probability of a system, in an additive white Gaussian noise channel, is a function of the free squared Euclidean distance d^2_{min}. Since the error probability decreases with the increase of d^2_{min}, the combinations of encoder, mapping rule and modulator, which maximise d^2_{min} are investigated. In order to validate the outcomes of the results, the computer simulation of the whole transmission system is performed. Receiver structures are proposed and presented to recover these coded signals under the frequency selective Rayleigh fading channel.

The bit error rate (BER) performances of Trellis coded 8-PSK and coded 4-level 3-SP (Sine pulse) DPM schemes under frequency selective Rayleigh fading channel are evaluated through the use of computer simulations. It is found that trellis coded 8-PSK provides a small amount of coding gain when compared with the uncoded 4-PSK, which has the same spectral efficiency as the coded 8-PSK. For the partial response DPM case, some coded schemes with the same spectral efficiencies as the uncoded ones and as some coded CPM schemes, but with higher power efficiencies, are presented.

LIST OF ABBREVIATIONS AND SYMBOLS

AWGN	Additive white Gaussian noise
BER	Bit error rate
CIR	Channel impulse response
CPFSK	Continuous phase frequency shift keying
CPM	Continuous phase modulation
DFE	Decision feedback equalisers
DPM	Digital phase modulation
FIR	Finite impulse response
FSRF	Frequency selective Rayleigh fading
GMSK	Gaussian minimum shift keying
ISI	Intersymbol interference
LFE	Linear feedback equaliser
LMS	Least mean square
LSB	Least significant bit
L-SP DPM	Digital phase modulation with Sin pulse, length L
MLSE	Maximum likelihood sequence estimation
MSB	Most significant bit
MSE	Mean square error
MSK	Minimum shift keying
NSMED	Normalized squared minimum Euclidean distance
OI	Observation interval
PSK	Phase shift keying
QAM	Quadrature amplitude modulation
QPSK	Quadrature phase shift keying
RF	Radio frequency

SNR	Signal to noise ratio
VDFE	Viterbi decision feedback equaliser
VLSI	Very large scale integration
TCM	Trellis coded modulation
TDMA	Time division multiple access
2RC	Double-raised-cosine
3RC	Triple-raised-cosine
d^2_{min}	Free squared Euclidean distance
$S_n(t)$	Transmitted signal
$d(S_1(t), S_2(t))$	The distance between two signals
$\Phi_l(t)\Phi_k(t)$	Orthonormal waveforms
$P[e]$	The probability of error
$S_n(f)$	Spectral density of signal $S_n(t)$
$erfc(x)$	The complementary error function
$R_x(\tau)$	The autocorrelation function of a stationary stochastic process $x(t)$
$g(t)$	Frequency pulses
f_c	Carrier frequency
$\Phi(t, \alpha)$	The information carrying phase
$q(t)$	Phase pulses
l	The pulse duration which is measured by symbol intervals T
η	The oversampling ratio
T_m	Multipath spread
$X(t)$ and $Y(t)$	Real and imaginary parts of a transmitted signal
$E\{\alpha_i^2\}$	Expected value of α_i
$Y_n(i)$ or C_n	Tap coefficients of the transmission channel
$\hat{Y}_n(i)$	The estimated tap coefficients
Δ	The gradient step size
e_n	The signal error

Δ_t	The minimum distance between parallel transitions in trellis coded 8-PSK
r_{nI}, r_{nQ}	The baseband components of the n th received signal
a_{nI}, a_{nQ}	The baseband components of the n th expected symbol
S_{iI} and S_{iQ}	The in-phase and quadrature components of the transmitted signal
$W_I(i)$, $W_Q(i)$	The simulated noise samples (in phase and quadrature)
C/D	The ratio between the sequential $E\{\alpha_i^2\}$ in dB
S/N	Signal to noise ratio
M	Modulation level
$D^2_{m,m'}(S_m(t), S_{m'}(t))$	The squared Euclidean distance between two signals $S_m(t)$ and $S_{m'}(t)$
E_s	The signal energy
E_b	The bit energy
$d^2_{m,m'}$	The squared Euclidean distance normalised by bit energy between two signals $S_m(t)$ and $S_{m'}(t)$
$\alpha_{m,i}$	Data sequence
$\gamma_{mm',i}$	The difference sequence between two data sequences $\alpha_{m,i}$ and $\alpha_{m',i}$
$d^2_{up}(h)$	The upper bound on $d^2_{min}(h)$
B	Bandwidth
$S_c(w)$	Continuous part of the spectrum
S	the number of state in Viterbi algorithm
v	The constraint length of a convolutional encoder
g^i	The generator vector to represent an encoder
$d^2_{min,OI}(h)$	Normalized squared minimum Euclidean distance corresponding to the time interval $(OI)T_s$
c_k^{asc}	The symbol corresponding to the transition from state a to the state c
$W_{sa}(k-1)$	The total accumulated error distance corresponding to the time instant $(k-1)$

ACKNOWLEDGMENTS

I would like to express my sincere gratitude to my supervisors Dr. F.S.F. Poon and Dr. P.N. Denbigh for their invaluable guidance and support throughout the research work, and reviewing the draft of the thesis.

My thanks also to Dr. A. Denker of Bogazici University, Istanbul for his very helpful observations and discussions and to Dr. U. Berkok of University of Sussex for the reviewing the draft of the thesis.

Helps from all my friends, at the University of Sussex are gratefully appreciated.

For his invaluable support from Bremen, I would like to thank to my nephew Orhan Yilmaz.

I am especially grateful to my wife Figen and my daughter Ozgun for their encouragement and for their understanding during the many hours spent away from them. I am also greatful to my parents, and my brothers and sisters. Without their invaluable support, this thesis would never have been written.

Finally, I would also like to thank Dokuz Eylul University for the financial support.

CHAPTER 1

INTRODUCTION

1.1 Motivation of the project

Digital transmission techniques of both voice and data are growing quickly in importance. In digital transmission systems, the transmitted signals are discrete in time, amplitude, phase, or frequency. One advantage of this form of digital is that the impairments such as noise and interference introduced in the transmission medium can be corrected [72][75] [74][68]. That can be achieved by coding techniques. This is one of the most primary advantages of digital transmission. One other advantage in digital transmission systems is that encryption techniques can be used to obtain privacy in communication. As far as implementation is concerned, digital transmission systems are attractive because of the rapid development of complex very large scale integrated (VLSI) circuits. This rapid development causes the digital signal processing to become inexpensive.

Three prevailing requirements in transmission systems are to increase the transmitted information per unit of spectral bandwidth, to decrease the power needed for reliable transmission (for desirable bit error rate), and to use a modulation technique which is easy to implement. Hence, power, bandwidth and implementation efficiencies are the most important requirement in a modulation technique. [19][10][32][68] [60][13]. The bandwidth itself is basically the range of frequency that a modulation scheme occupies. In this thesis, the bandwidth is defined as the range of frequency containing some fixed percentage of the total signal power. For spectrum conservation, the band occupancy of the chosen modulation scheme has to be small so that as many channels as possible can be transmitted in a given band. In addition to spectral efficiency, the modulation scheme should be power efficient as well. As the available transmitter power is limited or there is a power usage restriction, the system should be designed to use its power efficiently. It is also favourable for modulation schemes used in digital mobile systems to have a constant

envelope because of the need for a nonlinear amplifier. The constant envelope is useful because of the need to communicate over a mobile channel which is corrupted by severe fading. Another criterion to be considered in choosing a modulation scheme for mobile systems is how easily it can be implemented.

1.2 Overview of power and bandwidth efficient modulation techniques

In recent years, efforts have been made in the search for power- and bandwidth-efficient modulation techniques. Over the last ten years two different classes of coding methods related to the bandwidth efficiency have been developed. One of them is the combination of convolutional coding with continuous phase modulation (CPM), trellis coded CPM, which was proposed by Sundberg, [64] [65], Aulin [66], Anderson [77], and Wilson [70]. A detailed discussion about CPM will be given in Chapter2. The other one is Trellis coded modulation (TCM) combined with PSK, pioneered by Ungerboeck [27] [28] [29]. The modulation schemes used with TCM by Ungerboeck are M-ary PSK or M-ary Quadrature phase shift keying (QPSK). These are not constant envelope signals and the spectral efficiency is obtained by post filtering. A detailed discussion of trellis coded modulation is given in Chapter4.

Trellis-coded modulation proposed by Ungerboeck [27] [28] and studied by others [32] [33] [34] [40] is a combination of coding and modulation techniques for digital transmission over band-limited additive white Gaussian noise (AWGN) channels. Ungerboeck [27] [28] showed that TCM schemes can provide coding gains of 3-6 dB relative to an uncoded scheme with the same spectral efficiency. The appropriate criterion for designing good TCM schemes in the AWGN channel is to maximise the free Euclidean distance [27] [28] [29] [30]. M-ary PSK TCM was studied by some authors [27] [28] [32] [33] [34] [40] under the AWGN channel. More recently, TCM has been investigated for other channels as well, including the Rician channel [30] [36] [38] and the Rayleigh channel [31] [35] [37] [41] [42] [43].

Convolutional coding combined with continuous phase modulation (CPM) has been studied by several authors i.e. the coding combined with continuous phase frequency shift keying (CPFSK) in [66], [67] and [70] and coding with double-raised-cosine (2RC) and

triple-raised-cosine (3RC) in [70].

1.3 Research objectives

In this thesis, the search for improving power efficiency is addressed. The advantages that can be obtained with specific coded modulations as compared to their uncoded cases are studied. Two kind of coding techniques are examined, namely trellis coded modulation (TCM) combined with PSK and the combination of convolutional coding with partial response digital phase modulation (DPM).

For TCM, there are still open questions concerning coding gains under the intersymbol interference (ISI) and frequency selective Rayleigh fading channels. In this study, the Ungerboeck 4-state rate 2/3 8-PSK TCM scheme is examined for time invariant ISI and frequency selective Rayleigh fading channels (wideband channels). The main concern is whether the coding gains obtained for additive white Gaussian noise channels will degrade or stay the same when the channel is an intersymbol interference channel or a frequency selective Rayleigh fading channel. Receiver structures to recover the data corrupted in these channels, are presented. For a channel with time invariant ISI, three types of equaliser are examined. Two of them are known algorithms, namely the linear feedback equaliser, and the decision feedback equaliser. The third algorithm is the proposed algorithm which will be called Viterbi decision feedback equaliser (VDFE). To evaluate and compare the performance of these three algorithms, computer simulation is used. The simulation is performed for a time invariant ISI channel, namely telephone channel 2 [49]. For the frequency selective Rayleigh fading channel, a receiver structure which is based on the VDFE, is proposed and presented. The bit error rate (BER) performance of the system under this channel is found through computer simulations.

Since the coding gain achieved in trellis coded (TC) 8-PSK is low, searches have been conducted for improving this gain. A modulation scheme called Hybrid trellis-coded 8/4 PSK presented by Sundberg [44], which is the combination of the TC 8-PSK and the uncoded 4-PSK, has been studied under the frequency selective Rayleigh fading. The BER performance is also found by using computer simulations.

Modulation schemes such as band limited M-ary PSK are usually used due to their high spectral and power efficiencies. However, the rf envelope of the modulated carrier is not constant and, if a non-linear amplifier is used in the transmitter, the spectral side-lobes of the signal increase due to the non-linear effects of the amplifier. This causes serious adjacent channel interference. This is unfortunate since, as far as mobile radio is concerned, the available power is limited and this makes it necessary to use a non-linear amplifier. One way to overcome this problem is to use spectrally efficient but constant or low-fluctuation envelope signals, such as continuous phase modulation (CPM) [68] or digitally phase modulated (DPM) signals [60] [61] [13]. Because they have phase shaping before or within the modulator, rather then after the modulator, their rf envelopes are constant and their spectral side-lobes are reduced compared to M-ary PSK. One disadvantage of partial response DPM, mentioned in [60], is that it has a broader main lobe in the power spectrum than partial response CPM. However, as far as implementation is concerned, DPM [60] [61] [13] signals have some advantages over CPM signals. This is because phase modulation is used instead of frequency modulation. Thus carrier recovery needed for coherent modulation is simpler to implement. In demodulator, there is no need for the carrier phase to be accumulated continuously as in the case for CPM. The other advantage of DPM is that it is well suited for VLSI implementation [60] [61] [13]. These advantages of DPM signals motivated a consideration of these signals in mobile radio environments.

In this thesis, the study was restricted to a binary and 4-level partial response DPM with a sine pulse (SP) and a duration LT, known as an L-SP pulse [60], where T is the symbol interval and $L = 3$. The scheme will be called 3-SP DPM. According to the study in [60], this pulse has a good properties.

Firstly, the general properties such as free Euclidean distance (d^2_{min}) and power spectrum of binary and 4-level partial response DPM systems are studied in detail. A fast algorithm developed by Aulin [65] for CPM system has been modified in order to evaluate the free Euclidean distance of binary and 4-level $3 - SP$ DPM signals.

Secondly, the effects of the coding in improving the power efficiency of partial response DPM signals are examined. The main interest is to investigate what improvements may

be obtained by coding. The goal is to find schemes which are both power and bandwidth efficient.

The error probability of a system, in an additive white Gaussian noise channel, is a function of the free squared Euclidean distance d^2_{min} [76] [72] [73]. Since the error probability decreases with the increase of d^2_{min}, the combinations of encoder, mapping rule and modulator, which maximise d^2_{min} are investigated for each memory length and modulation index.

The study is carried out to show how the minimum Euclidean distances grow with the observation interval length for these combinations. The observation interval lengths for which the free Euclidean distance is reached are found for each of the best combinations. This length is the minimum decision depth length of the receiver.

In order to validate the outcomes of the results, computer simulation of the whole transmission system is performed. Receiver structures are proposed and presented to recover these coded signals under the frequency selective Rayleigh fading channel. The bit error rate (BER) performance of a coded 4-level 3-SP DPM scheme under a frequency selective Rayleigh fading channel is evaluated through the use of computer simulation.

1.4 An outline of the thesis

Chapter 2 describes some basic concepts of the modulation schemes. These are the signal space distance, the bit error rate, exponential bound parameter R_o and the bandwidth and power spectrum. A brief introduction on some modulation schemes is given in the same Chapter. The mathematical model of the frequency selective Rayleigh fading channel used in this study is introduced in Chapter 3. In the same Chapter, two arrangements of a channel estimator are put forward based on the least-mean-square algorithm and, to find the accuracies of the channel estimators over a frequency selective Rayleigh fading (FSRF) channel, computer simulation tests are presented. In Chapter 4, the error performances of the Ungerboeck's 4-state rate 2/3 8-PSK TCM scheme under additive white Gaussian noise (AWGN), under a time invariant intersymbol interference and under frequency selective Rayleigh fading (FSRF) channels are evaluated through the use of computer simulations. To obtain these results, receiver structures to recover these coded signals are

first proposed and presented. In the same chapter, a modulation scheme which combines the TCM 8-PSK and the uncoded 4-PSK signals is studied under the frequency selective Rayleigh fading channel. In Chapter 5, some properties i.e free Euclidean distance, power spectrum and bandwidth are studied for both binary and 4-level DPM signals. Using the receivers proposed, the bit error rate (BER) performances of binary and 4-level partial response DPM under frequency selective Rayleigh fading channel are evaluated through the use of computer simulation. Chapter 6 describes the principal results of this research, which is the combination of short constraint length, rate 1/2 convolutional coding and binary/4-level partial response DPM. In the same chapter, some coded schemes which are power and bandwidth efficient are examined under a frequency selective Rayleigh fading channel, through the use of computer simulations. A conclusion is given in Chapter 7.

Part of this thesis has been presented at the IEEE SICON/ICIE 1993 [80], and another part of this thesis has been accepted for presentation at the IEEE MELECON'94 [81].

CHAPTER 2

CONCEPTS AND CHARACTERISTICS OF THE MODULATION SCHEMES

2.1 Signal space distance

Signals used in all communication systems can be expressed and visualised geometrically. By using this, the performance of many communication systems can be analysed. In fact many signals in communication systems are expressible in only two dimensions.

An appropriate measure of the distance between two finite energy signals $S_1(t)$, $S_2(t)$ is [76]

$$d(S_1(t), S_2(t)) = \left(\int_0^T (S_1(t) - S_2(t))^2 dt \right)^{1/2} \tag{2.1}$$

If the signals are written in terms of the same orthonormal basis then

$$\begin{aligned} S_1(t) &= \sum_{l=1}^{N} S_{1l} \Phi_l(t) \\ S_2(t) &= \sum_{l=1}^{N} S_{2l} \Phi_l(t) \end{aligned} \tag{2.2}$$

where

$$\int_0^T \Phi_l(t) \Phi_k(t) dt = \begin{cases} 1; & for \quad k = l \\ 0; & for \quad k \neq l \end{cases} \tag{2.3}$$

for $k, l = 1, 2, \ldots N$, and

$$S_{mn} = \int_0^T S_m(t) \Phi_n(t) dt \tag{2.4}$$

where $m = 1, 2, \ldots M$ and $n = 1, 2, \ldots N$ and M is the modulation level, and N is the number of dimensions. Using equations 2.2, 2.3, equation 2.1 can be rewritten as

$$\begin{aligned} d(S_1(t), S_2(t)) &= (\int_0^T (\sum_{k=1}^N (S_{1k}\Phi_k(t) - S_{2k}\Phi_k(t))^2 dt)^{1/2} \\ &= (\int_0^T (\sum_{k=1}^N (S_{1k} - S_{2k})\Phi_k(t))^2 dt)^{1/2} \\ &= (\sum_{k=1}^N (S_{1k} - S_{2k})^2)^{1/2} \end{aligned} \tag{2.5}$$

An important example for actual applications is the set of multilevel quadrature amplitude modulated (QAM) signals. In this case, there are $\Phi_1(t) = \sqrt{2/T}cosw_c t$ and $\Phi_2(t) = \sqrt{2/T}sinw_c t$ as orthonormal waveforms for $0 \leq t \leq T$. If $\mp A_c$ are the amplitudes in each direction, then the 4 transmitted signals are:

$$\begin{aligned} S_1(t) &= A_c\Phi_1(t) + A_c\Phi_2(t) \\ &= A_c\sqrt{2/T}cosw_c t + A_c\sqrt{2/T}sinw_c t \\ S_2(t) &= A_c\Phi_1(t) - A_c\Phi_2(t) \\ &= A_c\sqrt{2/T}cosw_c t - A_c\sqrt{2/T}sinw_c t \\ S_3(t) &= -A_c\Phi_1(t) + A_c\Phi_2(t) \\ &= -A_c\sqrt{2/T}cosw_c t + A_c\sqrt{2/T}sinw_c t \\ S_4(t) &= -A_c\Phi_1(t) - A_c\Phi_2(t) \\ &= -A_c\sqrt{2/T}cosw_c t - A_c\sqrt{2/T}sinw_c t \end{aligned} \tag{2.6}$$

This set of signals can be represented by vectors in two dimensional signal space as $S_i = [S_{i1} \;\; S_{i2}]$

$$\begin{aligned} S_1 &= [A_c \;\; A_c] \\ S_2 &= [A_c \;\; -A_c] \\ S_3 &= [-A_c \;\; A_c] \\ S_4 &= [-A_c \;\; -A_c] \end{aligned} \tag{2.7}$$

The signal set in Equation 2.7 is plotted and shown in Fig 2.1. This coordinate representation of all the signals in the set is called the signal constellation or signal space diagram. If we want to calculate the distance between any two signals, Equation 2.5 can be used. For example the distance between the first and the third signal is:

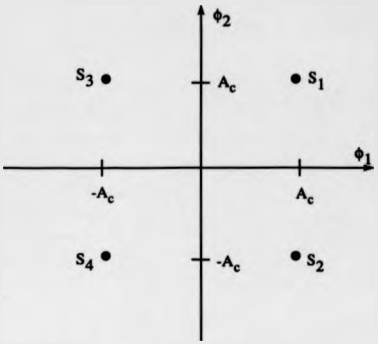

Figure 2.1: The signal constellation for 4-level QAM

$$\begin{aligned} d(S_1(t), S_2(t)) &= (\sum_{k=1}^{N}(S_{1k} - S_{2k})^2)^{1/2} \\ &= ((Ac - (-A_c))^2 + (A_c - A_c)^2)^{1/2} \\ &= 2A_c \end{aligned}$$

which is obviously true by inspection of Fig. 2.1.

2.2 The error probability

The probability of error of a modulation scheme is effected by the distances between the signals. If there is an M-ary signal set consists of the M signals $S_1(t)$, $S_2(t), \ldots, S_M(t)$ then, since the total probability of error over the entire signal set is of interest, the probability of error can be written as

$$P[\epsilon] = \sum_{i=1}^{M} P[\epsilon \mid S_i(t)]P[S_i(t)] \tag{2.8}$$

where $P[S_i(t)]$ denotes the probability that signal $S_i(t)$ is transmitted, and $P[\epsilon \mid S_i(t)]$ denotes the probability of error when signal $S_i(t)$ is transmitted. Assuming the signals to be

equiprobable, which is the case in maximum likelihood detection [68], then the Equation 2.8 becomes

$$P[\epsilon] = 1/M \sum_{i=1}^{M} P[\epsilon \mid S_i(t)] \tag{2.9}$$

To calculate the $P[\epsilon]$ for a signal set when it is used in additive white Gaussian noise of spectral density $S_n(f)$, where

$$S_n(f) = N_0/2, \qquad -\infty < f < \infty \tag{2.10}$$

equation 2.8 can be lower bounded by [76]:

$$P[\epsilon] \geq erfc(d_{min}/\sqrt{2N_0}) \tag{2.11}$$

and, equation 2.8 can be upper bounded by [76]:

$$P[\epsilon] \leq (M-1)erfc(d_{min}/\sqrt{2N_0}) \tag{2.12}$$

$$erfc(x) = 1/\sqrt{2\pi} \int_x^{\infty} exp(-u^2/2)du \tag{2.13}$$

where d_{min} represents the minimum distance between all pairs of signals in the M-ary set, and $erfc(.)$ denotes the complementary error function.

Equations 2.11 and 2.12 show that the probability of error for any signal set is dependent on the minimum distance between the signals in the set.

2.3 Exponential bound parameter R_o

The exponential bound parameter or, in other words, the cutoff rate [26] [70] [63] [76] is an indicator of the potential performance of a modulation scheme when coding is to be used with it. Actually, R_o gives the rates where reliable transmission is possible and gives an exponential to the bound error probability.

Let S_1 and S_2 be two code words chosen from a randomly selected code, then the probability that a maximum likelihood decoder selects S_2, when S_1 is transmitted, is [70] [63] [76]

$$P_{2,e} = Q(d(S_1, S_2)\sqrt{E/2N_o} \tag{2.14}$$

where $d(S_1, S_2)$ is the signal space distance between signals S_1 and S_2, and $Q(.)$ is the Gaussian error probability defined by Equation 2.15

$$Q(x) = 1/\sqrt{2\pi}\int_x^\infty exp(-u^2/2)du \tag{2.15}$$

R_o specifies the exponential bound on the mean probabillty of error:

$$P[e] \leq e^{-N(R_o - R)} \tag{2.16}$$

where N is the number of dimensions and R is the desirable rate in bits/dimension, and

$$\begin{aligned} R_o &= -(1/N)log_2 P_{2,e} \\ &= -(1/N)log_2(E[Q(d(S_1, S_2)\sqrt{E/2N_o}]) \end{aligned} \tag{2.17}$$

2.3.1 R_o for M-ary PSK

If the signal vectors S_i are transmitted with q_i probabilities where $i = 1, 2 \ldots M$ over the additive white Gaussian noise channel then,

$$R_o = -log_2(\sum_{i=1}^{M}\sum_{j=1}^{M} q_i q_j e^{-|S_i - S_j|^2/4N_o}) \tag{2.18}$$

For M-ary PSK, when the signals have the same probabilities then R_o can be seen in Fig. 2.3.1. An example which is given in [63] can explain the necessity of coding. Assume that we want to transmit two bits per waveform. The natural candidate would be 4-PSK, which requires E_b/N_o of 7 dB. However this figure shows that using 8-PSK, the same desirable 2 bits per waveform can be achieved with only E_b/N_o of 3 dB. When coding is used, 8-PSK can be made to transmit 2 bits/waveform. This example shows that 4 dB coding gain is achievable. Also, if we use 16-PSK, more coding gain is achievable.

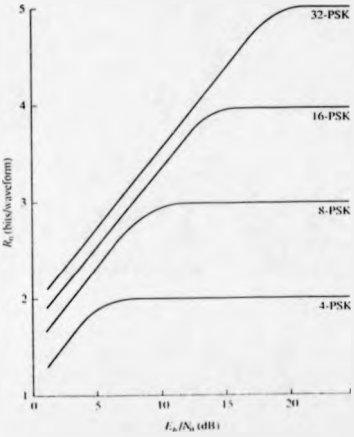

Figure 2.2: R_a for M-ary PSK signals

2.4 Bandwidth and power spectrum

The bandwidth of any signal is defined as the range of frequency containing some fixed percentage of the total signal power. Thus the bandwidth of any signal can be evaluated from the power spectrum of the signal set. The power spectrum of a signal set represents the average amount of energy at a given frequency. For a stationary stochastic process x(t), the power spectrum $S(f)$ can be obtained from the Fourier transform of the auto-correlation function.

$$S(f) = 1/2\pi \int_{-\infty}^{\infty} R_x(\tau) e^{-j2\pi f\tau} d\tau \tag{2.19}$$

where $R_x(\tau)$ is the autocorrelation function of $x(t)$.

The bandwidth used in this thesis is defined as double-sided bandwidth which contains the 99 percent of the total power.

2.5 Modulation schemes

2.5.1 M-ary phase shift keying (PSK)

Phase shift keying (PSK) involves transmitting digital information by shifting the phase of a carrier among several discrete values. The transmitted signal s(t) is

$$s(t) = A_c cos[w_c t + \Phi_i]$$

$$s(t) = A_c cos\Phi_i cos w_c t - A_c sin\Phi_i sin w_c t$$

where $i = 1, 2, \ldots M$, $cos\Phi_i$ is called the in phase component I, and $sin\Phi_i$ is the quadrature component Q.

In binary PSK case (M=2), the phase switches between 0° and 180°. Thus, the transmitted signal s(t) is

$$s(t) = \begin{cases} A_c cos w_c t & for\ "1" \\ -A_c cos w_c t & for\ "0" \end{cases}$$

In 4-ary PSK, each pair of binary digit is represented by a different transmitted phase. Since there are four possible pairs, the signal can take on four phases during an interval.

Input dibit	Phase of 4-ary PSK signal
00	+45
01	-45
10	+135
11	-135

Table 2.1: 4-ary PSK

These phases are equally spaced so that the transmitted phases for 4-ary PSK are 90° apart. These are shown in Table 2.1.

2.5.2 Continuous phase modulation (CPM)

The continuous phase modulation (CPM) scheme has received considerable attention as an efficient technique for digital transmission [62]-[70]. Its constant envelope property makes it insensitive to nonlinearities. CPM is a frequency modulation scheme.

The block diagram of a CPM transmitter is shown in Fig.2.3. A data source generates M-ary symbols α_k at rate 1/T. The symbols are shaped by a linear filter into frequency pulses $g(t)$, which are fed to a frequency modulator. The transmitted symbol is therefore

$$S(t,\alpha) = cos(2\pi f_c t + \Phi(t,\alpha)) \tag{2.20}$$

where f_c is the carrier frequency and $\Phi(t,\alpha)$ is the information carrying phase which is

$$\Phi(t,\alpha) = 2\pi h \int_{-\infty}^{t} \sum_{i=-\infty}^{\infty} \alpha_i g(\tau - kT) d\tau \tag{2.21}$$

where α_i takes one of the values

$$\alpha_i = \mp 1,\ \mp 3, \ldots, \mp(M-1) \qquad i = 0,\ \mp 1,\ \mp 2 \ldots,$$

h is the modulation index, and where $\Phi(t,\alpha)$ is a continuous function of time t. This means the frequency baseband pulse $g(t)$ does not contain any impulses. The frequency

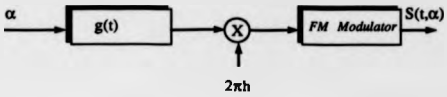

Figure 2.3: The block diagram of a CPM transmitter

pulse $g(t)$ is sometimes defined in terms of a phase pulse $q(t)$ as

$$q(t) = \int_{-\infty}^{\infty} g(\tau)d\tau \qquad -\infty < t < \infty \tag{2.22}$$

It is seen that the pulse of the CPM signal is formed by

$$\Phi(t,\alpha) = 2\pi h \sum_{i=-\infty}^{\infty} \alpha_i q(t-iT); \qquad -\infty < t < \infty \tag{2.23}$$

A CPM system is obtained when the frequency pulse $g(t)$ is

$$g(t) \cong 0; \qquad t < 0,\ t > LT$$
$$g(t) \cong 0; \qquad 0 \leq t \leq LT$$

where L denotes the pulse duration which is measured by symbol intervals T. In the case of $L = 1$, the scheme is called full response; If $L > 1$, then it is called partial response CPM. CPM schemes are denoted by their phase response function or by frequency response function. Some of them are:

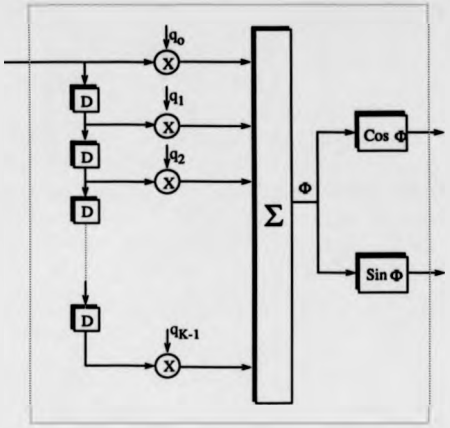

Figure 2.4: The block diagram of a DPM transmitter

Continuous phase frequency shift keying (CPFSK). When the modulation index $h = 1/2$, then CPFSK scheme is called Minimum shift keying (MSK). The Gaussian MSK (GMSK) and raised cosine with pulse length L (LRC) are also kinds of CPM schemes.

2.5.3 Digital phase modulation (DPM)

As described above, CPM is a frequency modulation scheme. Viewed as a phase modulation, it has pulses of infinite length. The slightly simpler digital phase modulation (DPM) has phase pulses with finite length and shares some of the advantages which CPM has. As pulse shaping is used within the modulator in DPM, rather then after the modulator, the rf envelope is constant as in CPM. These features are important in satellite and mobile communications. However, as far as implementation is concerned, DPM [60] [13] signals have some advantages over CPM signals. This is because the filter design is simpler and there is no need for the carrier phase to be accumulated continuously as in the case for CPM. The other advantage of DPM is that it is well suited for VLSI implementation [60] [13].

A DPM signal is represented as in [60]:

$$S(t) = \sqrt{2E/T}\, cos(w_o t + \Phi(t)) \tag{2.24}$$

where T is the signalling interval, E is the energy per symbol, w_o is the carrier frequency, and Φ is the time varying phase given by

$$\Phi(nD) = \sum_{i=-\infty}^{\infty} \alpha_i q_{n-i\eta} \tag{2.25}$$

where the data symbols $\alpha_i \in \{1, -1, 3, -3, \cdots, M-1, -(M-1)\}$, q_n are the filter coefficients, and η is the oversampling ratio, which is the integer ratio between the signalling interval T and the duration D of each element in the digital filter, i.e.

$$\eta = T/D \tag{2.26}$$

The pulse used for the DPM scheme is a sine pulse (SP) with a duration LT, known as an L-SP pulse [60]. Here, we consider the partial response DPM scheme for $L = 3$ only. This scheme will be called 3-SP DPM. The filter coefficients can be written as in [60]

$$q_i = \sum_{l=0}^{\eta-1} d_{i-l} \qquad i \in 0, 1, \ldots, (K-1) \tag{2.27}$$

where

$$d_i = \beta sin(\pi(i+1)/(N+1)) \qquad i \in 0, 1, \ldots, (N-1) \tag{2.28}$$

β is the constant which regulates Eq.2.28 in order to have the desired modulation index. The modulation index is the maximum possible phase change during one symbol interval and is defined in [60] as

$$(M-1)\pi h = max\{\Phi(t+T) - \Phi(t)\} \tag{2.29}$$

2.5.4 Comparison between CPM and DPM signals

In digital form of CPM which is called digital frequency modulation (DFM) or in any similar modulation technique such as Gaussian minimum shift keying (GMSK), the carrier

phase at any time instant is the accumulated phase of all the previous symbols. This can be seen from Equation 2.30.

$$\begin{aligned} \Phi(t,\alpha) &= 2\pi h \sum_{n=i-L+1}^{i} \alpha_n q(t-nT) + \pi h \sum_{n=-\infty}^{i-L} \alpha_n \\ &= \phi(t,\alpha) + \phi_i \end{aligned} \tag{2.30}$$

In DPM, the last term which is the phase of the sum of all previous symbols is not found. That gives DPM an implementation simplicity when compared to DFM or to any similar modulation. The phase of DPM signal can be seen in the following equation (when $\eta = 1$):

$$\Phi(nD) = \sum_{i=n-L-1}^{n} \alpha_i q_{n-i} \tag{2.31}$$

CHAPTER 3

ON MOBILE RADIO CHANNELS AND CHANNEL ESTIMATORS

3.1 Introduction

Several experimental studies agree in confirming [1][2] [10][15][16][17][19] that the statistical characteristics of the mobile channel are well known. The techniques for simulation of the mobile channel behaviour are well established [1] - [9]. According to these studies, the signal in the mobile communication channel is affected by multipath interference which is caused by:

- Reflection from a hill, a building, a truck, an airplane.
- The delay spread of the received signal.
- Random frequency modulation due to different Doppler shifts.

In mobile radio telephone systems, propagation takes place by multiple-path reflections. The received signal envelope fluctuates about the local mean with Rayleigh statistics, and the RF phase is uniformly distributed [1] [10] [11] [19]. In a mobile system operating at a high bit rate, the delay spread causes intersymbol interference. Hence, the communication channel is a frequency selective Rayleigh fading channel (FSRF). There are many papers published on the modelling of mobile radio channels in urban environments[1][18]. The communication channel, namely a Rayleigh fading channel, based on the model introduced by Lee [10] is computer simulated. Frequency selective fading is generated by including path delay. The intersymbol interference introduced by the channel can be suppressed by an adaptive equaliser. As the channel characteristics are not known and change in time, the equaliser should be adaptive i.e. should follow the rapid variations in the channel impulse response. A detailed discussion about the adaptive equaliser will be given in Chapter4. A channel estimator is employed to find the tap coefficients of the equaliser. Several papers have already shown that a variety of algorithms can be used to find the

channel impulse responses. Some of them employ the gradient algorithm [21] [23] [74], the least-square Lattice algorithm [22], and the fast Kalman algorithm [74] [58] [24]. In this thesis, two arrangements of a channel estimator are put forward based on the least-mean-square algorithm [25]. They are implemented by applying the steepest descent (gradient) algorithm for minimisation of the mean square error (MSE) [74]. 8-level PSK signals are transmitted to find the accuracies of the channel estimators, over a FSRF channel. The results of computer simulation tests are presented.

3.2 Fading in mobile radio environment

In a typical mobile radio communication the propagation between the base station and the mobile station is usually not (only) by a line-of-sight path, but by many paths, largely by way of scattering from the surfaces of the buildings or by diffraction around buildings and terrain. Thus, many different paths between the transmitter and receiver occur. This is known as multipath propagation. The radio waves arriving from different directions with different time delays combine vectorially at the receiver antenna. The combined signal level will be fluctuated with time, this is known as fading. The envelope of the fading signal contains long-term and short-term fading components. The long-term fading is the average of the fading signals, as the dotted curve shows in Fig 3.2. The terrain configuration (open area, flat terrain, hilly terrain and mountain area) between the base station and the mobile unit cause the long-term fading [19]. This long term fading causes long-term variation in mean signal level. The long-term variations can be eliminated by increasing margins in transmitter power [20].

Short-term fading is caused by multipath reflections of a transmitted wave by houses, buildings, and other human-built structures, or by natural obstacles such as forest surrounding a mobile unit. It is also known as fast-fading. Whenever relative motion exists between the transmitter and receiver, there is a frequency variation in the received signal due to the Doppler effect. This also causes short-term fading. Since short-term fading falls within a statistical distribution known as Rayleigh distribution, it is also called Rayleigh fading. However, the deep rapid fades, in other words the short-term variations, degrade the communication quality. In this thesis the focus of the attention will be on the short-term fading, i.e. Rayleigh fading.

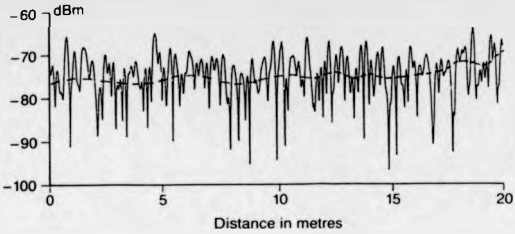

Figure 3.1: A typical fading signal envelope in an urban area. Source: D. PARSONS, The mobile Radio Propagation Channel, p.110.

3.2.1 Frequency selective Rayleigh fading channel

As the transmitted signal follows several paths in the mobile radio environment, signals arrive at the receiver with different delays. This phenomenan can be seen in Fig. 3.2.1. The range of delays that the paths introduce to the signal is referred to as the multipath spread T_m of the channel. Frequency selective fading is closely related to the multipath spread (delay spread). For a delay spread equal to zero, selective fading does not exist. When frequency selective fading exists in channels, the multipath spread is large enough that more than one transmitted symbol affects the received signal at a given instant. This is equivalent to time varying intersymbol interference (ISI), where the channel memory is defined by the delay spread. In digital systems, the degree of intersymbol interference depends on the transmitted bit rate (or symbol rate if modulation level ≥ 4). Let us consider the case of $T_m = 1\mu s$ and the bit transmission rate of 400 kilobits per second, and 2-level modulation scheme. Each symbol would consume 2.5 μs which would refer to a symbol overlap of 40 percent.

As its name indicates, signals with different frequencies will be differently affected by this channel i.e.frequency selective fading also affects the frequency spectrum of the received signal.

3.3 Computer generated frequency selective Rayleigh fading channel

The modelling of mobile radio channels is covered in a number of papers [1][18]. These modelling channels can be used to predict the signal transmitted in this channel. In this study, the simulated Rayleigh multipath fading channel is based on the model introduced

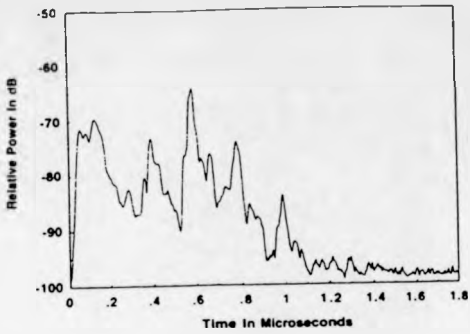

Figure 3.2: Illustration of delay spread. Source: G. CALHOUN, Digital Cellular Radio, p.215.

by Lee [10]. The model described in [10] is used to simulate a Rayleigh fading signal. N low-frequency oscillators with frequencies equal to the Doppler shifts $(2\pi V/\lambda)cos(2\pi n/N)$, $n = 1, 2, \ldots N$, are used to generate signals frequency-shifted from a carrier frequency w_c. Each generated signal consists of real and imaginary parts, $X(t)$ and $Y(t)$.

$$X(t) = \sum_{n=1}^{N=9} [A_n cos(2\pi V/\lambda t cos\Phi_n) + B_n sin(2\pi V/\lambda t cos\Phi_n) \tag{3.1}$$

$$Y(t) = \sum_{n=1}^{N=9} [B_n cos(2\pi V/\lambda t cos\Phi_n) - A_n sin(2\pi V/\lambda t cos\Phi_n) \tag{3.2}$$

where A_n and B_n are N Gaussian random variables with zero mean and variance one, $\Phi_n = 2\pi n/N$, and V is the speed of the vehicle. According to [10][1], N must be greater than 8. In this study N is chosen to be 9. If the sampling interval, $\Delta t = t_i/i$, then, $X(t)$ and $Y(t)$ become:

$$X_i = \sum_{n=1}^{N=9} [A_n cos(2\pi V/\lambda i \Delta t cos\Phi_n) + B_n sin(2\pi V/\lambda i \Delta t cos\Phi_n) \tag{3.3}$$

$$Y_i = \sum_{n=1}^{N=9} [B_n cos(2\pi V/\lambda i \Delta t cos\Phi_n) - A_n sin(2\pi V/\lambda i \Delta t cos\Phi_n) \tag{3.4}$$

PAGE(S) MISSING
NOT AVAILABLE

P23

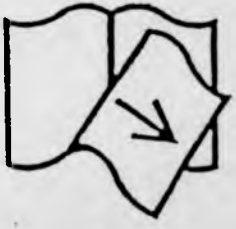

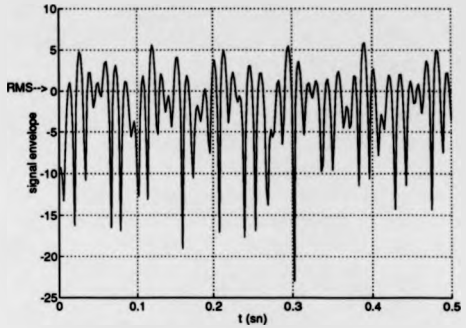

Figure 3.3: Simulated Rayleigh fading signal envelope

At the specific transmission rate and the given delay spread, any signal is assumed to be effected by three subsequent ones. Thus, the impulse response of the channel is expressed by the four ray model:

$$h(kT_s) = \alpha_1 e^{j\theta_1}\delta(kT_s) + \alpha_2 e^{j\theta_2}\delta(kT_s - \tau) + \alpha_3 e^{j\theta_3}\delta(kT_s - 2\tau) + \alpha_4 e^{j\theta_4}\delta(kT_s - 3\tau) \quad (3.7)$$

where α_1, α_2, α_3 and α_4 are independent and have Rayleigh distributed amplitudes. θ_1, θ_2, θ_3 and θ_4 are independent and have uniformly distributed phases on 0 to 2π, and τ is the time delay between the rays. The sum of $E\{\alpha_1^2\}$, $E\{\alpha_2^2\}$, $E\{\alpha_3^2\}$ and $E\{\alpha_4^2\}$ is set to unity in the simulation so the channel has unity gain. Two different channel characteristics with different $E\{\alpha_i^2\}$ are examined. The ratio between the sequential $E\{\alpha_i^2\}$ is denoted as C/D. In other words, the ratio between $E\{\alpha_1^2\}$ and $E\{\alpha_2^2\}$, $E\{\alpha_2^2\}$ and $E\{\alpha_3^2\}$ and $E\{\alpha_3^2\}$ and $E\{\alpha_4^2\}$ will be called C/D. Different channel characteristics will be taken to mean different C/D ratios. The signal $S_T(t)$ is modulated by a Rayleigh envelope $\alpha_1(t)$ and a uniform phase $\theta_1(t)$. The first delayed signal $S_T(t-\tau)$ is modulated by a Rayleigh envelope $\alpha_2(t)$ and a uniform phase $\theta_2(t)$. The second delayed signal $S_T(t-2\tau)$, and the third $S_T(t-3\tau)$ are modulated by Rayleigh envelopes $\alpha_3(t)$ and $\alpha_4(t)$ and by uniform

phases $\theta_3(t)$ and $\theta_4(t)$ respectively. The combinations of $S_T(t)$, $S_T(t-\tau)$, $S_T(t-2\tau)$ and $S_T(t-3\tau)$ account for the frequency selective fading. The output signal of this filter is then added to a white Gaussian noise.

In this thesis the fading process is assumed to be slow enough that the channel impulse response is constant over the length of a block of data. For these simulations a block size of 125 data bits is used. Assume that time division multiple access (TDMA) is used in this transmission. If the data transmission rate is 500 kb/s, then the duration of a time-slot, consisting of 125 bits, will be 0.25 ms. The TDMA frame period (consisting of 8 time slots) will be 2 ms. As the time slot corresponding to a user is sent with a period of 2 ms then, for each 2 ms, a sample must be taken from the simulated Rayleigh fading signal. This means the channel impulse responses change during each time slot.
The samples (amplitude values) are first normalised to have desired decibel mean and then stored in memory. As mentioned before, 750 samples were taken 2 ms apart, and an envelope is produced that is 1.5 s long. This is done for each tap as shown in Fig. 3.4.

3.4 On Channel estimators

As the communication channel is a frequency selective Rayleigh fading channel, the inter-symbol interference introduced by the channel can be suppressed by an adaptive equaliser. As the channel characteristics are not known and change with time, the equaliser should be adaptive i.e. it should be able to follow rapid variations in the channel impulse response. The structure of the adaptive algorithm, which is going to be discussed in details later, can be seen in Fig. 3.5. In this figure, Y represents the unknown mobile channel which has to be compensated by an adaptive filter Y'. The objective of the compensation is to reach the case in which $X = Z$. A channel estimator is employed to estimate the channel impulse responses (CIR). It performs the identification (estimation) by a known training sequence transmitted periodically at every TDMA frame. By using these (CIR)s, the tap coefficients of the feedforward and feedback sections of this equaliser can be found. Various papers have already shown that several algorithms can be used to find the channel impulse responses. Amongst these are gradient, Kalman and fast Kalman algorithms. What they all have in common is that they evaluate the difference between known or estimated reference symbols and equaliser output values, and update the coefficients by iterative feedback.

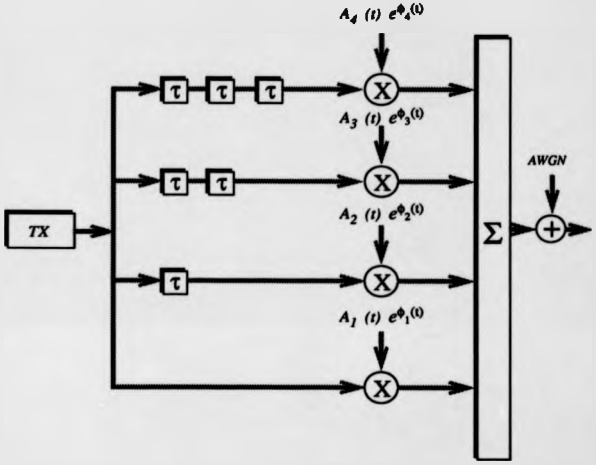

Figure 3.4: The block diagram of a frequency selective Rayleigh fading channel

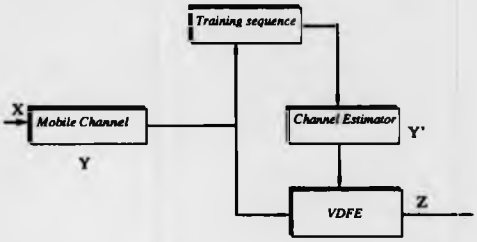

Figure 3.5: The block diagram of the adaptive algorithm

The channel estimators proposed in this thesis are based on the least-mean-square algorithm [25]. They are implemented by applying the steepest descent (gradient) algorithm for minimisation of the mean square error (MSE) [74].

3.4.1 The simulated channel estimator

The objective of the channel estimator to be presented within this section is to obtain an optimum estimate of the channel characteristics, by using a known training sequence. A channel estimator is identical in structure to a linear transversal equaliser. In fact, a channel estimator is a replica of the equivalent channel. The estimated tap coefficients, denoted as $\hat{Y}_n(i)$, are adjusted recursively to minimise the MSE between the actual received sequence and the output of the estimator. The simulated channel estimator using the Least mean square (LMS) algorithm is illustrated in Fig.3.6. The algorithm operates as follows. The training sequence S_i is passed through a shift register. The channel tap gains are adjusted according to [23][24][25]

$$\hat{Y}_n(i+1) = \hat{Y}_n(i) + \Delta e_i U_{i-n} \tag{3.8}$$

where $n = 0, 1 \ldots L$, and Δ is the gradient step size. If the value of Δ is kept small, the effect of the additive white noise on $\hat{Y}_n(i)$ will be small. On the other hand the rate of response of $\hat{Y}_n(i)$ to become $Y_n(i)$ will be small. In other words, more iteration will be needed for $\hat{Y}_n(i)$ to change to $Y_n(i)$. e_n is the signal error which is:

$$e_i = R_i - \hat{R}_i = R_i - \sum_{k=0}^{L} \hat{Y}_k(i) S_{i-k} \tag{3.9}$$

All training symbols S_i, S_{i-1}, S_{i-g} are multiplied by the corresponding channel tap gains $\hat{Y}_L(i)$, $\hat{Y}_{L-1}(i), \ldots \hat{Y}_0(i)$ respectively, and then added to give the estimate $\hat{R}_i$ of the received symbol R_i. This can be seen from equation 3.9.

Two different arrangements of the LMS estimator have been tested. These use the algorithm given by equations 3.8 and 3.9 with the following modifications:

1) LMS estimator one: At each time slot the initial values of $\hat{Y}_n(i)$ are assumed to be zero (0). In other words, the tap coefficients of the channel estimator at each time slot (at each step) are reset.

2) LMS estimator two: The initial values of $\hat{Y}_n(i)$ are assumed to be the same as the previous one. In other words, the tap coefficients of the channel estimator are not reset at each time slot (at each step).

3.4.2 Performance results

An extensive series of computer simulation tests have been carried out to compare the performances of these arrangements with a different number of training sequences over a frequency selective Rayleigh fading channel. An 8-level PSK signal is transmitted over the frequency selective Rayleigh fading channel.

The tests are carried out for 3 different signal to noise ratios(SNR), SNR=20 dB, 30 dB and 40 dB, and for a training sequence with three different numbers(amounts) of symbols,

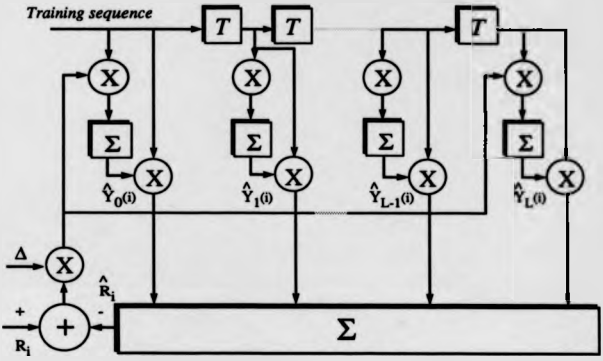

Figure 3.6: Adaptive channel estimator

15, 20 and 25 symbols. The gradient values, Δ, between 0.10 and 0.30, are considered for both LMS channel estimator 1 and 2. The mean-square error (MSE) in $\hat{Y}_n(i)$ is measured in dB, and is given by

$$MSE = 10\log_{10}(1/N \sum_{n=1}^{N}\sum_{i=1}^{L}|Y_n(i) - \hat{Y}_n(i)|^2). \tag{3.10}$$

where N is the number of the transmitted symbol. In this study N is chosen to be 100. Table 3.2 and Table 3.3 show the measured mean-square error for LMS estimator 1 and LMS estimator 2, respectively, for given Δ's, training sequences and SNR's.

The optimum values of gradient step size Δ are found and given in Table 3.4. Each LMS estimator is optimised for each signal/noise ratio and for each training sequence considered in this study.

Figs. 3.7, 3.8 and 3.9 show the variation of MSE with gradient step size Δ, for the LMS estimator 2. As seen in these figures, a very small value of Δ degrades the performance because it prevents the estimator from tracking the variations in $Y_n(i)$ correctly. In other words, more iterations will be needed for $Y_n(i)$ to change to $Y_n(i)$. A degradation in performance can also be seen when the Δ is very large. Another common result is that increasing the SNR increases the performance of the estimator, and also an increase is observed in optimal gradient step sizes Δ. As can be seen from Table 3.4, this is valid for LMS estimator 2 with with three different training sequences. In fact, this is true for LMS estimator 1 as well. For example, for a training sequence of 15 symbols and a SNR equal to 20, 30 and 40 dB, the optimal Δ values for LMS 1 and LMS 2 are, 0.22, 0.26, 0.28 and 0.14, 0.20, 0.28, respectively. It is clear that, increasing the SNR will cause an increase in optimal gradient step sizes.

The results of the tests tabulated in Tables 3.2, 3.3 and 3.5 demonstrate that, for all given training sequences and SNR values considered here, the LMS estimator 2 has a slightly better performance than the LMS estimator 1. The optimal estimators and corresponding mean-square errors are given in Table 3.5. Fig. 3.10 shows the performances of two LMS estimators where the training sequence is composed of 25 symbols. As seen in this figure, the LMS estimator 2 has 1-2 dB better MSE performance than the LMS estimator 1, for fixed SNR's.

Training seq.	20 dB	30 dB	40 dB
Δ =0.10			
15	-13.739	-13.975	-14.015
20	-19.015	-19.891	-20.029
25	-22.297	-24.558	-24.920
Δ =0.12			
15	-16.170	-16.751	-16.802
20	-21.964	-24.402	-24.800
25	-24.270	-28.910	-30.132
Δ =0.14			
15	-18.110	-19.271	-19.337
20	-22.601	-28.413	-29.580
25	-23.798	-31.406	-34.944
Δ =0.16			
15	-19.261	-21.058	-21.463
20	-23.076	-30.900	-33.942
25	-23.145	-32.164	-38.322
Δ =0.18			
15	-20.138	-22.606	-23.164
20	-22.358	-31.755	-37.128
25	-22.626	-32.261	-40.380
Δ =0.20			
15	-19.788	-23.839	-24.748
20	-21.963	-31.785	-39.430
25	-21.395	-31.699	-41.752
Δ =0.22			
15	-20.285	-24.970	-26.222
20	-21.000	-31.048	-40.241
25	-21.513	-31.084	-40.777

(a)

Table 3.2: Mean-square errors given by LMS estimator 1

Training seq.	20 dB	30 dB	40 dB
Δ =0.24			
15	- 19.532	-26.069	-27.716
20	- 20.441	-30.161	-39.793
25	- 20.848	-30.572	-40.519
Δ =0.26			
15	-19.331	-26.748	-29.333
20	-19.723	-29.597	-39.564
25	-19.655	-30.066	-39.656
Δ =0.28			
15	-18.460	-26.557	-30.348
20	-18.796	-29.090	-38.294
25	-18.831	-29.181	-39.200
Δ =0.30			
15	-17.899	-26.303	-30.341
20	-18.067	-28.258	-37.200
25	-18.245	-28.314	-37.971

Table 3.2b: Continued from Table 3.2a.

Training seq.	20 dB	30 dB	40 dB
Δ =0.10			
15	-21.803	-23.339	-23.547
20	-24.322	-30.158	-31.379
25	-25.578	-33.533	-36.330
Δ =0.12			
15	-22.954	-26.543	-26.940
20	-24.631	-32.739	-36.096
25	-25.029	-34.329	-40.607
Δ =0.14			
15	-22.956	-28.312	-29.752
20	-24.058	-33.279	-39.948
25	-24.341	-34.040	-42.593
Δ =0.16			
15	-22.761	-30.084	-32.296
20	-23.773	-33.118	-41.817
25	-23.179	-32.860	-42.708
Δ =0.18			
15	-22.139	-30.656	-33.987
20	-22.577	-32.465	-42.036
25	-22.477	-32.429	-42.212
Δ =0.20			
15	-21.478	-30.720	-35.568
20	-21.975	-31.760	-41.553
25	-21.871	-31.492	-41.289
Δ =0.22			
15	-21.054	-30.420	-36.867
20	-21.026	-30.908	-40.898
25	-21.372	-30.951	-40.756

(a)

Table 3.3: Mean-square errors given by LMS estimator 2

Training seq.	20 dB	30 dB	40 dB
Δ =0.24			
15	-20.443	-30.190	-37.222
20	-20.626	-30.230	-40.389
25	-20.345	-30.305	-40.513
Δ =0.26			
15	-20.053	-29.236	-37.350
20	-19.547	-29.829	-39.433
25	-19.604	-29.745	-39.803
Δ =0.28			
15	-18.681	-28.807	-37.361
20	-18.862	-29.206	-38.807
25	-18.970	-29.193	-39.124
Δ =0.30			
15	-17.764	-28.089	-36.913
20	-18.042	-28.074	-38.138
25	-18.098	-28.085	-38.228

Table 3.3b: Continued from Table 3.3a.

	LMS 1			LMS 2		
Training seq.	20 dB	30 dB	40 dB	20 dB	30 dB	40 dB
15	0.22	0.26	0.28	0.14	0.20	0.28
20	0.16	0.20	0.24	0.12	0.14	0.18
25	0.12	0.18	0.20	0.10	0.12	0.16

Table 3.4: Optimum values of Δ

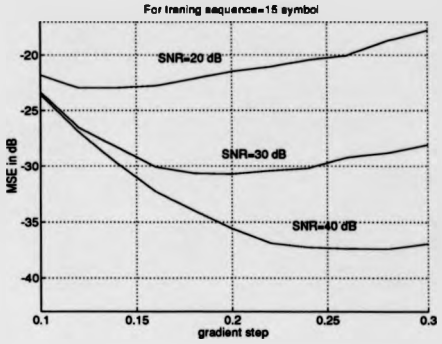

Figure 3.7: Variation of mean-square error MSE with gradient step Δ, for LMS estimator 2 and training sequence=15 symbol

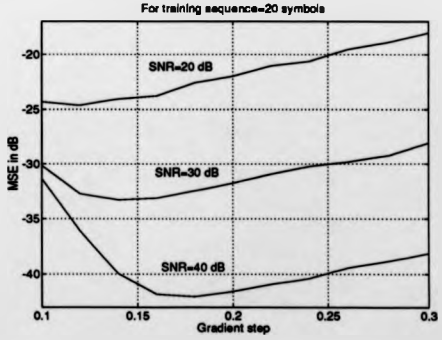

Figure 3.8: Variation of mean-square error MSE with gradient step Δ, for LMS estimator 2 and training sequence=20 symbol

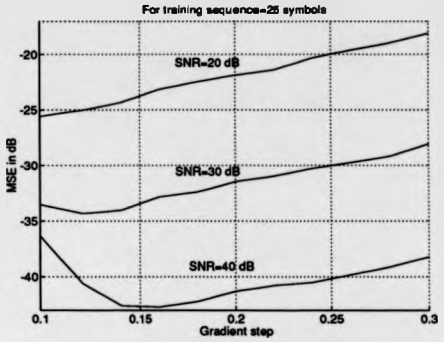

Figure 3.9: Variation of mean-square error MSE with gradient step Δ, for LMS estimator 2 and training sequence=25 symbol

In this study, the LMS estimator 2 with training sequence of 25 symbols is employed as a part of the receiver. A gradient step size, Δ, of 0.14 is chosen. The reason for choosing it is that when considering three given SNR's, this size is the optimal one.

Training seq.	20 dB		30 dB		40 dB	
	LMS #	MSE	LMS #	MSE	LMS #	MSE
15	2	-22.956	2	-30.720	2	-37.361
20	2	-24.631	2	-33.279	2	-42.036
25	2	-25.578	2	-34.329	2	-42.708

Table 3.5: Optimum LMS estimators and their MSE values

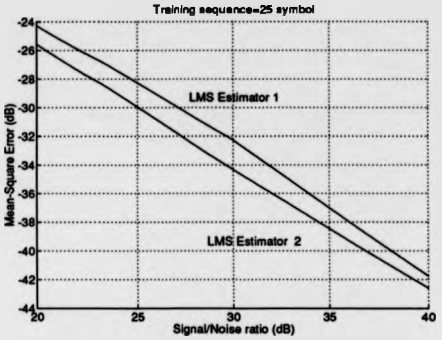

Figure 3.10: Comparison of channel estimators LMS 1 and LMS 2, training sequence=25 symbol

3.5 Conclusion

The statistical characteristics of the mobile channel are well known. The signal in the mobile communication channel is affected by several factors; by multipath interference which is caused by reflection from a hill, a building, a truck, an airplane; by a delay spread of the received signal; by a random frequency modulation due to different Doppler shifts. These effects cause the received signal envelope to fluctuate about the local mean with Rayleigh statistics, and the RF phase with uniform distribution. In a mobile system operating at a high bit rate, the delay spread causes intersymbol interference. Hence, the communication channel is a frequency selective Rayleigh fading channel. A communication channel model has been computer simulated. The range of delays that paths introduce to the signal is known as the multipath spread of the channel. For frequency selective fading channels the multipath spread is large enough that the received signal has the effect of more than one transmitted symbol at a given instant. This has been established by introducing more than one path with independent Rayleigh distributed amplitudes and uniformly distributed phases. In this thesis, the impulse response of the channel has been expressed by the four ray model. This intersymbol interference introduced by the

channel can be suppressed by an adaptive equaliser. As the channel characteristics are not known and change with time, the equaliser should be adaptive i.e. it should be able to follow the rapid variations in the channel impulse response. To find the tap coefficients of the feedforward and feedback section of this equaliser, a channel estimator has been employed. In this thesis, two arrangements of a channel estimator based on the least-mean-square algorithm [25] have been proposed. They are implemented by applying the steepest descent (gradient) algorithm for minimisation of the mean square error (MSE). 8-level PSK signals are transmitted to find the accuracies of the channel estimators over a FSRF channel. The results of computer simulation tests have been presented.

CHAPTER 4

TRELLIS CODED M-ARY PHASE SHIFT KEYING (PSK) COMMUNICATION SYSTEMS

4.1 Introduction: On trellis coding modulation (TCM) technique

Trellis-coded modulation (TCM) proposed by Ungerboeck [27] [28] and studied by others [32] [33] [34] [40] is a combination of coding and modulation technique for digital transmission over additive white Gaussian noise (AWGN) channels. Ungerboeck [27] [28] showed that TCM schemes can provide coding gains of 3-6 dB relative to an uncoded scheme with the same spectral efficiency.

The appropriate criterion for designing good TCM schemes in the AWGN channel is to maximise the free Euclidean distance [27] [28] [29] [30]. The gain is accomplished by coding onto an expanded signal constellation so that the free Euclidean distance is maximised. The Hamming distance of the code, whether measured in code bits or code symbols, is not directly relevant [27] [28] [30] [75].

M-ary trellis coded (TC) PSK was studied by some authors [27] [28] [32] [33] [34] [40] under the AWGN channel. More recently, TCM has been investigated for other channels as well, including Rician channel [30] [36] [38] and Rayleigh channel [31] [35] [37] [41] [42] [43].

However, there were still open questions concerning coding gains under the time invariant intersymbol interference (ISI) and frequency selective Rayleigh fading channels. In this study, the Ungerboeck 4-state rate 2/3 8-PSK TCM scheme is examined for ISI and frequency selective Rayleigh fading channels. The main concern is whether the coding gains obtained for additive white Gaussian noise channels will degrade or stay the same when the channel is intersymbol interference or frequency selective Rayleigh fading channel.

Since the error rate is one of the primary measures of performance in digital transmission and since the computation of the error rate as a function of multipath parameters, filter characteristics, Doppler effect etc. is extremely complex, a simulation method is used to determine these performances. Hence, the bit error rate (BER) of each system considered in this study is evaluated through computer simulations.

Receiver structures, to recover the data corrupted in these channels, are presented. For a channel with time invariant ISI three types of equaliser are examined. Two of them are the known equalisers, namely the linear feedback equaliser, and the decision feedback equaliser. The third equaliser is the proposed equaliser, which will be called Viterbi decision feedback equaliser (VDFE). To evaluate and compare the performance of these three algorithms, computer simulation is used. The simulation is performed for a time invariant ISI channel, namely telephone channel 2 [49]. For frequency selective Rayleigh fading channel (studied in Chapter 3) a receiver structure which is based on the VDFE, is proposed and presented. The bit error rate (BER) performance of the system under this channel is found through computer simulations.

Since the coding gain achieved in TC 8-PSK is low, searches have been conducted in improving this gain. A modulation scheme called Hybrid trellis-coded 8/4 PSK presented by Sundberg [44], which is the combination of the TC 8-PSK and the uncoded 4-PSK, has been studied under the frequency selective Rayleigh fading. The BER performance is also found by using computer simulations.

Section 4.2 presents the system under consideration: The combination of trellis coding with 8-PSK. In Section 4.3 the Ungerboeck 4-state rate 2/3 8-PSK TCM scheme in AWGN channels is studied. In Section 4.4, receiver structures to recover the TC 8-PSK signal, which is passed through a time invariant intersymbol interference channel, are proposed. The BER performances are found in the same section. A receiver structure for the TC 8-PSK signal in frequency selective mobile radio channel is proposed and presented in Section 4.5. In the same section the BER performance of this system under frequency selective Rayleigh fading (FSRF) channel is computed. The same section discusses the performance results of uncoded and coded schemes. In Section 4.6 a modulation scheme which combines the TC 8-PSK and the uncoded 4-PSK signals is studied under the fre-

quency selective Rayleigh fading channel. Meanwhile the BER performance of this system under the frequency selective Rayleigh fading channel is evaluated through the use of computer simulation. The comparison with the others is also presented. The same section discusses the performance results. The chapter is summarised in Section 4.7.

4.2 Combining trellis codes with 8-PSK: TC 8-PSK

The general structure of 8-PSK trellis coded modulation is illustrated in Fig. 4.1. As shown in this figure, TC 8-PSK signals are generated as follows: There are two bits to be transmitted. One of them is coded onto two bits. These two bits are used to select one of the 4-subsets of a redundant 8-ary signal set. The remaining uncoded bit specifies one of the 2 signals in this subset (See Fig. 4.2).

The trellis codes arise from combining convolutional coding with modulation. This combination is called trellis coded modulation (TCM). It is based on set partitioning. Set partitioning divides a signal set into smaller subsets by increasing the smallest distances in the subsets. Set partitioning is repeated until Δ_i corresponding to the last subset is equal to the desired free Euclidean distance of TCM scheme to be designed.

The Trellis coded modulation (TCM) scheme used in this study is the 4-state TCM 8-PSK scheme presented by Ungerboeck. The design of this scheme is based on the free Euclidean distance [26] [28] [29]. The scheme shown in Fig. 4.3 consists of a rate 2/3 convolutional encoder and a 8-PSK signal mapper. The corresponding signal constellation and trellis of the code are shown in Fig. 4.4(a) and (b). In the 4-state 8-PSK code, the 8-signal set is divided first into two subsets, and then into four subsets where the free Euclidean distance $\Delta_4 = 2$.

The free Euclidean distance in the four-state 8-PSK code is defined as [29]

$$d_{free} = Min[\Delta_4, d_{free}(1)]$$

where Δ_4 is the minimum distance between parallel transitions and $d_{free}(1)$ denotes the minimum distance between any two signal paths which diverge from the same state and remerge in another state after more than one transition.

The distance between parallel transitions, Δ_4, is equal to 2. To find the $d_{free}(1)$ all the signal path pairs have to be considered. It has been shown that this distance is equal to $\Delta_2 + \Delta_1 + \Delta_2 = \Delta_1 + \Delta_4 = 2 + 2\sin(\pi/8)$. An example to these is the distance between the signal path 0-0-2 and the path 2-1-0 (see Figure 4.4). According to the equation above the free Euclidean distance is equal to 2. That means the free Euclidean distance for this scheme is the distance between the parallel transition. The free Euclidean distance corresponding to the uncoded 4-PSK scheme is $\sqrt{2}$. The probability of error can be written as [28]

$$P(e) = N_{free}Q[d_{free}/(2\sigma)] \tag{4.1}$$

where Q(.) is the Gaussian error probability integral which is defined in Equation 2.15, and N_{free} is the number of nearest neighbours signal sequences with distance d_{free}. For any state transition along any 4-state TC 8-PSK sequence transmitted, there exists just one nearest-neighbour signal at free distance. Now the achievable coding gain can be evaluated using Equation 4.1. If it is expressed in decibels, TC 8-PSK with 4-state can achieve 3 dB coding gain.

4.3 TC 8-PSK signal in an ideal channel

4.3.1 A receiver structure for the TC 8-PSK signal in an ideal (memoryless) channel with AWGN

In order to decode the TC 8-PSK signal a maximum likelihood sequence estimation (MLSE) algorithm can be used effectively. The best known of such algorithms is the Viterbi algorithm [73] [72] which is used throughout this study.

Decoding is accomplished as follows: The received noisy signal is compared with the corresponding components of the two possible signals (the two parallel signals) at each of the 8 possible branches (See Fig. 4.4). The symbol closest to the received signal is determined. In other words, a hard decision is made on the signal of each branch. That is why the parallel signals of each branch are designed to be as far from each other as possible. The error distances between the received signal and the four possible signals in each branch are compared and the signal with the smallest error distance is chosen. These signals are

The distance between parallel transitions, Δ_4, is equal to 2. To find the $d_{free}(1)$ all the signal path pairs have to be considered. It has been shown that this distance is equal to $\Delta_2 + \Delta_1 + \Delta_2 = \Delta_1 + \Delta_4 = 2 + 2\sin(\pi/8)$. An example to these is the distance between the signal path 0-0-2 and the path 2-1-0 (see Figure 4.4). According to the equation above the free Euclidean distance is equal to 2. That means the free Euclidean distance for this scheme is the distance between the parallel transition. The free Euclidean distance corresponding to the uncoded 4-PSK scheme is $\sqrt{2}$. The probability of error can be written as [28]

$$P(e) = N_{free}Q[d_{free}/(2\sigma)] \tag{4.1}$$

where Q(.) is the Gaussian error probability integral which is defined in Equation 2.15, and N_{free} is the number of nearest neighbours signal sequences with distance d_{free}. For any state transition along any 4-state TC 8-PSK sequence transmitted, there exists just one nearest-neighbour signal at free distance. Now the achievable coding gain can be evaluated using Equation 4.1. If it is expressed in decibels, TC 8-PSK with 4-state can achieve 3 dB coding gain.

4.3 TC 8-PSK signal in an ideal channel

4.3.1 A receiver structure for the TC 8-PSK signal in an ideal (memoryless) channel with AWGN

In order to decode the TC 8-PSK signal a maximum likelihood sequence estimation (MLSE) algorithm can be used effectively. The best known of such algorithms is the Viterbi algorithm [73] [72] which is used throughout this study.

Decoding is accomplished as follows: The received noisy signal is compared with the corresponding components of the two possible signals (the two parallel signals) at each of the 8 possible branches (See Fig. 4.4). The symbol closest to the received signal is determined. In other words, a hard decision is made on the signal of each branch. That is why the parallel signals of each branch are designed to be as far from each other as possible. The error distances between the received signal and the four possible signals in each branch are compared and the signal with the smallest error distance is chosen. These signals are

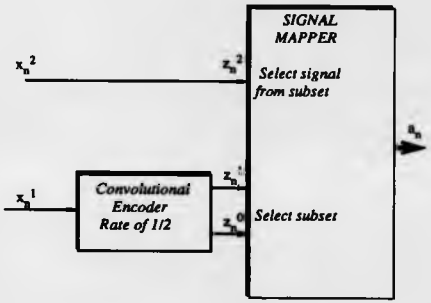

Figure 4.1: General structure of TCM 8-PSK

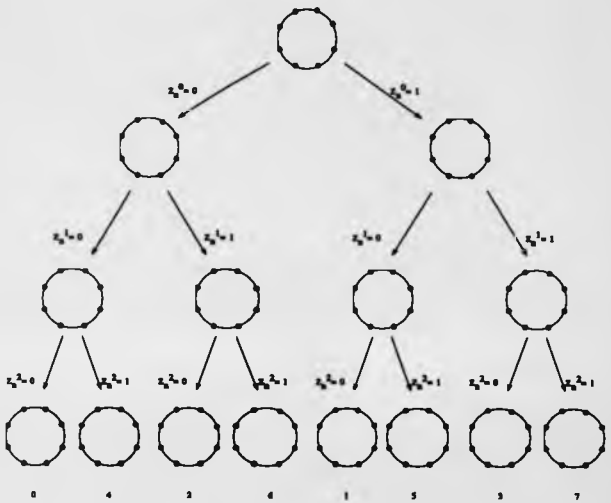

Figure 4.2: Set partitioning of the 8-PSK

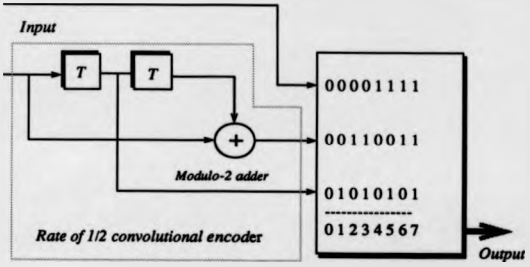

Figure 4.3: An encoder modulator for the four-state 8-PSK

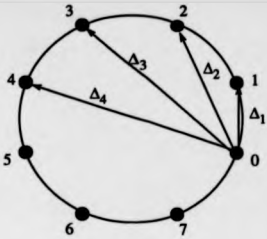

$\Delta_1 = 2\ \mathrm{Sin}(\pi/8)$

$\Delta_2 = \sqrt{2}$

$\Delta_3 = \sqrt{3.414}$

$\Delta_4 = 2$

(a)

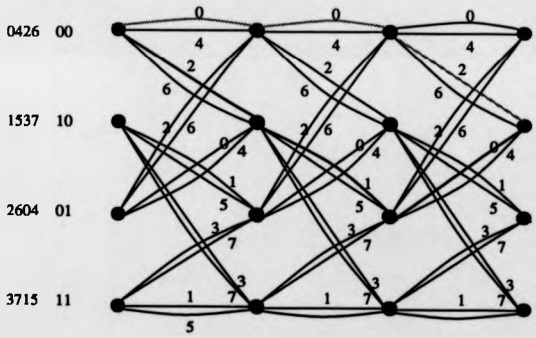

(b)

Figure 4.4: The trellis of the TCM 8-PSK

stored, together with their squared error distances from the received signal.

After a hard decision is made, there remains two possible signals leading to each of the four states in the trellis diagram (See Fig.4.5(a)). From the two signals leading to each of the four states, the one which gives less overall accumulated error distance is chosen and stored in a memory (see Fig.4.5(b)). The squared value of the error distance is used and is computed by:

$$\sum_{n}[(r_{nI} - a_{nI})^2 + (r_{nQ} - a_{nQ})^2]$$

where r_{nI}, r_{nQ} are the baseband components of the n th received signal and a_{nI}, a_{nQ} are the baseband components of the n th expected symbol of the trellis path concerned. According to this equation, each received signal is correlated with all possible transmitted signals.

When the length of the trellis (or observation length) reaches the decision depth, a hard decision is taken as to the oldest symbol in memory, which is then converted to a 2-bit message.

In the simulation, the decision depth length of 10 is used [79]. That means, when the observation interval length is equal to $10T_s$, a decision is taken as to the first symbol. It was also assumed that the receiver has full knowledge of the timing of the transmitted symbols.

4.3.2 The BER performance of the TC 8-PSK modulation in ideal channels with AWGN

In this section the BER performance of the 4-state TC 8-PSK scheme is studied over an ideal (memoryless) channel with AWGN through computer simulation. For comparison reasons the BER performance of uncoded 4-PSK scheme is also studied. The Gaussian noise source used in the simulation was generated from a uniformly distributed random source [46]. Fig.4.6 illustrates the signal transmission model used.

The results of the simulation for both 4-state TC 8-PSK and uncoded 4-PSK schemes are given in Fig.4.7. As observed, for all error probabilities considered here, the trellis coded scheme has better performance than the uncoded scheme. The coding gain of this

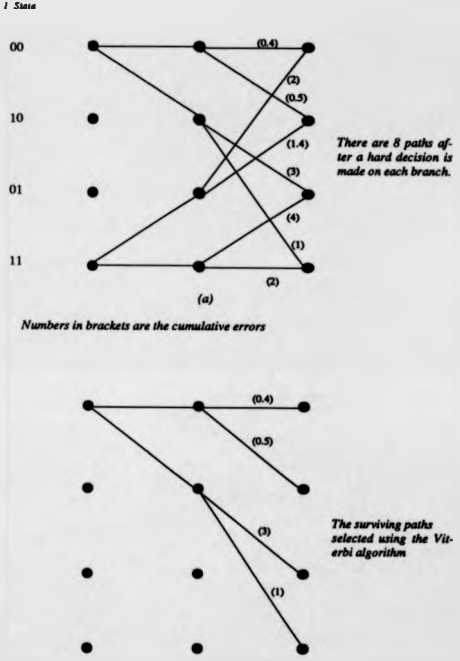

Figure 4.5: Trellis diagram of Viterbi decoding

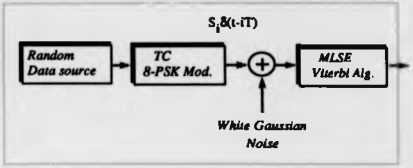

Figure 4.6: The block diagram of the transmission system for AWGN channel

code for bit error probabilities in the area of 10^{-3}, which is important in digital speech transmission, is about 1.5 dB. For error probabilities less than 10^{-3}, a gain increase is observed. For high S/N ratio this amount seems to reach 2 dB coding gain. It is observed that the simulation result is roughly 1 dB poorer than the expected (theoretical) coding gain given in [28].

The main conclusion concerning these results is that a significant gain can be achieved by trellis coding modulation in the presence of AWGN.

4.4 TC 8-PSK signal in a time invariant intersymbol interference channel with AWGN

The aim of the study in this section is to find out the obtainable coding gain of the 4-state TC 8-PSK modulation under the time invarying intersymbol interference channels.

The data transmission system considered here is shown in Fig.4.8. The information bits to be transmitted are generated from a random source. These are fed to the TC 8-PSK modulator. The low-pass envelope of the output symbol S_i is:

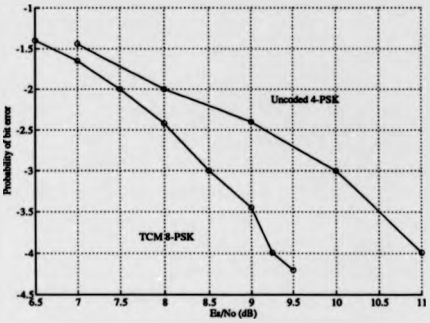

Figure 4.7: The BER performance of TC 8-PSK modulation in ideal channels with AWGN

$$S_i = S_{iI} + jS_{iQ}$$

where S_{iI} and S_{iQ} are the in-phase and quadrature components of the 8-PSK signal. The sequence of the complex data elements is fed to a transversal filter with complex coefficients $y(0), y(1), \ldots, y(m)$ and with a sampling rate equal to the symbol rate. This filter represents the baseband equivalent of the transmitter output filter, transmission path and receiver input filter, and will be referred to as an equivalent baseband channel. The in-phase and quadrature components of the received baseband signal for the ith symbol period, are denoted by R_I and R_Q respectively. The simulated noise samples $W_I(i)$ and $W_Q(i)$ from a Gaussian distribution with zero mean, are added to the filter output complex signal. The received signal is therefore (see Fig.4.9):

$$R_I + jR_Q = \sum_{k=0}^{m} (S_I(i-k) + jS_Q(i-k)) * y(k) + W_I(i) + jW_Q(i)$$

where i is denoting the current symbol period.

The bandpass transmission path is here taken to be a telephone circuit. Hence the complex time invarying intersymbol interference channel which is used in this simulation study is

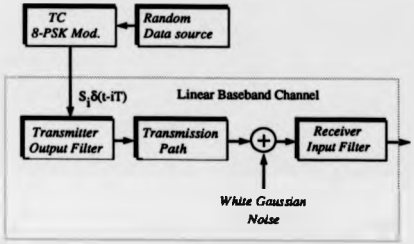

Figure 4.8: The data transmission system

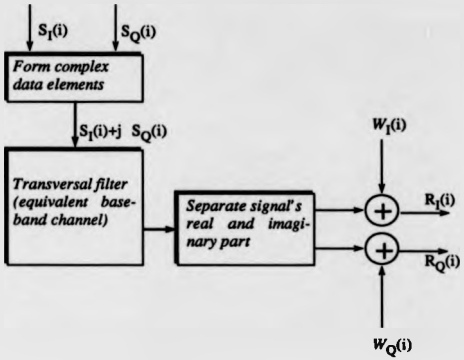

Figure 4.9: The block diagram of the transmission system for ISI channel

the telephone channel 2 in [49]. The channel impulse response coefficients are shown in Table 4.1.

When a digital signal is transmitted over a linear channel which distorts the signal, the resulting intersymbol interference can be removed or greatly reduced by employing an equaliser at the receiver [47][48][49][50][55][56][57][58]. Given the received signal $R(t)$, we need to know what is the best receiver for the TC 8-PSK signal under the time-invarying intersymbol interference channel. To find out, three kinds of receiver (equaliser) were investigated and proposed . All the equalisers studied here have the general structure shown in Fig.4.10.

4.4.1 A receiver structure using zero forcing linear feedback equaliser

A zero forcing equaliser is simply an inverse filter, which inverts the frequency response of the channel. The equaliser coefficients are chosen in such a way that the impulse response

Telephone channel 2	
Real part	Imaginary part
-0.0086	0.0030
0.0004	0.0042
0.0059	-0.0094
-0.0409	-0.0090
0.0043	0.0405
0.4725	0.0186
0.8081	-0.0218
0.0105	-0.0010
-0.1972	-0.0450
0.2039	0.0602
-0.1028	-0.0803
0.0287	0.0717
0.0208	-0.0461
-0.0406	0.0188
0.0403	0.0026
-.0340	-0.0138
0.0240	0.0177
-0.0158	-0.0190
0.0114	0.0184
-0.0088	-0.0176
0.0075	0.0165
-0.0052	-0.0148
0.0044	0.0126
-0.0045	-0.0110
0.0047	0.0097
-0.0042	-0.0017
0.0045	0.0062
-0.0051	-0.0040
0.0056	0.0023

Table 4.1: Sampled impulse responses of the telephone channel 2

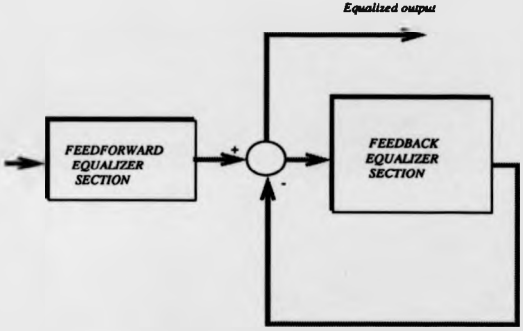

Figure 4.10: Generalised equaliser architecture

of the combined channel and equaliser are all zero except the first one. For more details about zero forcing equaliser, the reader can be referred to [48][58].

Linear feedback equaliser

Suppose that the Z-transform of the sampled impulse response of the baseband channel is:

$$C(z) = C_0 + C_1 Z^{-1} + C_2 Z^{-2} + \ldots + C_m Z^{-m}$$

where Z^{-i} represents the time instant $t = iT$ and $C_0 \neq 0$. This channel model is illustrated in Fig.4.11.

The received signal, which is the output signal of the channel in the absence of noise, is:

$$R_i = S_i C_0 + S_{i-1} C_1 + \ldots + S_{i-m} C_m.$$

The proposed linear feedback equaliser (LFE) is shown in Fig.4.12. What we want to see at the output of the LFE is: $X_i = S_i$, at the time instant $t = iT$. That is achieved. To prove that, assume that all the signals in the equaliser are zero. At the time instant $t = iT$, the output of the baseband channel (see Fig.4.11) is $R_i = S_i C_0$ which is the input signal of the equaliser. This will be multiplied by $1/C_0$ and become S_i. This amount will be subtracted from the signal coming from the adder, which is zero, at that time. Now the output of the equaliser is S_i, which is the desired amount. At the time instant $t = (i+1)T$, the output of the baseband channel is: $R_i = S_i C_0 + S_{i-1} C_1 / C_0$. That amount will be subtracted from the amount coming from the adder, which is $S_{i-1} C_1 / C_0$. The output of the equaliser is now S_i. This process continues in this way until the time instant equals $(i+m+1)T$. It is clear that the equaliser removes the intersymbol interference introduced by the channel.

In the presence of noise, if $|C_0|$ is small, then the noise and the signal will be amplified by multiplying them with $1/C_0$. This means noise magnification.

The proposed receiver structure is shown in Fig.4.13. As seen in this figure the equalised signal is passed through the Viterbi decoder to recover the coded data.

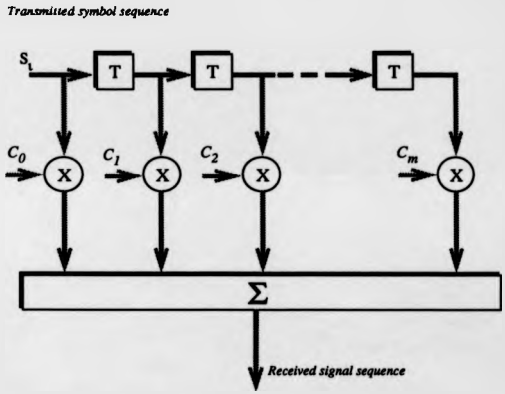

Figure 4.11: A channel model

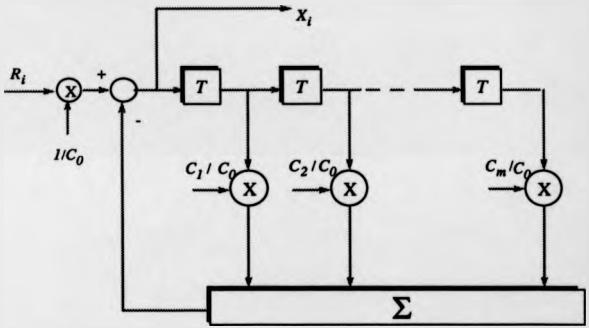

Figure 4.12: General structure of a linear feedback equaliser

Telephone channel 2 & feedforward equaliser	
Real part	Imaginary part
1.000	0.0000
0.5091	0.1960
-0.1465	0.0000
0.0323	-0.0171
0.0125	0.0200

Table 4.2: Sampled impulse responses of the combination of the telephone channel 2 and feedforward equaliser section

Real part	Imaginary part
0.5091	0.1960
-0.1465	0.0000
0.0323	-0.0171
0.0125	0.0200

Table 4.3: Sampled impulse responses of the feedback equaliser section

Simulation of the LFE

The general structure of the zero forcing LFE is as shown in Fig.4.10. The feedforward section is the combined section of the baseband channel (telephone channel 2) and the zero forcing equaliser. The impulse responses of this feedforward equaliser can be found in [48] and are shown in Table 4.2 (after removing the insignificant terms). In the simulation, noise is added to the output of the feedforward equaliser. This has been shown to be equivalent to adding noise at the output of the channel[49] [51]. The impulse responses of the feedback section are shown in Table 4.3.

The BER performance of the TC 8-PSK in a channel with time invariant ISI using linear feedback equaliser

In this section the BER performance of 4-state TC 8-PSK scheme is studied over the time invarying intersymbol interference channel, namely telephone channel 2 with AWGN through computer simulation. For comparison reasons, the BER performance of uncoded

4-PSK scheme is also studied. Fig.4.13 illustrates the signal transmission model used in this study. The equalised signal is passed through the Viterbi decoder to recover the data.

The results of simulation for both 4-state TC 8-PSK and uncoded 4-PSK schemes are given in Fig.4.14. As is observed, for error probabilities greater than 10^{-2}, the uncoded scheme has better performance. For error probabilities of 10^{-2} or less, the trellis coded scheme has better performance than the uncoded scheme. The coding gain of this code for bit error probabilities in the area of 10^{-3}, which is important in digital speech transmission, is about 0.25 dB.

The main conclusion concerning these results is that the coding gain which can be achieved by trellis coding modulation is not significant when LFE is used.

4.4.2 A receiver structure using decision feedback equaliser

It has been shown that decision feedback equalisers (DFE) can sometimes achieve better performance than linear equalisers [48][49][58]. As its basic structure is suitable for real time signal processing, the decision feedback equaliser is used widely in communication systems [56] [49].

The decision feedback equaliser is implemented as a linear feedforward transversal equaliser fed from the output of the detector, as shown in Fig.4.15. If the detector is removed from this figure then it will be seen that the Fig.4.12 is obtained. As the symbol detector (usually a threshold device) is nonlinear, it can be said that the DFE is nonlinear as well.

Suppose that the sampled channel impulse responses vector is:

$$C = [C_0, C_1, \ldots C_m].$$

The objective of the feedback transversal filter is to give at its output the transmitted symbol. At time instant $t = iT$, the received signal is:

$$R_i = \sum_{j=0}^{m} S_{i-j}C_j + W_i \quad = S_iC_0 + \sum_{j=1}^{m} S_{i-j}C_j + W_i.$$

Figure 4.13: The total transmission system using linear feedback equaliser

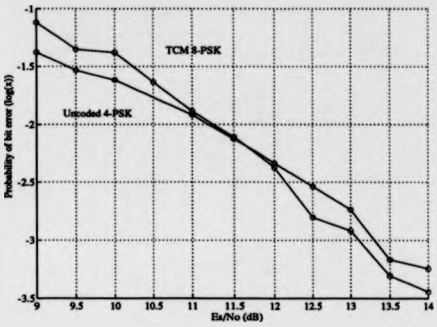

Figure 4.14: The BER performance of TC 8-PSK in a channel with ISI using linear feedback equaliser

If both sides of the equation are divided by C_0, which is the first impulse response of the channel, it becomes:

$$R_i/C_0 = S_i + \sum_{j=1}^{m_1} S_{i-j}C_j/C_0 + W_i/C_0. \tag{4.2}$$

The output of the equaliser shown in Fig.4.15 is:

$$X_i = R_i/C_0 - \sum_{j=1}^{m_2} S'_{i-j}C_j/C_0 \tag{4.3}$$

Substituting equation (4.2) in (4.3), we have:

$$X_i = S_i + \sum_{j=1}^{m_1} S_{i-j}C_j/C_0 + W_i/C_0 - \sum_{j=1}^{m_2} S'_{i-j}C_j/C_0 \tag{4.4}$$

In the presence of a correct decision, when $S_{i-j} = S'_{i-j}$, the equation (4.4) becomes

$$X_i = S_i + W_i/C_0 \tag{4.5}$$

where S_i is the desired symbol and W_i/C_0 is the noise. It is obvious that as long as correct detection is made, the DFE removes the intersymbol interference introduced by the channel.

The proposed receiver structure is shown in Fig.4.16. As seen in this figure the equalised signal is passed through the Viterbi decoder to recover the coded data.

The BER performance of the TC 8-PSK in a channel with time invariant ISI using decision feedback equaliser

The total transmission system as it has been simulated is shown in Fig.4.16, of which the receiver concept has already been described before. The receiver consists of the decision feedback equaliser and the Viterbi decoder, as shown in Fig.4.16. The impulse responses of these equalisers are the same as the zero forcing linear feedback equaliser's impulse responses. The only difference is that DFE has a hard-decision detector in its feedback section.

In this section the BER performance of 4-state TC 8-PSK scheme is studied over the time invarying intersymbol interference channel, namely telephone channel 2 with AWGN through computer simulation. For comparison reasons, the BER performance of uncoded 4-PSK scheme is also examined. Fig.4.16 illustrates the signal transmission model used in our study. As seen in this figure, the equalised signal is passed through the Viterbi decoder to recover the coded data.

Recall that, in this study the decision depth length is chosen to be 10 symbol intervals.

The results of computer simulation for both 4-state TC 8-PSK and uncoded 4-PSK schemes are given in Fig.4.17. As is observed, for all error probabilities considered here, the uncoded

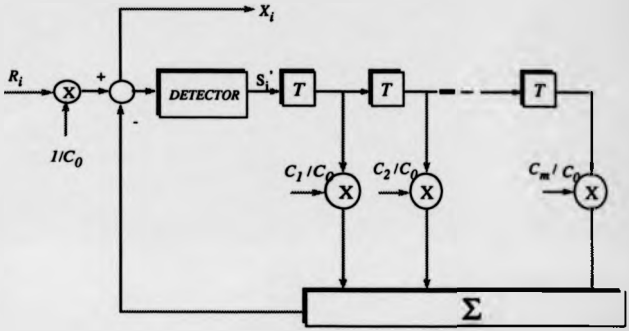

Figure 4.15: Decision feedback equaliser

scheme has better performance than the trellis coded scheme. For bit error probabilities in the area of 10^{-3}, which is important in digital speech transmission, the TC 8-PSK scheme is some 1.3 dB worse than the uncoded scheme. Such disappointing results are expected as the detector in the DFE makes hard decisions on the received signals and hence the potential benefit offered by trellis coding is lost.

4.4.3 A receiver structure using the VDFE

As undesired results in the DFE are due to the use of a hard decision device, the aim should be to improve the decision device to make a better decision. To gain the benefit offered by the trellis coding, a new idea is proposed. The idea is to integrate the Viterbi algorithm into the DFE architecture. This proposed algorithm will be called "Viterbi decision feedback equaliser (VDFE)".

The tapped delay line (or the shift register) of a decision feedback equaliser (see Fig.4.15) contains the values of the newest symbols determined by the detector using a hard decision algorithm. The required number of new symbols is the same as the number of tap coefficients in the feedback section. These symbols may or may not be correctly detected. If there are errors in these symbols, the received signal will be incorrectly equalised and more errors will follow if an incorrect decision is subsequently made. In a Viterbi decoder, however, a hard decision is made on the received signal after it has moved through the trellis for a time period equal to the decision depth. If the Viterbi decoder is used directly to replace the detector of the DFE, the symbols detected will be "too old" for the purpose of the equalisation. Fig.4.18 shows the memory containing the surviving paths schematically. The timing shown in the diagram is that when the ith symbol is received. It is clear that the preceding symbols required for equalisation are not available. However, the most probable combinations of these symbols are available in the newest part of the trellis memory (see Fig4.18). The equalised signal X_i of the ith path is given by:

$$X_i|_j = R_i - \sum_{m=1}^{n} X^i{}_{i-m,j} v_m$$

where n is the number of tap coefficients in the feedback section and j is the trellis state (or path) number . In the case of a 4-state trellis, which is considered in this study, there are 4 possible equalised signals corresponding to 4 surviving paths. Each of these equalised

Figure 4.16: The total transmission system using decision feedback equaliser

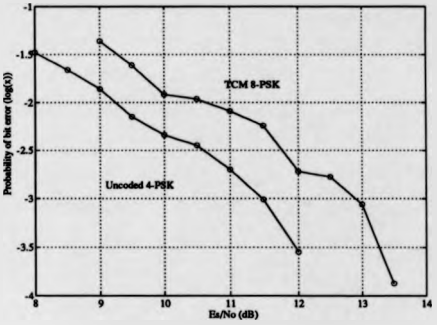

Figure 4.17: The BER performance of TC 8-PSK in a channel with ISI using decision feedback equaliser

signals is then used to determine the two most probable next symbols of the corresponding path. Now the number of symbols to be considered is eight. The metrics (squared error distances) corresponding to these eight symbols are first calculated and then added to the corresponding previous accumulated metrics. Then the four paths having smallest accumulative error distances of the eight paths are chosen as survived paths. n of the last(newest) symbols of these 4 paths are selected as the newest symbols of the feedback equaliser. It can be seen that the feedback section of the VDFE is used to remove the intersymbol interference introduced by the baseband channel while the Viterbi algorithm is used as a trellis decoder.

The BER performance of the TC 8-PSK in a channel with time invariant ISI using the new equalisation algorithm

The total transmission system as it has been simulated is shown in Fig.4.19, of which the receiver concept has already been described before. The receiver consists of the Viterbi decision feedback equaliser, as shown in Fig.4.16. The impulse responses of these equalisers are the same as the decision feedback equaliser's impulse responses. The only difference

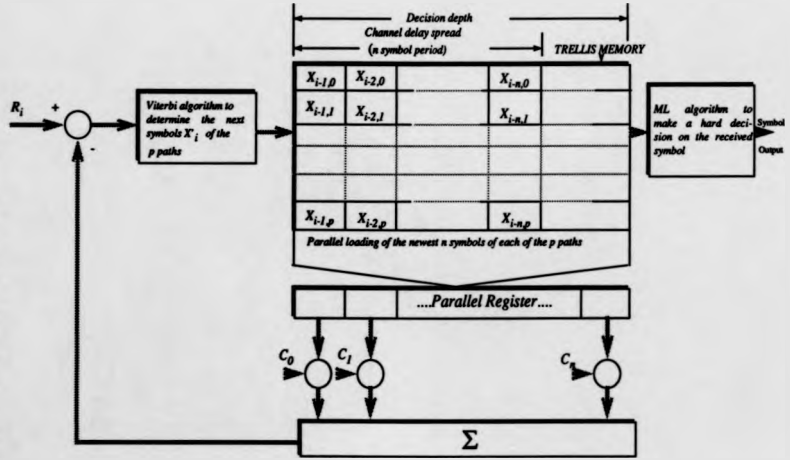

Figure 4.18: Viterbi decision feedback equaliser

is that VDFE has a Viterbi algorithm in its feedback section.

In this section the BER performance of 4-state TC 8-PSK scheme is studied over the time invariant intersymbol interference channel, namely telephone channel 2 with AWGN through a computer simulation. For comparison reasons, the BER performance of uncoded 4-PSK scheme is also examined. Fig.4.19 illustrates the signal transmission model used in our study.

The simulation results for both 4-state TC 8-PSK and uncoded 4-PSK schemes are given in Fig.4.20. As is observed, for all error probabilities considered here, the trellis coded scheme has better performance than the uncoded scheme. For bit error probabilities in the area of 10^{-3}, which is important in digital speech transmission, the TC 8-PSK scheme is some 1.6 dB better than the uncoded scheme.

4.4.4 Description of the results

To recover the TCM 8-PSK signal corrupted by the time invariant intersymbol interference channels, first, two known algorithms have been studied and examined through a computer simulation. The results show that the TC 8-PSK scheme has little or no advantage over the uncoded counterpart (uncoded 4-PSK). Such disappointing results can be expected as the detector in the DFE makes hard decisions on the received signals and hence the potential benefit offered by trellis coding is lost. Second, the new proposed algorithm, namely VDFE, was shown to be better than the other two algorithms. The results show that, using this algorithm, TC 8-PSK signal can be received with 1.6 dB lower S/N, when compared with uncoded 4-PSK scheme, for the BER in the area of 10^{-3}. Fig.4.21 shows the BER performances of the TC 8-PSK scheme using three different receiver algorithms. It is obvious that the new proposed algorithm, VDFE, is the superior one amongst them. It has remarkably good performance. When compared with the two others, it has approximately 3 dB better performance for bit error rates of around 10^{-3}.

Figure 4.19: The total transmission system using Viterbi decision feedback equaliser

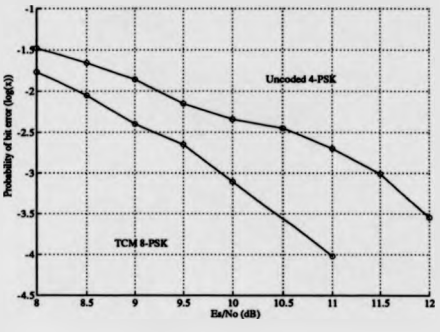

Figure 4.20: The BER performance of TC 8-PSK in a channel with ISI using Viterbi decision feedback equaliser

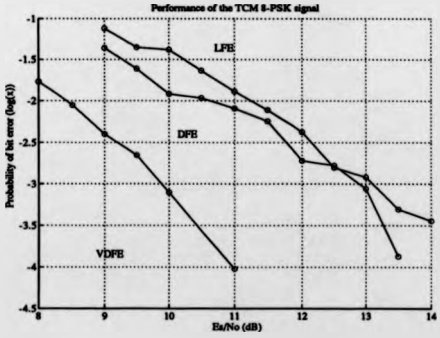

Figure 4.21: The BER performance of TCM 8-PSK in a channel with ISI using three different equalisers

4.5 TC 8-PSK in frequency-selective Rayleigh fading (FSRF) channel

As constant envelope schemes such as Gaussian minimum shift keying (GMSK) do not cause serious adjacent channel interference, they are used in mobile systems[2][11][13][71]. On the other hand, the bandwidth required to transmit the RF signals is considerably larger and the spectral efficiency is poor. As the demand for mobile communication increases, the spectral efficiency of the GMSK is no longer sufficient. In order to improve the spectral efficiency, the linear modulation schemes such as high-level PSK are considered again [52][53].

Multipath fading is a common impairment of mobile radio channels. It occurs when there are several radio paths between the transmitter and the receiver. In the presence of multipath fading, the received signal is the sum of signals received from the different paths. If these paths interfere destructively at the receiver then the signal is faded. The range of delays that paths introduce to the signal is known as the multipath spread of the channel. For frequency selective fading channels the multipath spread is large enough that the received signal has the effect of more than one transmitted symbol at a given instant. This is the same as the time varying intersymbol interference.
In this study, the performance of the TC 8-PSK scheme is going to be derived in a frequency-selective Rayleigh fading channel corrupted by AWGN. A receiver structure is proposed and presented in the following section.

4.5.1 Channel description

The channel imperfections which considered include:

- Fast fading which causes Rayleigh envelope fluctuation and uniform distributed phase.
- Delayed signal which causes frequency-selective fading
- Additive white Gaussian noise

Fig.3.4 shows the block diagram of a frequency selective Rayleigh fading channel corrupted by AWGN. The block TX is the transmitter of the desired symbol that transmits the TC 8-PSK signal:

$$S_T(t) = X(t)\cos w_c(t) - Y(t)\sin w_c(t) \tag{4.6}$$

where $X(t)$ and $Y(t)$ are the in-phase and quadrature baseband signals, respectively. The impulse response of the channel is expressed by the four ray model:

$$h(kT_s) = \alpha_1 e^{j\theta_1}\delta(kT_s) + \alpha_2 e^{j\theta_2}\delta(kT_s - \tau) + \alpha_3 e^{j\theta_3}\delta(kT_s - 2\tau) + \alpha_4 e^{j\theta_4}\delta(kT_s - 3\tau) \tag{4.7}$$

where α_1, α_2, α_3 and α_4 are independent and Rayleigh distributed amplitude. θ_1, θ_2, θ_3 and θ_4 are independent and uniformly distributed phase between 0 and 2π, and τ is the time delay between the rays. The sum of $E\{\alpha_1^2\}$, $E\{\alpha_2^2\}$, $E\{\alpha_3^2\}$ and $E\{\alpha_4^2\}$ is set to unity in the simulation, and so the channel has unity gain. Two different channel characteristics with different $E\{\alpha_i^2\}$ are examined. The ratio between the sequential values of $E\{\alpha_i^2\}$ is denoted as C/D. In other words, the ratio of $E\{\alpha_1^2\}$ to $E\{\alpha_2^2\}$, $E\{\alpha_2^2\}$ to $E\{\alpha_3^2\}$ and $E\{\alpha_3^2\}$ to $E\{\alpha_4^2\}$ will be called C/D. When two different channel characteristics are mentioned, channel characteristics with two different C/D ratios are meant. The signal $S_T(t)$ is modulated by a Rayleigh envelope $\alpha_1(t)$ and a uniform phase $\theta_1(t)$. The first delayed signal $S_T(t-\tau)$ is modulated by a Rayleigh envelope $\alpha_2(t)$ and a uniform phase $\theta_2(t)$. The second delayed signal $S_T(t-2\tau)$, and the third $S_T(t-3\tau)$ are modulated by a Rayleigh envelope $\alpha_3(t)$ and $\alpha_4(t)$ and a uniform phase $\theta_3(t)$ and $\theta_4(t)$ respectively. The combination of $S_T(t)$, $S_T(t-\tau)$, $S_T(t-2\tau)$ and $S_T(t-3\tau)$ accounts for the frequency selective fading. The output signal of this filter is then added to a white Gaussian noise. A software fading simulator, which is studied in Chapter 3, has been used to generate the amplitude and the phase of each ray in the four ray model. Only one receiver speed of 20 mph is examined in an urban area; this scenario then determine the parameters used in the fading channel model.

4.5.2 A receiver structure for the TC 8-PSK signal in frequency selective Rayleigh fading channel

In this section, a receiver structure is proposed to demodulate TC 8-PSK signals in the presence of frequency selective Rayleigh channel.

Figure 4.22: The receiver structure of TC 8-PSK signals

The proposed receiver, shown in Fig.4.22, consists of two principal components:

1. The Viterbi decision feedback equaliser (VDFE).
2. A channel estimator.

The receiver works as follows: While the Viterbi Algorithm is used to decode the TC 8-PSK signal, the feedforward and feedback sections of the VDFE are used to remove the channel intersymbol interference. As shown in Fig.4.22, both sections consist of a finite impulse response (FIR) filter, whose respective outputs are added to each other to form the equaliser output before Viterbi algorithm processing. As seen, the functioning principles of this receiver are the same as the receiver's proposed for the TC 8-PSK signal in ISI channel. One difference is that the FIR coefficients of the equalisers are computed by the channel estimator (for more details on the channel estimator see Chapter 3) using the training sequence at each time slot.

4.5.3 The BER performance of the TC 8-PSK signals

The error performances of the TC 8-PSK signal in a frequency selective Rayleigh fading channel are shown in Fig.4.23, Fig.4.24 and Fig.4.25 for two different C/D ratios. The channel in this study has a multipath spread which spans four symbol intervals. As C/D increases, the channels become less frequency-selective. If the C/D ratio is below 40 dB then the channel can be considered as a frequency selective channel [54].

For the case of C/D=10 dB, the results of computer simulation for both 4-state TC 8-PSK and uncoded 4-PSK schemes are given in Fig.4.23. As is observed, for error probabilities larger than $10^{-2.8}$, the uncoded scheme has better performance. For error probabilities of $10^{-2.8}$ or less, the trellis coded scheme has better performance than the uncoded scheme. The coding gain for bit error probabilities in the area of 10^{-3}, which is important in digital speech transmission, is about 0.5 dB. For high S/N ratios this gain is about 1.5 dB.

For the case of C/D=5 dB, the results of our simulation for both 4-state TC 8-PSK and uncoded 4-PSK schemes are given in Fig.4.24. As is observed, for error probabilities of 10^{-3} or more, the trellis coded scheme has no coding gain over uncoded scheme. For bit

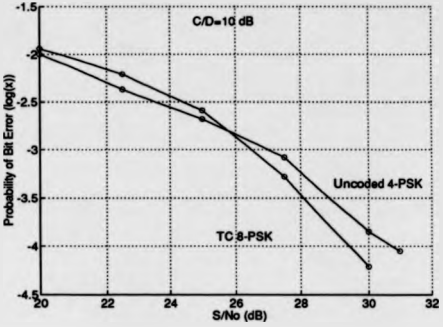

Figure 4.23: The BER performance of TC 8-PSK scheme in a FSRF channel (C/D = 10 dB)

error probabilities less than 10^{-3}, the coded scheme has better performance. The coding gain for bit error probabilities in the area of 10^{-4} is 1 dB.

Fig.4.25 shows the BER performance of TC 8-PSK scheme in frequency selective Rayleigh fading channel for two different C/D ratios. By comparing the results which are shown in this figure, the channel having C/D ratio of 10 has better performance than the one with C/D ratio of 5 for error probabilities of 10^{-3}. This result means, if the C/D ratio is decreased (which corresponds to more frequency selective) then performance degradation occurs.

4.6 A modulation scheme: combining the TC 8-PSK with the uncoded 4-PSK

The hybrid Trellis-coded 8/4-PSK presented by Sundberg [59] was proposed for such a phase error which can occur when the carrier phase varies during the transmission. This can be faced in mobile communications, fading channels, and jitter channels.

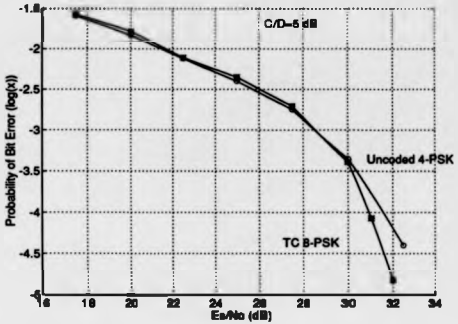

Figure 4.24: The BER performance of TC 8-PSK scheme in a FSRF channel (C/D = 5 dB)

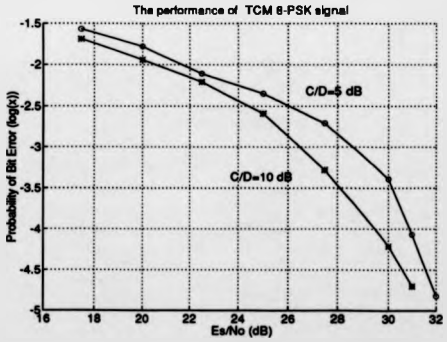

Figure 4.25: The BER performance of TC 8-PSK scheme in a FSRF channel for two different C/D ratios

In an uncoded 4-PSK receiver, the operating range is $\mp 45°$ in the absence of noise. If the phase error is inside this interval, the transmitted signal can be recovered. On one hand, the signal recovery fails if it is outside this interval. On the other hand, the signal recovery fails in a TC 8-PSK receiver, if the phase offset exceeds the critical value which is $\mp 22.5°$. This can cause a long error burst [29] [59]. By using the hybrid TC 8/4-PSK, the operating range of the receiver is increased compared to the TC 8-PSK case [59]. By this increase for hybrid 8/4-PSK, a lower BER than TC 8-PSK has, can be expected. The question is whether this scheme can be more efficient than the TC 8-PSK in frequency selective Rayleigh fading channel. As the analysis of this scheme in FSRF channel is too complex, the BER performance of a hybrid Trellis-coded 8/4-PSK in a FSRF channel is found through computer simulations.

The required bandwidth of this system is the same as the required bandwidth of the uncoded 4-PSK and TC 8-PSK systems[59]

4.6.1 System description

Hybrid TC 8/4-PSK, whose general structure is shown in Fig.4.26, is the combination of 4-state TC 8-PSK and uncoded 4-PSK. These are used in a time varying manner. As shown in Fig.4.26 the only difference from the block diagram of TC 8-PSK (shown in Fig.4.1) is that the mapper is changing periodically, whereas the convolutional code keeps generating the coded bits. During the odd-numbered symbol time intervals the 8-PSK mapper, and during the even-numbered symbol intervals the 4-PSK mapper, is used.

The general structure of hybrid trellis coded 8/4-PSK modulation is illustrated in Fig. 4.26. As shown in this figure, these signals are generated as follows: There are two bits to be transmitted. These are coded onto three bits. These three bits are the input bits to a mapper, which is periodically changed. The two mapping rules are shown in Table 4.4. The Trellis coded 8-PSK modulation scheme used in this study is the rate of 2/3 and 4-state TC 8-PSK scheme presented by Ungerboeck. The scheme is shown in Fig. 4.3. The corresponding trellis of the code is shown in Fig. 4.27. It can easily be seen that the squared Free Euclidean distance is 4 as in the TC 8-PSK.

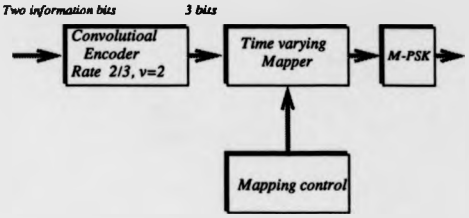

Figure 4.26: General block diagram for hybrid TC 8/4-PSK

Mapping Rules		
Encoder's output	TC 8-PSK	4-PSK
000	0	0
001	7	0
010	1	2
011	2	2
100	4	4
101	3	4
110	5	6
111	6	6

Table 4.4: The mapping rules for hybrid TC 8/4-PSK

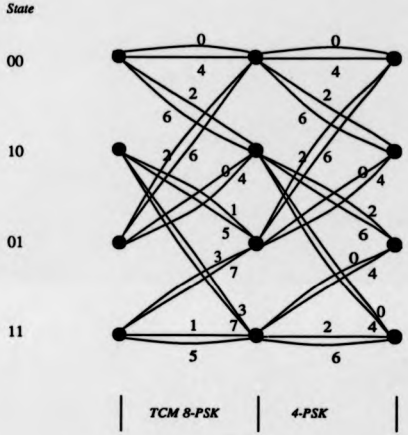

Figure 4.27: The trellis of the hybrid TC 8/4-PSK

4.6.2 A receiver structure for the hybrid TC 8/4-PSK signal in frequency selective Rayleigh fading channel

In this section, a receiver structure for recovering the hybrid TC 8/4-PSK signals in the presence of frequency selective Rayleigh channel is proposed.

The proposed receiver structure is the same as the receiver structure proposed for TC 8-PSK (see Fig.4.22). The only difference is that the Viterbi Algorithm, which is used to decode the TC 8-PSK signal, considers the two mapping rules.

Decoding is accomplished as follows: During the first (odd-numbered) symbol time interval, the received noisy signal is compared with the corresponding components of the two possible signals (the two parallel signals) at each of the 8 possible branches (See Fig. 4.27). There are 8 possible symbols for this time interval. The symbol closest to the received signal is determined. In other words, a hard decision is made on the signal of each branch. The error distances between the received signal and the four possible signals in each branch are compared and the signal with the smallest error distance is chosen. These signals are stored together with their squared error distances from the received signal. After a hard decision is made, there remain two possible signals leading to each of the four states in the trellis diagram. From the two signals leading to each of the four states, the one which gives less overall accumulated error distance is chosen and stored in a memory.

During the second (even-numbered) symbol time interval, the received noisy signal is compared with the corresponding components of the two possible signals (the two parallel signals) at each of the 8 possible branches (See Fig. 4.27). The same computation made during the first symbol time interval is required again. The only difference is that the total number of the symbol to be compared with is only four.

When the length of the trellis (or observation length) reaches the decision depth, a hard decision is made as to the oldest symbol in memory, which is then converted to a 2-bit message.

The feedforward and feedback sections of the VDFE are used to remove the channel intersymbol interference.

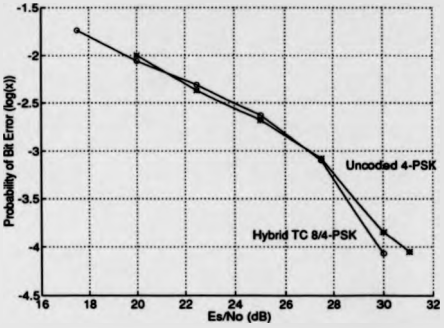

Figure 4.28: The BER performance of hybrid TC 8/4-PSK scheme in a FSRF channel.

4.6.3 The BER performance of this system in a FSRF channel

In this section the BER performance of hybrid TC 8/4-PSK scheme is studied in a FSRF channel with AWGN through computer simulations. The complete transmission system has been simulated. For comparison reasons, the BER performance of uncoded 4-PSK scheme is also studied.

The results of our simulation for both hybrid TC 8/4-PSK and uncoded 4-PSK schemes are given in Fig.4.28. As is observed, the coding gain of this scheme for bit error probabilities in the area of 10^{-3}, which is important in digital speech transmission, is negligible (almost 0). But for the error probabilities of 10^{-4}, the hybrid coded scheme has 1 dB better performance than the uncoded scheme.

For comparison, the BER performance of TC 8-PSK and hybrid TC 8/4-PSK systems are illustrated in Fig.4.29. As shown in this figure, for BER larger than $10^{-2.7}$ the hybrid TC 8/4-PSK has better performance. But for BER smaller than $10^{-2.7}$ the TC 8-PSK has better performance. In the area of 10^{-3}, the TC 8-PSK scheme has approximately 0.4 dB better performance than the hybrid TC 8/4-PSK scheme.

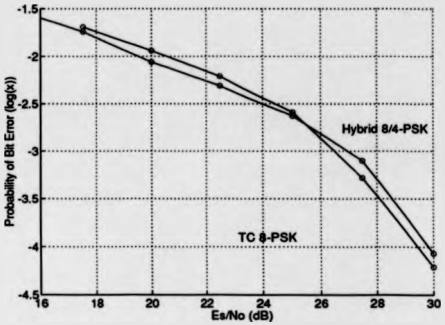

Figure 4.29: The BER performance comparison between TC 8-PSK and hybrid TC 8/4-PSK in a FSRF channel.

4.7 Conclusion

Trellis-coded modulation (TCM) proposed by Ungerboeck, which is a combination of coding and modulation technique for digital transmission over band-limited additive white Gaussian noise (AWGN) channels, has been shown that it can provide coding gains of 3-6 dB relative to an uncoded scheme with the same spectral efficiency.

In this study, Ungerboeck's 4-state rate 2/3 8-PSK TCM scheme, which has a theoretical 3dB coding gain in AWGN channels, has been examined. To prove the theoretical results, first the BER performance of this scheme is found through a computer simulation. The main conclusion concerning these results is that a significant gain can be achieved by trellis coding modulation in the presence of AWGN. For error probabilities of 10^{-2} or less, the trellis coded scheme has better performance than the uncoded scheme. The coding gain for bit error probabilities in the area of 10^{-3}, which is important in digital speech transmission, is about 1.5 dB. For error probabilities less than 10^{-3}, a gain increase is observed. For high S/N ratio this amount seems to reach the 2 dB coding gain. It is observed that the simulation result is roughly 1 dB poorer than the expected (theoretical)

coding gain.

However, there were still open questions concerning coding gains under the time invariant intersymbol interference (ISI) and frequency selective Rayleigh fading channels. In this study, Ungerboeck's 4-state rate 2/3 TC 8-PSK scheme has been proposed for ISI and frequency selective Rayleigh fading channels. Receiver structures, to recover the data corrupted by these channels, have been presented. For time invariant ISI channel three types of equalisers have been examined. Two of them are the known algorithms: Linear feedback and decision feedback equaliser. The third algorithm is the proposed algorithm called Viterbi decision feedback equaliser (VDFE) which is studied in details in Section 4.4.3.

To evaluate and compare the performance of these three algorithms, computer simulations have been executed for an time invariant ISI channel, namely telephone channel 2. For frequency selective Rayleigh fading channel (studied in Chapter 3) a receiver structure which is based on the VDFE, has proposed and presented. The bit error rate (BER) performance of the system under this channel has been found.The results for LFE show that the coding gain of this code for bit error probabilities in the area of 10^{-3}, which is important in digital speech transmission, is about 0.25 dB. The results for DFE show that the TC 8-PSK scheme has no advantage (or very small) over the uncoded counterpart (uncoded 4-PSK). Such disappointing results can be expected though as the detector in the DFE makes hard decisions on the received signals and hence the potential benefit offered by trellis coding is lost. The algorithm VDFE was shown to be better than the other two algorithms. The results show that using this algorithm, TC 8-PSK signal can be received with 1.6 dB lower S/N, when compared with uncoded 4-PSK scheme, for the BER in the range of 10^{-3}. The VDFE shows superior performance when compared to conventional hard-decision demodulation. It has remarkably good performance when compared with the other two, it has approximately 3 dB better performance for bit error probabilities in the area of 10^{-3}.

Ungerboeck's 4-state rate 2/3 TC 8-PSK scheme has also been examined in the presence of a FSRF channel. A receiver structure based on VDFE has been proposed. The complete transmission system has been simulated. The results of our simulation for TC 8-PSK show that the coding gain of this scheme, for bit error probabilities in the area of 10^{-3} is about

0.5 dB. With high S/N ratios, 1.5 dB coding gain is achievable.

A modulation scheme called Hybrid trellis-coded 8/4 PSK presented by Sundberg for phase jitter, which combines the TC 8-PSK and the uncoded 4-PSK, has been studied under the frequency selective Rayleigh fading. The BER performance has been found for this scheme also. The results of computer simulations for hybrid TC 8/4-PSK show that the coding gain of this scheme, for bit error probabilities in the area of 10^{-3}, which is important in digital speech transmission, is negligible. While the hybrid TC 8/4-PSK has better performance for the cases where BER is larger than $10^{-2.7}$, the TC 8-PSK becomes better for BER is smaller than $10^{-2.7}$. In the area of 10^{-3}, the TC 8-PSK scheme has approximately 0.4 dB better performance than the hybrid TC 8/4-PSK scheme. In conclusion, no significant advantage of hybrid TC 8/4-PSK over TC 8-PSK has been observed.

CHAPTER 5

THE ANALYSIS OF PARTIAL RESPONSE DPM SIGNALS AND A RECEIVER STRUCTURE FOR THESE SIGNALS IN A MOBILE RADIO CHANNEL

5.1 Introduction

Modulation schemes such as band limited M-ary PSK are usually used due to their high spectral and power efficiencies. However, the rf envelope of the modulated carrier is not constant and, if a non-linear amplifier is used in the transmitter, the spectral side-lobes of the signal increase due to the non-linear effects of the amplifier. This causes serious adjacent channel interference which increases the error probability. This is unfortunate since, as far as mobile radio is concerned, the available power is limited and this makes it necessary to use a non-linear amplifier. One way to overcome this problem is to use spectrally efficient but constant or low-fluctuation envelope signals, such as continuous phase modulation (CPM) [68] or digitally phase modulated (DPM) signals [13] [60]. Because they have phase shaping before or within the modulator, rather then after the modulator, their rf envelopes are constant and their spectral side-lobes are reduced compared to M-ary PSK. One disadvantage of partial response DPM, mentioned in [60], is that it has a broader main lobe in the power spectrum than partial response CPM. However, as far as implementation is concerned, DPM [13] [60] signals have some advantages over CPM signals. This is because phase modulation is used instead of frequency modulation. Thus carrier recovery needed for coherent modulation is simpler to implement. In demodulator, there is no need for the carrier phase to be accumulated continuously as in the case for CPM. The other advantage of DPM is that it is well suited for VLSI implementation [60] [13]. These advantages of DPM signals motivated a consideration of these signals in mobile radio environments.

In this thesis, the study was restricted to a binary and 4-level partial response DPM

scheme with pulse duration LT, where T is the symbol interval and $L = 3$. In the second Section of this Chapter, general properties such as squared free Euclidean distance (d^2_{min}) and power spectrum of binary and 4-level partial response DPM systems are studied in detail. A fast algorithm developed by Aulin [65] for CPM system has been modified in order to evaluate the free Euclidean distance of binary and 4-level partial response DPM signals.

In [60] these properties have been studied for binary L-SP DPM cases. But the following details were not considered:

- The observation interval (OI) length which gives d^2_{min}. In fact this interval length is the decision depth length of the Viterbi algorithm which is used in the receiver section.
- The case of $M > 2$ is not studied.

In Section 6.2, these are studied. In the third section of this chapter, to recover these signals which are affected by the frequency selectivity of the mobile channel, a receiver structure is proposed and presented. In the fourth section, computer simulations of whole transmission system were performed in order to validate the numerical results found. The bit error rate (BER) performances of binary and 4-level 3-SP DPM under frequency selective Rayleigh fading channel are evaluated through the use of computer simulation. The Chapter is summarised in Section 5.5.

5.2 Some properties of the partial response DPM signals

In this section, general properties such as free Euclidean distance and power spectrum of binary and 4-level partial response DPM systems are studied in detail. The observation interval lengths which give d^2_{min} are studied and evaluated.

5.2.1 Free Euclidean distance and upper bounds on free Euclidean distance

In mobile cellular radio systems, the total power which can be transmitted from the base station is limited [69]. Because of this restriction it is of vital importance that the transmitted information is detected with as low an error probability as possible at the receiver end with a given SNR [13] [68].

As the error probability of a system is a function of d^2_{min} in the presence of additive white Gaussian noise (AWGN), d^2_{min} is the one parameter which simplifies the search for reliable data communication systems. In other words, d^2_{min} is the appropriate criterion of the error probability [72] [73] [76]. Throughout the study it is assumed that this parameter is also a criterion of the error probability in the presence of frequency selective Rayleigh fading channels, though it is not the only appropriate criterion. This will be proved in the forthcoming sections. The free Euclidean distance for DPM is the smallest distance between all possible pairs of signals where the phase trajectories of these signals differ only over a finite interval of time. The distance between two DPM signals $S_m(t)$ and $S_{m'}(t)$ over the interval $[(n-1)T_s, nT_s]$ can be derived. Recalling the form of DPM signals from Chapter 2:

$$S_m(t) = \sqrt{2E_s/T_s}cos(w_c(t) + \phi_1(t))$$

$$S_{m'}(t) = \sqrt{2E_s/T_s}cos(w_c(t) + \phi_2(t))$$

Where $\phi_n(t)$ is the time varying phase of the DPM signal. $n = 1, 2, \ldots$. According to the definition of the distance given in equation (2.1) and assuming w_c is much greater then $1/T_s$, then

$$\begin{aligned} D^2_{m,m'}(S_m(t), S_{m'}(t)) &= \int_{(n-1)T_s}^{nT_s} [S_m(t) - S_{m'}(t)]^2 dt \\ &= \int_{(n-1)T_s}^{nT_s} S^2_m(t)dt + \int_{(n-1)T_s}^{nT_s} S^2_{m'}(t)dt \\ &\quad -2\int_{(n-1)T_s}^{nT_s} S_m(t)S_{m'}(t)dt \\ &= E_s + E_s - 2\int_{(n-1)T_s}^{nT_s} cos(w_c t + \phi_m(t))cos(w_c t + \phi_{m'}(t))dt \\ &= 2E_s - 2E_s/T_s 2\int_{(n-1)T_s}^{nT_s} 1/2[cos(2w_c t + \phi_m(t) + \phi_{m'}(t)) \\ &\quad + cos(\phi_m(t) - \phi_{m'}(t))]dt \end{aligned}$$

$$= 2E_s - 2E_s/T_s \int_{(n-1)T_s}^{nT_s} cos(2w_c t + \phi_m(t) + \phi_{m'}(t))dt$$

$$-2E_s/T_s \int_{(n-1)T_s}^{nT_s} cos(\phi_m(t) - \phi_{m'}(t))dt$$

(5.1)

The first integral is negligible relative to the second integral (when the carrier frequency w_c is much greater than $1/T_s$, giving

$$D^2_{m,m'}(S_m(t), S_{m'}(t)) = 2E_s(1 - 1/T_s) \int_{(n-1)T_s}^{nT_s} cos(\phi_m(t) - \phi_{m'}(t))dt$$

$$= 2E_s/T_s \int_{(n-1)T_s}^{nT_s} (1 - cos\Delta\phi(t))dt \quad (5.2)$$

where

$$\Delta\phi(t) = \phi_m(t) - \phi_{m'}(t) \quad (5.3)$$

The squared Euclidean distance normalised by bit energy is [65] [66] [68]:

$$d^2_{m,m'} = D^2_{m,m'}/2E_b \quad (5.4)$$

where E_b is the bit energy. The normalisation of the Euclidean distance is necessary for the comparison of systems having different M's.

Using equation (5.2), equation (5.4) becomes:

$$d^2_{m,m'} = \log_2 M/T_s \int_{(n-1)T_s}^{nT_s} (1 - cos\Delta\phi(t))dt = 2\log_2 M/T_s \int_{(n-1)T_s}^{nT_s} sin^2[\Delta\phi(t)/2]dt \quad (5.5)$$

where $E_s = E_b \log_2 M$.

The squared Euclidean distance, the distance between two signals, normalised by bit energy for partial response DPM system is:

$$d^2_{m,m'} = \log_2 M 2\eta^{-1} \sum_{n=0}^{N_T} \sin^2 \left(1/2 \sum_{i=\lfloor (n-K-1)/\eta \rfloor}^{\lfloor n/\eta \rfloor} \gamma_{mm',i} q_{n-i\eta} \right) \tag{5.6}$$

where N_T is the length of the observation interval, $\lfloor x \rfloor$ denotes the integer part of x, and $\gamma_{mm',i}$ are the difference sequences between two data sequences which are:

$$\gamma_{mm',i} = (a_{m,i} - a_{m',i}) \tag{5.7}$$

where q_n are the filter coefficients, and η is the integer between the signalling interval T and the duration D of each element in the digital filter, and is known as the oversampling ratio.

To calculate d^2_{min} the difference sequences should be in the form:

$$\begin{aligned} \gamma_i &= 0, && for \quad i < 0 \\ \gamma_0 &= \pm 2, \pm 4, \pm 6 \ldots 2(M-1), && \\ \gamma_i &= 0, \pm 2, \pm 4, \pm 6 \ldots 2(M-1), && for \quad i = 1, 2 \ldots N_T - 1 \end{aligned} \tag{5.8}$$

The first symbol of difference sequences for time instant $i = 0$ must not be zero [68]. That is the condition of a merge. As the cosine function is an even function, it is sufficient to consider just the positive part of the first symbol in the difference sequences. To find the free Euclidean distance the observation interval length should be infinitely long. The Euclidean distance corresponding to all phase trajectories over an infinitely long N_T symbol interval is first found according to equation 5.6. The distance corresponding to the one having the smallest distance is taken as the free Euclidean distance. To find the upper bound on d^2_{min}, just a few pairs of infinitely long sequences can be considered over observation interval length N_T. Suitable candidates for these infinitely long pairs are the pairs that diverge at the same stage and merge as soon as possible after one time interval. The time instant they first merge will be called N_i. At the time intervals after N_i they have the same phase. Such merges certainly occur. It is easy to consider this kind of pairs, because the observation interval length is now finite. There is no need to consider the time instants after N_i, at which the difference between pairs are always zero. It means

no effect on changing the Euclidean distance.

For partial response DPM signals, the first time instant for these two pairs to merge is $t = LT_s$. This is known as the first merge. At $t = (L+1)T_s$ the second merge may occur. For L-SP DPM the upper bound of the free Euclidean distance does not decrease significantly as the number of merges extends above L. For the case of 3-SP DPM, three merges were considered. For the first merge, the corresponding normalised Euclidean distances for different sequence pairs are computed and the one giving the minimum value is recorded. The same computations were carried out for the second and third merge. Next, the minimum value of these three values is chosen as an upper bound on the minimum Euclidean distance (free Euclidean distance), for given modulation indices (h). In the following two sections the upper bounds on the minimum Euclidean distance are derived for binary and 4-level 3-SP DPM using techniques in [64], [65], [72], [73].

Finding the upper bounds for binary 3-SP DPM

The difference sequences to obtain the first three merges have been found. If l is the time interval, then the first, second and the third merges can be obtained when the differences are:

For the first merge:

$$\gamma_i = \begin{cases} 0, & \text{if } i < 0 \\ 2, & \text{if } i = 0 \\ 0, & \text{if } i = 1 \\ -2, & \text{if } i = 2 \\ 0, & \text{if } i > 2 \end{cases}$$

First the squared Euclidean distances corresponding to these difference sequences above are found, by using equation (5.6). The one having minimum distance is chosen as an upper bound for the first merge and stored in memory. This has been done for all modulation indices between 0.05 and 1.45 in steps of 0.05.

For the second merge:

$$\gamma_i = \begin{cases} 0, & \text{if } i < 0 \\ 2, & \text{if } i = 0 \\ \alpha, & \text{if } i = 1 \\ 0, & \text{if } i = 2 \\ -\alpha, & \text{if } i = 3 \\ 0, & \text{if } i > 3 \end{cases}$$

where $\alpha \in \{0, \pm 2\}$.

For the third merge:

$$\gamma_i = \begin{cases} 0, & \text{if } i < 0 \\ 2, & \text{if } i = 0 \\ \alpha, & \text{if } i = 1 \\ 0, & \text{if } i = 2 \\ 0, & \text{if } i = 3 \\ 0, & \text{if } i = 4 \\ 0, & \text{if } i > 4 \end{cases}$$

where $\alpha \in \{0, \pm 2\}$.

$$\gamma_i = \begin{cases} 0, & \text{if } i < 0 \\ 2, & \text{if } i = 0 \\ 0, & \text{if } i = 1 \\ \beta, & \text{if } i = 2 \\ 0, & \text{if } i = 3 \\ -\beta, & \text{if } i = 4 \\ 0, & \text{if } i > 4 \end{cases}$$

where $\beta \in \{\pm 2\}$.

The upper bounds for the second and third merges are also found and stored in memory. The minimum of these three values is chosen as an upper bound on d^2_{min} for given

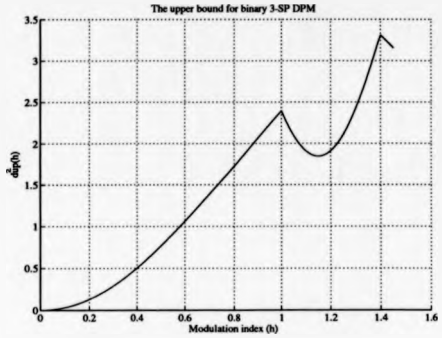

Figure 5.1: The upper bound on d^2_{min} for binary 3-SP DPM

modulation indices. Even the Euclidean distance is a non-decreasing function of the observation interval [64][65]; for some modulation indices, the Euclidean distance, corresponding to higher merges, might be smaller then the Euclidean distance corresponding to lower merges. That is the reason for considering more than one merge. In Fig. 5.1 the normalized upper bounds on d^2_{min} are shown for different h values. These can be seen in Table 5.1 as well.

Finding the upper bounds for 4-level 3-SP DPM

The difference sequences to obtain these merges have been evaluated. If i is the time interval, then the first merge can be obtained when the difference sequences are:

$$\gamma_i = \begin{cases} 0, & \text{if} \quad i < 0 \\ \alpha, & \text{if} \quad i = 0 \\ 0, & \text{if} \quad i = 1 \\ -\alpha, & \text{if} \quad i = 2 \\ 0, & \text{if} \quad i > 2 \end{cases}$$

where $\alpha \in \{2,4,6\}$.

The second merge can be obtained when the difference sequences are:

$$\gamma_i = \begin{cases} 0, & \text{if } i < 0 \\ 2,4,6 & \text{if } i = 0 \\ \alpha, & \text{if } i = 1 \\ 0, & \text{if } i = 2 \\ -\alpha, & \text{if } i = 3 \\ 0, & \text{if } i > 3 \end{cases}$$

where $\alpha \in \{0,2,4,6\}$.

The third merge can be obtained when the difference sequences are:

$$\gamma_i = \begin{cases} 0, & \text{if } i < 0 \\ 2,4,6 & \text{if } i = 0 \\ \beta, & \text{if } i = 1 \\ \alpha, & \text{if } i = 2 \\ 0, & \text{if } i = 3 \\ -\alpha, & \text{if } i = 4 \\ 0, & \text{if } i > 4 \end{cases}$$

where $\alpha \in \{0,2,4,6\}$ and $\beta \in \{\pm 2, \pm 4, \pm 6\}$.

As for the binary case, using equation (5.6), the squared Euclidean distances corresponding to difference sequences are first derived for the first merge above. The distance having the minimum value is chosen as an upper bound for the first merge, as a function of the modulation indices. Then the computation is made for the second and third merges. The smallest value of these three values is chosen as an upper bound on the minimum Euclidean distance for different h values. In fig. 5.2 the normalized upper bounds on d^2_{min}

	Binary 3-SP DPM	*4-level 3-SP DPM*
h	$d^2_{up}(h)$	$d_{up}(h)^2$
0.05	0.008	0.037
0.10	0.033	0.148
0.15	0.074	0.330
0.20	0.131	0.579
0.25	0.203	0.891
0.30	0.290	1.257
0.35	0.390	1.671
0.40	0.503	2.123
0.45	0.628	2.431
0.50	0.764	1.925
0.55	0.909	1.544
0.60	1.061	0.866
0.65	1.221	0.893
0.70	1.385	1.016
0.75	1.553	1.925
0.80	1.723	1.024
0.85	1.893	0.607
0.90	2.063	0.532
0.95	2.230	0.920
1.00	2.394	0.835
1.05	2.100	1.133
1.10	1.912	1.943
1.15	1.846	1.103
1.20	1.912	0.478
1.25	2.109	0.928
1.30	2.424	0.185
1.35	2.838	0.858
1.40	3.309	2.180
1.45	3.153	2.057

Table 5.1: Upper bounds on $d^2_{min}(h)$ for uncoded binary and 4-level 3-SP DPM.

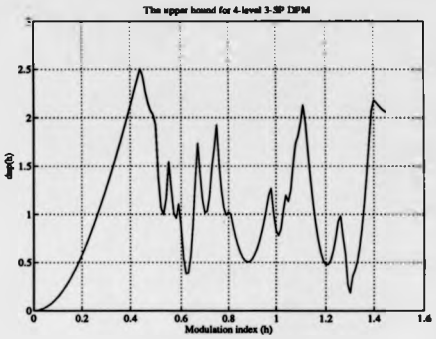

Figure 5.2: The upper bound on d^2_{min} for 4-level 3-SP DPM

are shown for different modulation indices, and M=4. These also can be seen in Table 5.1.

A modified algorithm to compute the free Euclidean distances

An algorithm developed by Aulin [64] [65] has been modified in order to evaluate d^2_{min} of partial response DPM signals. Using this algorithm, the growth of the Euclidean distance with incremental observation interval length is observed.

The squared Euclidean distances for DPM signals are additive, as for a CPM system [65]. That means when the Euclidean distance is calculated for the N th observation interval (OI), the Euclidean distance for the $(N+1)$ th observation interval is the Euclidean distance corresponding to the N th symbol interval, plus the distance for the last time interval. That is clear from the expression of the normalized squared Euclidean distance which is:

$$d^2_{m,m'}(\alpha_N, h) = \log_2 M 2 \sum_{n=0}^{N-1} \sin^2 \left(1/2 \sum_{i=(n-L-1)}^{n} \gamma_i \varphi_{n-i} \right)$$

where

$$d^2_{m,m'}(a_{N+1},h) = d^2_{m,m'}(a_N,h) + \log_2 M 2 \sum_{n=N}^{N+1} \sin^2\left(1/2 \sum_{i=(n-L+1)}^{N} \gamma_i q_{N-i}\right)$$

To calculate d^2_{min} in a conventional method, $(M-1)(2M-1)^{N-1}$ difference sequences should be considered [64] [65]. It is seen that when the observation interval length grows the number of calculations required grows exponentially. The algorithm developed by Aulin [64] [65] deals with this problem. The required number of calculations grows linearly with N.

The basic principle of the algorithm is not to consider all the difference sequences defined by equation (5.8). The idea is to compare the Euclidean distance corresponding to the first OI length with the upper bound for a given value of h. If the calculated distance is larger than $d^2_{up}(h)$ then this first value of the difference sequnce will never be used again [65]. In other words any subtree having this value as a first value will never be considered again when finding the Euclidean distance for the next observation interval. The Euclidean distance for the next OI length will be calculated using $\gamma_0, \gamma_1 \cdots \gamma_{OI-1}$ values whose corresponding distances do not exceed the upper bound. The subtrees are continuously deleted up to the maximum observation interval length (OI_{max}).

The flowchart for this algorithm is illustated in Fig. 5.3.

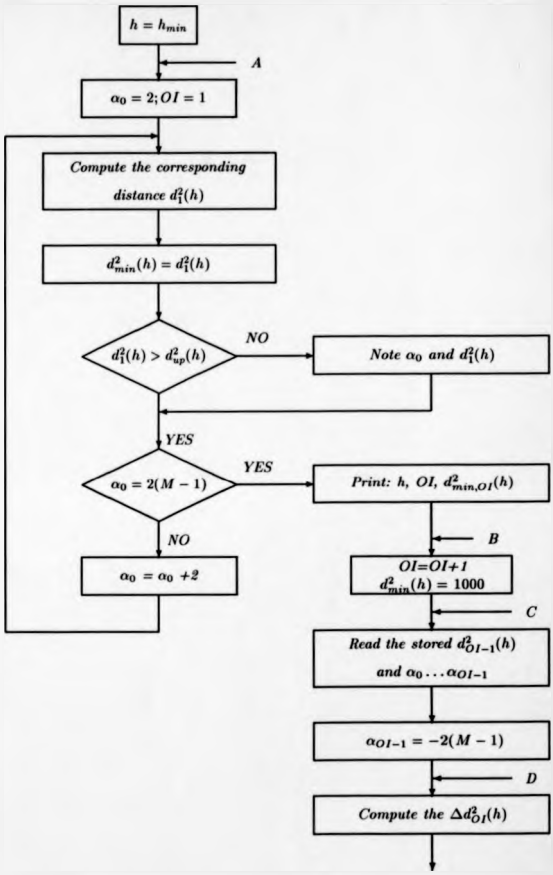

Figure 5.3a:The flowchart of the algorithm used to find $d_{min}^2(h)$

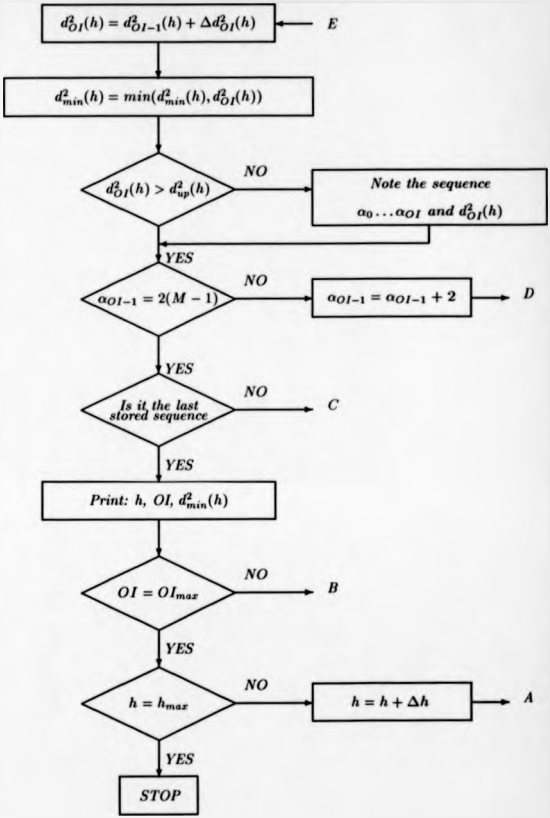

Figure 5.3b:Continued from Fig.5.3a

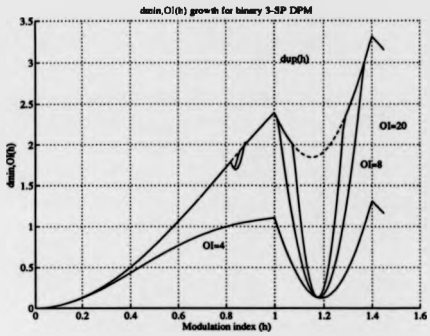

Figure 5.4: The growth of Euclidean distance with observation interval length for binary 3-SP DPM

The numerical results on free Euclidean distance

In this part of the thesis, the free Euclidean distances for partial responce 3-SP DPM signals have been evaluated using the computer simulated algorithm. The computations have been performed for binary and 4-level cases, varying the modulation index h from 0.05 to 1.45, in steps of 0.05. Meanwhile the study is carried out to observe how the Euclidean distance grows with the observation interval length (OI). The OI lengths which give the free Euclidean distances are also found. Table 5.2 shows the values of d^2_{min} and corresponding observation interval lengths for binary and 4-level 3-SP DPM. The '*' shown in this Table means that d^2_{min} corresponding to this OI length is not the upper bound. If the OI length is increased it might reach the upper bound.

Fig. 5.4 shows the growth of normalized squared Euclidean distances for binary 3-SP DPM and given h values. The upper bound on d^2_{min} is shown with dashed line. As is seen in Fig. 5.4, the normalized squared Euclidean distance corresponding to OI=4 is poor for

	Binary 3-SP DPM		*4-level 3-SP DPM*	
h	d^2_{min}	OI Length	d^2_{min}	OI Length
0.05	0.008	3	0.037	3
0.10	0.033	3	0.148	8
0.15	0.074	6	0.330	8
0.20	0.131	6	0.579	8
0.25	0.203	6	0.891	15
0.30	0.290	6	1.257	35
0.35	0.390	6	0.676	*40
0.40	0.503	6	1.123	*40
0.45	0.628	6	1.342	*40
0.50	0.764	6	1.563	*40
0.55	0.909	6	1.544	40
0.60	1.061	6	0.866	8
0.65	1.221	8	0.893	8
0.70	1.385	8	1.016	14
0.75	1.553	8	1.925	35
0.80	1.723	8	0.874	*40
0.85	1.893	25	0.230	*40
0.90	2.063	8	0.532	30
0.95	2.230	8	0.920	8
1.00	2.394	8	0.835	8
1.05	2.100	15	1.133	40
1.10	1.912	40	1.943	40
1.15	0.374	*50	1.103	40
1.20	0.488	*50	0.478	2
1.25	2.109	40	0.928	8
1.30	2.424	20	0.185	12
1.35	2.838	15	0.858	40
1.40	3.309	8	2.180	30
1.45	3.153	8	2.057	30

Table 5.2: d^2_{min} and corresponding observation interval lengths for binary and 4-level 3-SP DPM.

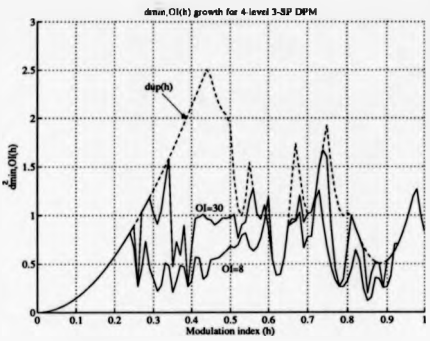

Figure 5.5: The growth of Euclidean distance with obsevation interval length for 4-level 3-SP DPM

almost all modulation indices. But increasing the OI length to 8 increases this distance significantly. It reaches the upper bound for almost every modulation index, except in the region $1 < h < 1.35$. For the OI length equal to 20, this region becomes narrower. For $h = 1.17$, increasing the OI length does not have the effect of increasing the Euclidean distance. When this happens the modulation index is called a weak modulation index. It occurs when [60]

$$\sum_{i=0}^{N-1} d_i = n\pi \qquad n = 1, 2, 3 \ldots$$

where d_i is as in Equation 2.28

Fig. 5.5 shows the growth of the Euclidean distance with the observation interval length for 4-level 3-SP DPM signals. For some modulation indices the upper bound cannot be reached. These are, $0.35 \leq h \leq 0.50$ and $h = 0.80, 0.85$.

For the binary 3-SP DPM system, the maximum value of the minimum Euclidean distance is 3.309 when $h = 1.40$ and $OI = 8$. For small modulation indices, the OI lengths which reach the upper bounds (d^2_{up}) are smaller then OI lengths which are needed to reach the upper bounds for high modulation indices, except for a few modulation indices. For ex-

ample, the case of $h = 0.85$. The upper bounds on free Euclidean distance are not reached for some modulation indices and for a given finite number of observation intervals. These are $h = 1.15$ and 1.20, and OI=50. The upper bounds corresponding to these modulation indices are 1.846 and 1.912 (see Table 5.1), but the corresponding free Euclidean distances are 0.374 and 0.488 (see Table 5.2), respectively. If the OI length is increased then the normalized squared Euclidean distances might increase. OI lengths of more than 50 are not considered.

For the 4-level 3-SP DPM system, the maximum value of the minimum Euclidean distance is 2.180 when $h = 1.40$ and $OI = 30$. This can be seen from Table 5.2. The upper bounds on free Euclidean distance are not reached for some modulation indices and for a given finite number of observation intervals. These are $h = 0.35, 0.40, 045, 0.50, 0.80$ *and* 0.85, and $OI = 40$. The upper bounds corresponding to these modulation indices are 1.671, 2.123, 2.431, 1.925, 1.024, and 0.607 but the free Euclidean distances obtained are 0.676, 1.123, 1.342, 1.563, 0.874, and 0.230, respectively. If the OI length is increased then the Euclidean distances increase. The OI lengths of more than 40 is not considered. For some modulation indices the OI lengths which reach the upper bounds are extremely large. These are $h = 0.30$, 0.55 and the h values between 1.05 and 1.15. These modulation indices must be avoided.

The main conclusion concerning these results is that, for both binary and 4-level 3-SP DPM, increasing the observation interval length increases d^2_{min} except for weak modulation indices. Moreover, increasing the modulation index up to a certain value also increases d^2_{min}; however the required OI length increases. This can be seen from Table 5.2. Corresponding to modulation indices between $0.05 \leq h \leq 0.55$ for the 4-level case, $d^2_{min}(h)$ is larger then $d^2_{min}(h)$ for the binary case. But as it can be seen from Table 5.2 the required OI lengths are larger too.

5.2.2 Power spectral density and bandwidth

The most important parameter to consider apart from the minimum Euclidean distance is the power spectral density of the signal [68][74]. The power spectra of partial response DPM signals can be obtained by numerical calculations using formulae in [60]. The com-

puter calculations are performed for binary and 4-level 3-SP DPM and given h values.

The power spectrum is the Fourier transform of the autocorrelation function of 3-SP DPM signal, which is [60]:

$$R_n = \eta^{-1} \sum_{p=0}^{\eta-1} \prod_{i=0}^{[(K+n)/\eta]} \prod_{l=0}^{\log_2(M)-1} cos(2^l(q_{p+i\eta} - q_{p+i\eta-n})) \tag{5.9}$$

where the symbol $\lfloor X \rfloor$ denotes the integer part of X. $q_i = 0, \quad if \quad i \in [0, 1 \ldots, (K-1)]$. The oversampling ratio η is chosen to be 8. In other words, the complex envelope $e^{j\phi(t,\alpha)}$ has been sampled eight times per symbol interval, and $K = 24$.
The autocorrelation values corresponding to $n \geq K$ will be [60]:

$$R_{K+m} = R_{K+m+i\eta} \tag{5.10}$$

where $m, i \geq 0$.

That means R_K is periodic for multiples of η. This causes spectral lines at multiple frequencies of the symbol rate [60]. Thus the power spectrum of DPM signal consists of two parts: a continuous and a discrete part. In the thesis the continuous part of the spectrum is considered, which is:

$$S_c(w) = -R_0 + R_{J\eta} + 2\sum_{p=0}^{\eta-1}\sum_{n=0}^{J}(R_{p+n\eta} - R_{p+Jn})cos[(R_{p+n\eta})Dw] \tag{5.11}$$

where $J = [K/\eta] = 3$.
The power spectrum of partial response DPM signal is:

$$S(w) = D[sin(Dw/2)/(Dw/2)]^2 S_c(w) \tag{5.12}$$

Fig. 5.6 and Fig. 5.7 show the power spectra of binary and 4-level 3-SP DPM systems corresponding to certain modulation indices. The frequency is normalised with bit rate

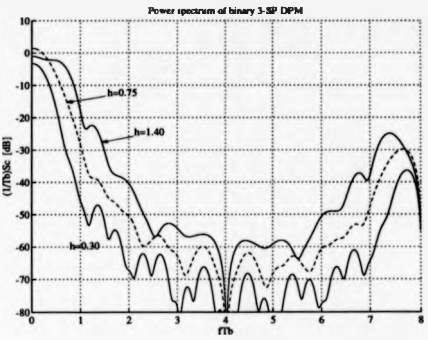

Figure 5.6: Power spectrum of binary 3-SP DPM signal

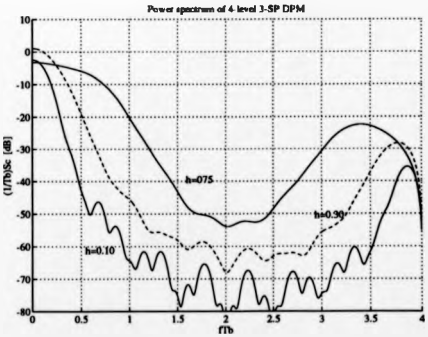

Figure 5.7: Power spectrum of 4-level 3-SP DPM signal

$1/T_b$, where $T_s = T_b \log_2(M)$. As it is seen in these figures, the main lobe and sidelobes of the power spectrum get broader by increasing the modulation index.

To reduce the amount of the sidelobes, a large value of η and K must be chosen [60].

The bandwidth

The bandwidth is defined as the range of frequencies containing some fixed percentage of the total signal power. This percentage will be 99% in this thesis. The normalised bandwidth ($B_{99}T_b$) contains 99% of the total power.

The bandwidth for binary and 4-level 3-SP DPM schemes are given in Table 5.3. It is obvious that the required bandwidth is dependent on the modulation index. Increasing the modulation index increases the bandwidth of the signal. Thus for 4-level case, the required bandwidth for modulation indices larger than 0.65 are not evaluated. The values η and K can effect the bandwidth as well. Larger values of η and K can reduce the required bandwidth [60].
For small modulation indices, the required bandwidth for a 4-level 3-SP DPM signal is smaller than for a binary 3-SP DPM signal.

5.3 A receiver structure for 3-SP DPM signals in mobile radio channel

In this section, a receiver structure is described for demodulating partial response DPM signals in the presence of frequency selective Rayleigh channel .

The receiver, shown in Fig.5.8, consists of two principal components:

1. An integration of the optimum coherent maximum likelihood sequence estimator (MLSE), which is called the optimum Viterbi algorithm, with a decision feedback equaliser.
2. A channel estimator.

Optimum Viterbi Algorithm: The maximum likelihood sequence estimation algorithm principally correlates all possible data sequences which could have been transmitted with received data sequences at every symbol time interval. It is done by computation of a

	Binary 3-SP DPM	*4-level 3-SP DPM*
h	$B_{99}T_b$	$B_{99}T_b$
0.05	0.96	0.48
0.10	0.96	0.52
0.15	0.96	0.60
0.20	1.00	0.68
0.25	1.00	0.78
0.30	1.04	0.88
0.35	1.04	1.00
0.40	1.08	1.12
0.45	1.12	1.26
0.50	1.16	1.40
0.55	1.20	1.56
0.60	1.24	1.74
0.65	1.28	2.02
0.70	1.36	
0.75	1.40	
0.80	1.44	
0.85	1.48	
0.90	1.52	
0.95	1.56	
1.00	1.64	
1.05	1.68	
1.10	1.72	
1.15	1.72	
1.20	1.76	
1.25	1.80	
1.30	1.84	
1.35	1.88	
1.40	1.92	
1.45	2.00	

Table 5.3: The normalised bandwidth ($B_{99}T_b$) for binary and 4-level 3-SP DPM signals

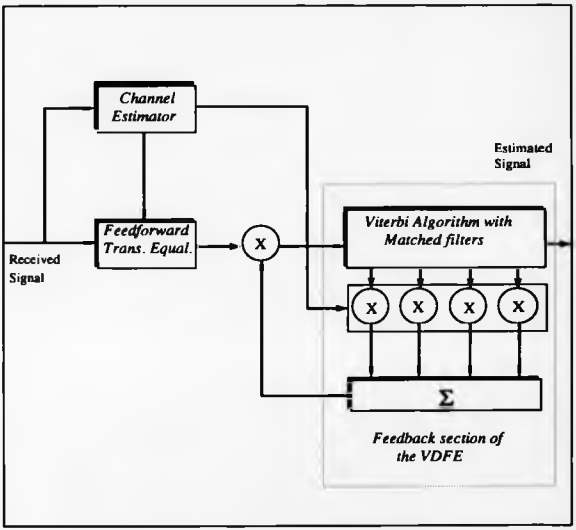

Figure 5.8: The receiver structure of partial response DPM signals

weighting parameter, called the metric, and then selecting the sequence having the highest metric [72] [74].

The Viterbi algorithm with M^L matched filters is shown in Fig. 5.9. The outputs of these filters are sampled once every symbol interval. The metrics or, in other words, the decision variables are computed for MLSE.

The MLSE receiving can be obtained by maximising the log likelihood function [65], which is:

$$\ln(P_r(t)|\alpha') \approx -\int_{-\infty}^{\infty}[r(t)-s(t,\alpha')]^2 dt \tag{5.13}$$

Sequence α' is the maximum likelihood sequence estimate and $(P_r(t)|\alpha')$ is the probability density function for the received signal. The maximisation of equation (5.13) is equivalent to the maximisation of the correlation [68]:

$$J(\alpha') \approx \int_{-\infty}^{\infty} r(t)s(t,\alpha')dt \tag{5.14}$$

This means that each received signal is correlated with all possible transmitted signals. The sequence α' which maximises this equation is chosen first. The oldest symbol of this sequence is chosen as an estimated symbol which is then converted to the message bit. Because equation (5.14) is not a feasible structure in practice this equation is defined [68] as:

$$J_n(\alpha') \approx \int_{-\infty}^{(n+1)T} r(t)s(t,\alpha')dt \tag{5.15}$$

Thus it can be written as:

$$J_n(\alpha') = J_{n-1}(\alpha') + Z_n(\alpha') \tag{5.16}$$

where

$$Z_n(\alpha^i) = \int_{nT}^{(n+1)T} r(t)cos[w_0 t + \phi(t,\alpha^i)]dt \tag{5.17}$$

Metric $Z_n(\alpha^i)$ is the correlation between the received signal and an estimated signal over the n th symbol interval. First the metric $Z_n(\alpha^i)$ is calculated and then added to $J_n(\alpha^i)$ recursively.

If the received signals quadrature components are $I^i(t)$ and $Q^i(t)$ then the equation (5.17) becomes:

$$\begin{aligned} Z_n(\alpha^i) &= \int_{nT}^{(n+1)T} I^i(t)cos[\phi(t,\alpha^i)]dt \\ &+ \int_{nT}^{(n+1)T} Q^i(t)sin[\phi(t,\alpha^i)]dt \end{aligned} \tag{5.18}$$

For DPM signals this is equal to M^L baseband filters with the impulse response:

$$h_{cj}(nD) = \begin{cases} cos(\sum_{i=1}^{L} \alpha_{ij} q((1-i)T - nD)), & \text{for} \quad 0 \le nD \le T \\ 0, & \text{for} \quad nD > T \quad or \quad nD < 0 \end{cases}$$

$$h_{sj}(nD) = \begin{cases} sin(\sum_{i=1}^{L} \alpha_{ij} q((1-i)T - nD)), & \text{for} \quad 0 \le nD \le T \\ 0, & \text{for} \quad nD > T \quad or \quad nD < 0 \end{cases} \tag{5.19}$$

where $j = 1, 2, \ldots M^L$ and $T = \eta$ D

At the output of the filters the following metrics will be produced:

$$1/T \int_0^T cos(\phi(t) - \phi_j(t))dt \tag{5.20}$$

where $\phi(t)$ is the phase of the received signal and $\phi_j(t)$ is the phase corresponding to the filter j. The matched filters can be presented in the way shown in Fig. 5.9.

In the Viterbi algorithm, the sequence that has the largest metrics up to the N_T th symbol interval is selected as the detected sequence. At that time a hard decision is made on a received signal. The total number of states in the Viterbi algorithm is $S = M^{(L-1)}$.

Up to now the section of the receiver involving the Viterbi algorithm is explained. The other section is the equaliser, which is presented in detail in chapter 4. The receiver works as follows: While the Viterbi Algorithm removes the intersymbol interference introduced by the partial response DPM modulator, the feedforward and feedback section of the Viterbi decision feedback equaliser (VDFE) are used to remove the channel intersymbol interference. As shown in Fig.5.8, both parts consist of a finite impulse response filter (FIR), and their respective outputs are added to each other to form the equaliser output before processing by the Viterbi algorithm . The FIR coefficients of the equalisers are computed by the channel estimator (for more details on the channel estimator see Chapter 3) using the training sequence at each time slot.

5.4 Performance studies of the scheme

The total transmission system, as it has been simulated, is shown in Fig. 5.10, of which the receiver concept has already been described in the previous section.

The coefficients of the pulse shaping filter which are used in modulator are chosen according to equation (2.31). For each different modulation index, h, there are different coefficients.

The fading channel in this study has a multipath spread T_M which spans four symbol intervals. The fading channel is modelled by a transversal filter with four taps and a memory of 3 symbols (see Fig.5.11). Each tap in the transversal filter has a Rayleigh distributed magnitude, and a uniformly distributed phase. white Gaussian noise is then added to the output signal of this filter. More details on the mobile channel can be found in chapter 3.

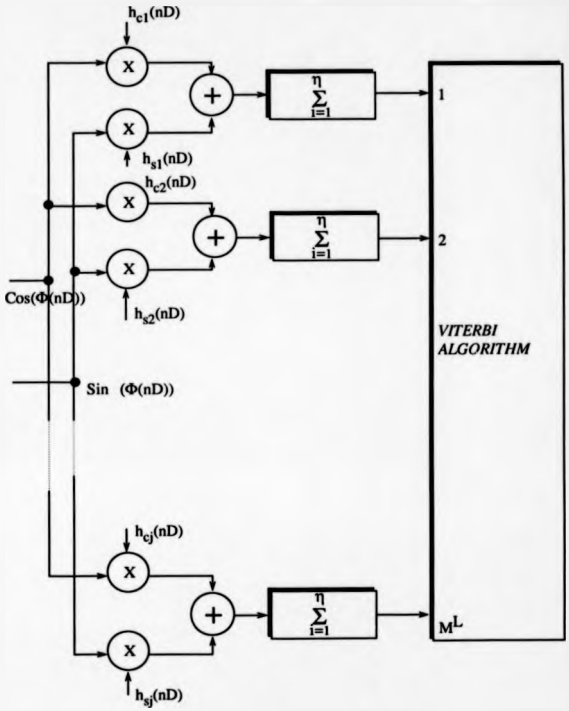

Figure 5.9: Matched filter section of the partial response DPM receiver

Figure 5.10: The block diagram of total simulated system

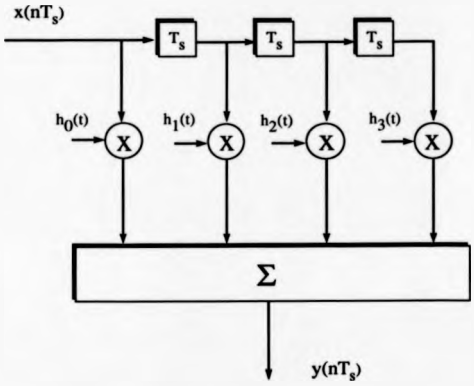

Figure 5.11: The discrete time model of the frequency selective Rayleigh fading channel

The decision depth length of the Viterbi algorithm is the observation interval length which gives d^2_{min} of the combined system. For different combination of modulation index and M-level modulator, the observation interval length which gives d^2_{min} might be different. The OI lengths which give d^2_{min} for both binary and 4-level cases are shown in Table 5.2.

5.4.1 Bit error rate (BER) calculation

The minimum number of bits which must be sent to perform the BER of a system is provided from [75]. This amount depends on the expected BER. In a particular simulation run the required number of bits is 100 times the reciprocal of the error rate [75]. In other words, in order to measure an average probability of bit error as low as 10^{-3}, the required number of transmitted bits must be at least as large as 10^5.

BER calculation for binary 3-SP DPM signals

For binary 3-SP DPM schemes with different modulation indices, the plot of BER vs. S/N under frequency selective Rayleigh fading channel is shown in Fig. 5.12. The cases of h=0.50 and 1.00 are considered. As it can be seen from Table 5.2, the values of d^2_{min} for these modulation indices are 0.764 and 2.394, respectively. As it is seen in Fig 5.12, the BER corresponding to the binary scheme with $h = 1.00$ is lower than the schemes with $h = 0.5$, for all observed signal/noise (S/N) ratios. This means increasing d^2_{min} decreases the BER of the system. Studying the BER of 10^{-3}, which is the acceptable BER amount in speech transmission, shows that, for binary 3-SP DPM, the system with modulation index h=1.00 is more power efficient (about 3.5 dB) than the system with h=0.50.

BER calculation for 4-level 3-SP DPM signals

The variation of BER with S/N ratio under frequency selective Rayleigh fading channel, for 4-level 3-SP DPM schemes with different modulation indices, is shown in Fig. 5.13. The cases of h=0.15, 0.45 and 0.50 are considered. As it can be seen from Table 5.2, the d^2_{min} values for these modulation indices are 0.33, 1.342 and 1.563 respectively. Fig 5.13 shows that, as for the binary case, increasing d^2_{min} decreases the BER of the system. An examination of the BER of $10^{-2.5}$ shows that for 4-level 3-SP DPM system with modulation index h=0.50 is more power efficient (about 6 dB) than the system with h=0.15. The one with modulation index h=0.50 is better than the one with h=0.45 (about 0.3 dB).

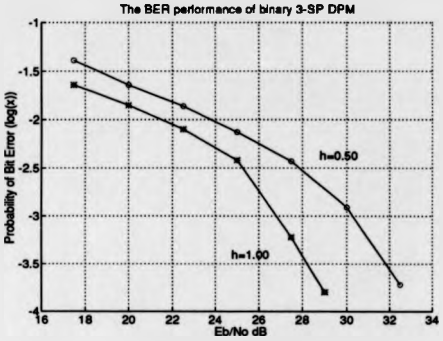

Figure 5.12: The BER performance of binary 3-SP DPM for the FSRF channel

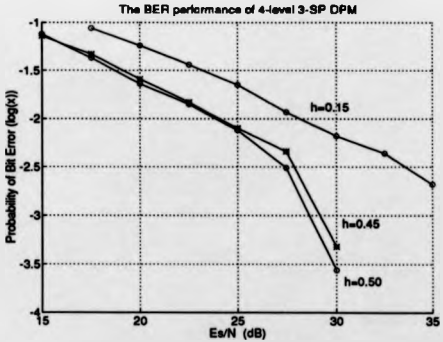

Figure 5.13: The BER performance of 4-level 3-SP DPM for the FSRF channel

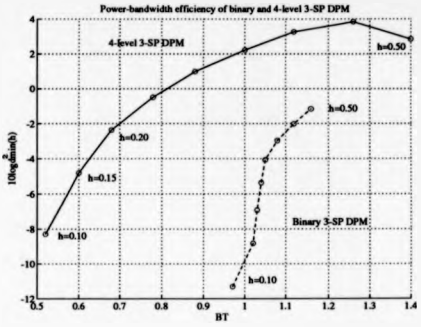

Figure 5.14: The power-bandwidth efficiency of binary and 4-level 3-SP DPM signals

5.5 Conclusion

In this chapter the free Euclidean distance and spectral properties of partial response binary and 4-level 3-SP DPM signals have been analysed. The required bandwidths of these signals have been evaluated for given modulation indices. The power-bandwidth efficiencies of these systems are illustrated in Fig. 5.14.

The free Euclidean distances corresponding to different 3-SP DPM schemes with a different modulation index have been investigated. The observation interval lengths which give d^2_{min} are found. In fact this length is the decision depth length of the Viterbi algorithm which is used in the receiver section. A receiver structure to recover the transmitted data, corrupted by the frequency selectivity Rayleigh fading, is presented. The total transmission systems for both binary and 4-level 3-SP DPM schemes are simulated. The bit error rate (BER) of these schemes is presented.

The results show that increasing the free Euclidean distance of a 3-SP DPM system improves the BER performance. Thus d^2_{min} can be considered as a criterion of power efficiency for 3-SP DPM even under the frequency selective Rayleigh fading channel.

CHAPTER 6

COMBINING CONVOLUTIONAL CODES WITH DPM

6.1 Introduction

Three prevailing requirements in transmission systems are decreasing the power needed for reliable transmission, reducing the required bandwidth and using a modulation technique which is easy to implement. For spectrum conservation, the band occupancy of the chosen modulation scheme has to be small so that as many channels as possible can be transmitted in a given band. In addition to spectral efficiency, the modulation scheme should be power efficient as well. As the available transmitter power is limited, the system should be designed to use its power efficiently. Another criterion to be taken into account in choosing a modulation scheme for mobile systems is the implementation difficulty.

In this Chapter, the effects of the coding in improving the power efficiency of partial response DPM signals are examined. The main interest is to investigate what improvements may be obtained by coding.

A convolutional code is generated by passing the information bit sequence to be transmitted through a linear finite-state shift register. The purpose of the coding is to gain noise immunity, in other words, to minimise the effect of the channel noise. The memory introduced by the encoder in the signals can be used by the receiver to improve the bit error rate.

Over the last ten years two different classes of coding methods related to the bandwidth efficiency have been developed. One of them is the combination of convolutional coding with CPM: Trellis coded CPM, which was proposed by Sundberg [64] [65], Aulin [66], Anderson [77], and Wilson [70]. The other one is Trellis coded modulation (TCM) combined with PSK pioneered by Ungerboeck [27] [28] [29]. CPM is a constant-amplitude

modulation scheme which has a good spectrum efficiency, where there is no need for further filtering. The modulation schemes used with TCM by Ungerboeck are M-ary PSK or M-ary Quadrature phase shift keying (QPSK). These are not constant envelope signals and the spectral efficiency is obtained by post filtering. Because partial response DPM is a constant-amplitude modulation scheme, it is in the first classes mentioned above.

The main interest of this study is to find the best combinations of 1/2 rate convolutional encoder, mapping rule and partial response DPM modulator (binary and 4-level) for given memory length and modulation index. The type of convolutional encoders which are considered are of short constraint lengths. The constraint length (or memory length) v varies from 1 to 3. The binary mapping rule is used for the binary case, and 2 different mapping rules are used for the 4-level case. The modulation index is between $0.05 \leq h \leq 1.20$.

The error probability of a system, in an additive white Gaussian noise channel, is a function of the free squared Euclidean distance d^2_{min} [76] [72] [73]. Since the error probability decreases with the increase of d^2_{min}, the combinations of encoder, mapping rule and modulator, which maximise d^2_{min} are investigated for each memory length and modulation index. As for any state transition along any DPM sequence transmitted there does not exist identical sets of neighbour distances, N_{free}(defined in Chapter 4) are not taken into account. More exact study, as has been suggested in [68] [70] for CPM codes is averaging against all transmitted sequences and finding the minimum distance for each one.

The study is carried out to show how the minimum Euclidean distances grow with the observation interval (OI) length for these combinations. The observation interval lengths for which the free Euclidean distance is reached are found for each of the best combinations. This length is the decision depth length of the MLSE receiver. A small value of OI length is desirable.

In order to validate the outcomes of the results found, computer simulation of the whole transmission system is performed. Receiver structures are proposed and presented to recover these coded signals under the frequency selective Rayleigh fading channel. The bit error rate (BER) performances of coded 4-level 3-SP DPM scheme under a frequency selective Rayleigh fading channel are evaluated through the use of computer simulation.

Section 6.2 presents the system under consideration which consists of a 1/2 convolutional encoder, a mapping rule and a modulator. In Section 6.3 the upper bounds on free Euclidean distance are discussed. An extended algorithm to compute the free Euclidean distances is described in Section 6.4. In Section 6.5 the optimal codes are presented for the case of rate 1/2 convolutional encoder combined with the binary partial response DPM system. Meanwhile the optimal combinations of encoder, mapping rule and 4-level partial response DPM are also presented in the same section. The growth of Euclidean distances with the observation interval length is studied in Section 6.6. Section 6.7 presents the power spectral density and the bandwidth of these coded signals and discusses the power and bandwidth efficiencies of coded 3-SP DPM signals and compares them with those of the uncoded cases. In Section 6.8, to recover these coded signals which are effected by the frequency selectivity of a mobile channel, a receiver structure is proposed and presented. In Section 6.9, the bit error rate (BER) performances of some coded 4-level 3-SP DPM schemes under frequency selective Rayleigh fading channel are evaluated with the use of computer simulation. The same section discusses the performance results of uncoded and coded schemes. The Chapter is summarised in Section 6.10.

6.2 System description

The system under consideration is illustrated by the block diagram in Fig. 6.1. It consists of a trellis encoder and a partial response DPM modulator. The trellis encoder, as shown in Fig. 6.1, combines a convolutional encoder and a signal mapper. The convolutional encoders and the signal mapping rules which are considered will be presented in the following subsections. For information about partial response DPM system, the reader can be referred to Section 2.2.3.

6.2.1 Rate of 1/2 convolutional encoders with short constraint length

The input to the channel encoder is a sequence of independent equiprobable bits a_m of rate $1/T_b$, while its output is the 2-bit coded word $b_m^i = [b_m^1, b_m^2]$ of rate $1/T_s$ where $T_s = \log_2(M)T_b$. a_m and $b_m^i (1 \leq i \leq 2)$ take values from the set 0,1. The rate of code R_c, is k/n information bits/coded symbol. Here, the case of $k = 1$ and $n = 2$ is used.

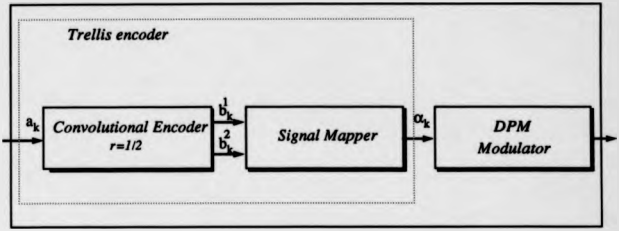

Figure 6.1: The Block diagram of coded DPM transmitter

One method for describing a convolutional encoder is to give its generator matrix. To specify the generator matrix, a functionally equivalent representation will be used in which a set of vectors is specified, one vector for each of the n modulo-2 adders. A "1" in the ith position of the vector indicates that the corresponding stage in the shift register is connected to the modulo-2 adder and a "0" in a given position indicates that no connection exists between that stage and the modulo-2 adder. To be specific, consider the binary convolutional encoder with memory length $v = 3$, and $k = 1$, $n = 2$ (rate of 1/2), which is shown in Fig. 6.2. Since the first and the second stages are connected to the first function generator, its matrix is:

$$g^1 = [1\ 1\ 0\ 0]$$

The second function generator is connected to the second and fourth stages. Hence,

$$g^2 = [0\ 1\ 0\ 1]$$

In decimal form, these generators are (12,5). This encoder can be named a (12,5)-encoder, with $v = 3$.

The encoding operation can be written as

$$b_m^i = \sum_{j=0}^{v} g^i(j) a_{m-j} \qquad i = 1, 2 \ldots$$

where the summations are modulo-2.

The number of encoders to be considered depends on the memory length of the encoder. Increasing the memory length increases the number of encoders also. Especially for a large memory length, the number of encoders is very large. Reducing this number is necessary. One way of reducing the number of encoders is to use a non-catastrophic modulation scheme [64] [65] [68] [70]. A modulation scheme is called catastrophic if there exist two data symbol sequences with infinite Hamming distance such that the corresponding Euclidean distance in signal space between these two signals is finite. When the convolutional encoder is non-catastrophic then the modulation scheme is also non-catastrophic for all rational h values [68] [73] [72]. That means it is necessary not to consider catastrophic encoders.

Another way to reduce the number of encoders to be searched is to check the output effect of the input bits in the required amount of time. For example, if the memory length of an encoder is 2, then (1,3), (1,2), (3,1), and (3,2)-encoders are not appropriate encoders. As seen in Fig. 6.3 the first input bit does not effect the first output symbol. For a memory length bigger than 2, the number of encoders which are not appropriate is quite large. If the first input bit to the encoder does not effect the first output symbol, then the first amount of the data difference sequence is zero, which has the effect of decreasing the Euclidean distance.

6.2.2 Mapping rules

The coded sequence b'_m is the input to the mapper. The signal mapper translates the sequence b'_m into one of the M different symbols α_m. For the binary case, there is only one mapping rule, namely the natural binary mapping rule, which is defined by:

$$\alpha_m = \sum_{i=1}^{\log_2(M)} 2^{i-1}(2b'_m - 1) \qquad (6.1)$$

For the case of $M = 4$, there are $M! = 24$ mapping rules. From equation 2.5 it can be seen that if γ were replaced by $-\gamma$ the Euclidean distance would be the same i.e. the mapping rules can be reduced to $M!/2 = 12$. These are shown in the Table 6.1.

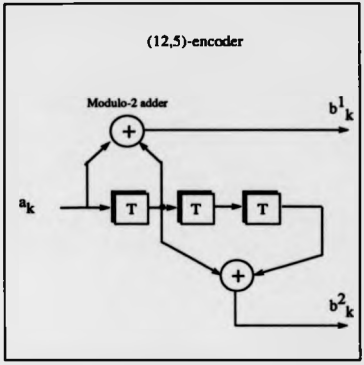

Figure 6.2: The (12,5)-convolutional encoder with memory length $v = 3$, and $k = 1$, $n = 2$ (rate of 1/2)

Input to the mapper		*Output symbol (Map#)*											
MSB	*LSB*	1	1a	1b	1c	1d	1e	2	2a	2b	2c	2d	2e
0	0	-3	-3	-3	-3	-3	-3	-1	-1	-1	-1	-1	-1
0	1	-1	1	3	-1	1	3	-3	-3	1	1	3	3
1	0	1	-1	-1	3	3	1	3	1	-3	3	1	-3
1	1	3	3	1	1	-1	-1	1	3	3	-3	-3	1

Table 6.1: Mapping rules for 4-level case

Table 6.2: Mapping rules which are considered for 4-level case

Input to the mapper		*Output symbol*	
MSB	*LSB*	Map# 1	Map # 2
0	0	-3	-1
0	1	-1	-3
1	0	1	3
1	1	3	1

It can be easily shown that these rules can be reduced to two [66] [70]. There are just two, because one encoder with a mapping rule can be transformed into any encoder with a different mapping rule, except these two mapping rules. These rules will be called map# 1 and map# 2. These are shown in Table 6.2. The map# 1 is the natural binary mapping and map# 2 is the natural binary mapping rule with LSB complemented.

For example: Suppose we want to transform the (1,6)-encoder with mapping rule map#1c (see Fig. 6.1) into an encoder with a mapping rule map#1d. In other words, we want to create a new encoder with mapping rule map# 1d from the combination of (1,6)-encoder and map# 1c. As shown in Table 6.1, the symbol "-1" should be converted to the symbol "1" and the symbol "1" to "-1". In other words, the inputs to the mapper, namely the coded bits "11", should be converted to bits "01" and "01" to "11". In Fig. 6.4, it can be seen that the least significant bit (LSB) is used to create the new encoder. If we add the LSB of the (1,6)-encoder to the MSB, to create the most significant bit (MSB) bit of the new encoder and leave LSB unchanged for the LSB of the new encoder, the new encoder can be created with mapping rule map# 1d, which is identical to the (1,6)-encoder with mapping rule map# 1c. The new encoder is (7,6)-encoder.

6.3 Finding the upper bounds on free Euclidean distance

The squared Euclidean distance, the distance between two signals, normalised by bit energy for partial response DPM system is:

$$d^2_{m,m'} = \log_2 M 2\eta^{-1} \sum_{n=0}^{N_T} \sin^2 \left(1/2 \sum_{i=\lfloor (n-K-1)/\eta \rfloor}^{\lfloor n/\eta \rfloor} \gamma_{mm',i} q_{n-i\eta} \right) \qquad (6.2)$$

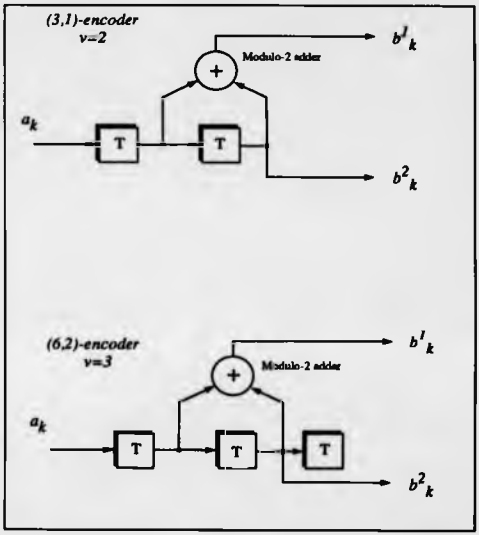

Figure 6.3: Some encoders, which are not considered

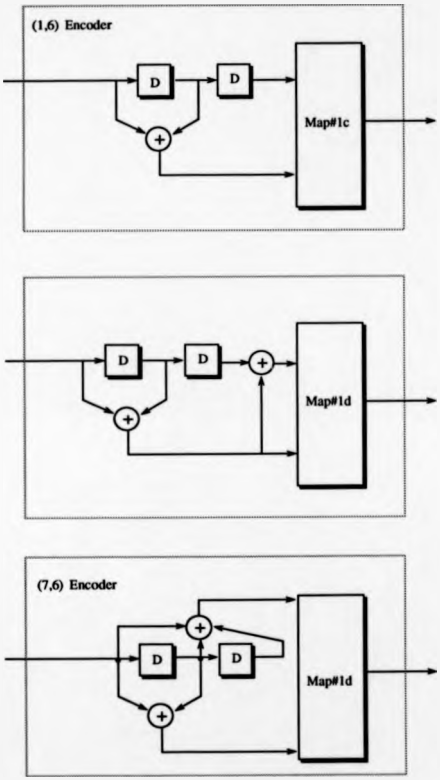

Figure 6.4: Transforming an encoder with a 4-level mapping rule to encoders with different mapping rules

where N_T is the length of the observation interval, $\lfloor x \rfloor$ denotes the integer part of x, and $\gamma_{mm',i}$ is the difference sequence between two data sequences, which is:

$$\gamma_{mm',i} = (\alpha_{m,i} - \alpha_{m',i})$$

where q_n are the filter coefficients, and η is the integer between the signalling interval T and the duration D of each element in the digital filter and is known as the oversampling ratio.

To find the upper bound of d^2_{min}, just a few pairs of infinitely long sequences can be considered. Suitable candidates for these infinitely long pairs are the pairs that diverge at the same stage and merge as soon as possible after one time interval. For the coded DPM case, the two sequences should, in addition to having the same phase as in the uncoded case, also have the same state in the convolutional encoder. Then it can be said that they have a state and phase merge [65]. For partial response modulation scheme it is not sufficient to consider just the first state and phase merge [68]. For L-SP DPM, the upper bound of d^2_{min} does not decrease significantly as the number of merges extends above L. For our case of 3-SP DPM, three merges were considered.

To produce a state merge, two data sequences take on the same pairwise values for a number of end elements exactly equal to the memory length of the encoder. For the partial response signal ($L > 1$) and for the case of $v \leq L$, the phase and state merge can be produced by adding the same pairwise values for a number of L to the end of the difference sequences. If $v > L$, this number will be v.

For example: Fig 6.5a shows the modulation scheme consisting a (7,2)-encoder with rate of 1/2, and memory length $v = 2$, a mapper (Map# 1) and a 4-level 3-SP DPM modulator. To find an upper bound corresponding to the first merge a few pairs of data sequences which have phase and state merge can be found. The minimum Euclidean distances corresponding to these all pairs are computed first. The smallest distance is considered as an upper bound on the free Euclidean distance. Let assume that the starting states of the convolutional encoder are [0, 0]. If the two data sequences are $data1 = \{0\ 0\ 0\ 1\ 0\ 0\}$ and $data2 = \{1\ 0\ 0\ 1\ 0\ 0\}$ then the output of the mapper for the first data sequence is $\alpha_1 = \{-3,\ -3,\ -3,\ 1,\ 3,\ 1\}$ and for the second data sequence is $\alpha_2 = \{1,\ 3,\ 1,\ 1,\ 3,\ 1\}$. Fig 6.5b shows that these two signals have a phase and state merge, at $t = 6T$. The

last state of the encoder is [0, 0]. That means they have a state and phase merge. The difference sequence between these two data sequences is

$$\gamma = \alpha_1 - \alpha_2$$

$$= \{-4, -6, -4, 0, 0, 0\}$$

The normalized squared minimum Euclidean distance (NSMED) can be derived by using equation (6.2) and the γ -sequence. The N_T in equation (6.2) will be 6. To find an upper bound, all NSMED corresponding to all pairs of data sequences which have merge should be found. The smallest distance is the upper bound for considered combination of encoder and modulator.

For binary 3-SP DPM cases the upper bounds, for each combination of encoder and the modulator, have been evaluated. The natural binary mapping rule is used.
The upper bounds for each combination of encoder, mapping rule and 4-level 3-SP DPM modulator have been also evaluated. The mapping rules are map# 1 and map#2.

For both binary and 4-level cases, the memory length of $1 \leq v \leq 3$, and the modulation indices between 0.05 and 1.20, in steps of 0.05 are considered. The computed upper bound for each of these combinations are stored in a memory. These will help with finding the free Euclidean distances.

6.4 An extended algorithm to compute the free Euclidean distance

The algorithm which is used to find the free Euclidean distance of uncoded 3-SP DPM system has been extended to find the free Euclidean distances for coded cases. The flowchart of the algorithm is illustrated in Fig. 6.6. The modulation indices between 0.05 and 1.20 are considered in steps of 0.05. The memory length of the encoder varies from 1 to 3. The free Euclidean distance for each combination of encoder, mapping rule, and modulator is evaluated using this algorithm.

In the first step, the states of the encoder is set to zero, and the first bit of the first sequence to "1", and the first bit of the second sequence to "0". That is the condition of diverge.

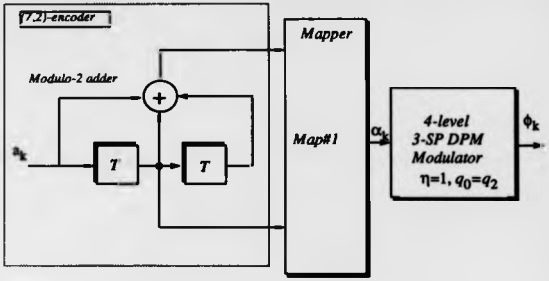

(a)

Figure 6.5: A minimum distance pair: An example to find a state and phase merge

At this stage the observation interval length is equal to N (The length N which is seen in the flowchart equals 2 for the binary case, and 1 for 4-level case). Then the difference sequence γ is computed. After that the normalized squared minimum Euclidean distance corresponding to this sequence is first found using equation (6.2); then this distance is compared with the evaluated upper bound, $d^2_{up}(h)$, as found in the section above. If this distance is smaller than $d^2_{up}(h)$ then these data sequences (a^1_{OI} *and* a^2_{OI}) and the current states ($state^1_1, state^1_2, \ldots state^1_v$ *and* $state^2_1, state^2_2, \ldots state^2_v$) are stored, where v is the memory length of the encoder. At this time, the $d^2_{min\,OI}(h)$ corresponding to the first observation interval length is stored.

In the second step, the observation interval length is increased by N. Now there are four possible new data pairs. These are ($a^1_{OI} = 0$ $a^2_{OI} = 0$), ($a^1_{OI} = 0$ $a^2_{OI} = 1$), ($a^1_{OI} = 1$ $a^2_{OI} = 0$), ($a^1_{OI} = 1$ $a^2_{OI} = 1$). These four possible new data pairs will be used with the previous data pairs and states, to evaluate normalized squared minimum Euclidean distance corresponding to this time interval. The total normalized squared minimum Euclidean distance is

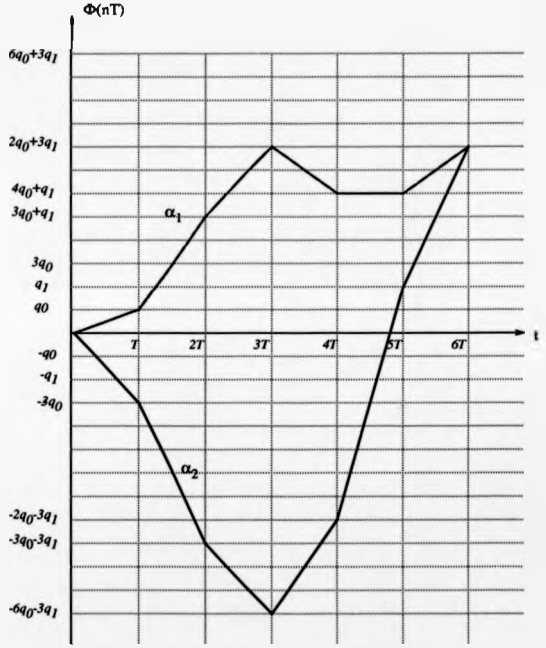

Figure 6.5 b: Continued from Figure 6.5 a.

$$d^2_{OI}(h) = d^2_{OI-1}(h) + d^2_{\Delta}(h)$$

where $d^2_{\Delta}(h)$ is the normalized squared Euclidean distance corresponding to the time interval $((OI-1)T \leq t \leq (OI)T)$. Now, the minimum distance of these two distances ($d^2_{min\,OI}(h)$ *and* $d^2_{OI}(h)$) is chosen as a normalized squared minimum Euclidean distance. In the following stage, the comparison between $d^2_{min,OI}(h)$ and $d^2_{up}(h)$ is accomplished. If $d^2_{min\,OI}(h)$ is smaller than or equal to $d^2_{up}(h)$ then this distance and the corresponding data and state sequences are saved for the computation of the minimum distance corresponding to the next observation interval length. The minimum of these stored distances is the normalized squared minimum Euclidean distance corresponding to OI=2N ($d^2_{min,2N}$). The saved data and state sequences are

$$(a^1_N,\ a_2N^1, \ldots a^1_{OI}\ \textit{and}\ a^2_N,\ a_2N^2,\ a^2_{OI})$$

$$(state^1_1,\ state^1_2, \ldots state^1_v\ \textit{and}\ state^2_1,\ state^2_2, \ldots state^2_v)$$

At this stage, loop is compared with 4. If it does not reach 4, then it is increased by 1, and the new data (new bits to the encoder) a^1_{OI} *and* a^2_{OI} are entered. If loop is already 4 then the stored sequences are checked. If all the stored sequences are read then the corresponding $d^2_{min}(h), OI$ and h are printed. This process continues until d^2_{min} is found. When $d^2_{min,OI}$ equals to d^2_{up} then the computation finishes. That means $d^2_{min,OI} = d^2_{up}$. At this time, the corresponding OI length is noted. If $d^2_{min,OI}$ does not equal to d^2_{up} then the process starts from the stage A again.For some modulation indices this distance (d^2_{up}) might not be reached by the maximum observed OI time.

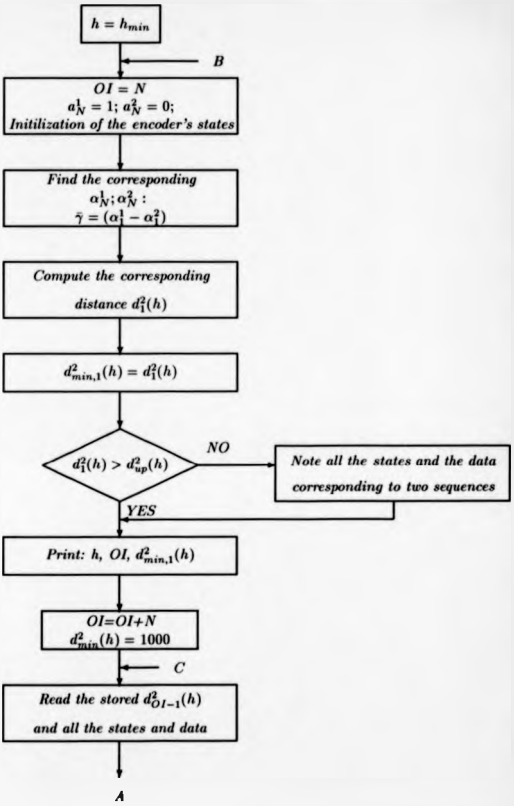

Figure 6.6a:The flowchart of an extended algorithm to compute the free Euclidean distance

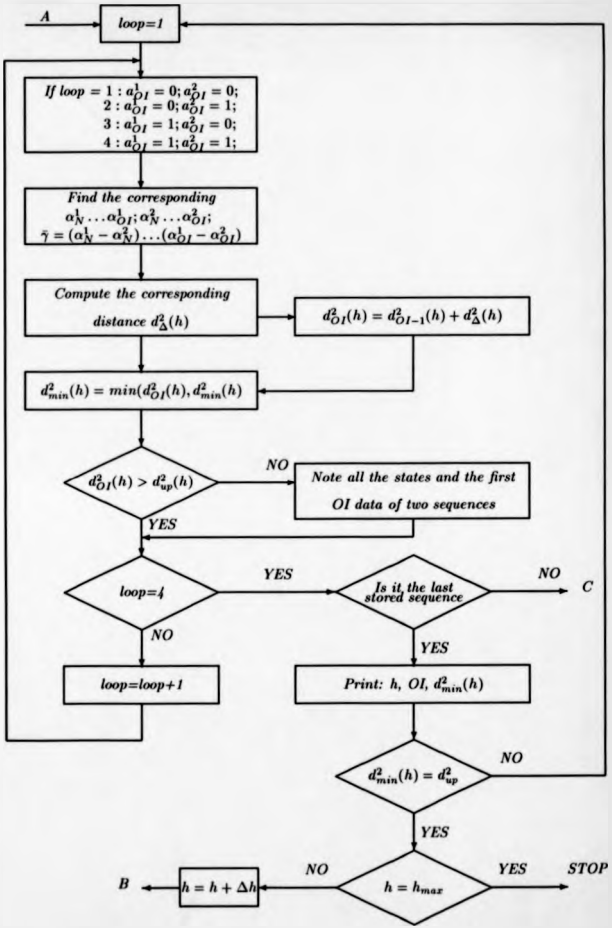

Figure 6.6b Continued from Fig. 6.6a

6.5 The optimal combinations of 1/2 rate encoder, mapping rule and 3-SP DPM modulator

In this section, the best (optimal) combinations of 1/2 rate convolutional encoder, mapping rule and 3-SP DPM modulator (binary and 4-level) are searched for given modulation indices h and memory length v. To be more specific, the best combination is found for every modulation index h and memory length v.

Since the error probability of a system is a function of the free Euclidean distance d^2_{min}, the combinations which maximise this distance are investigated. The optimal combination will contain the type of the encoder, the mapping rule, corresponding d^2_{min}, and the OI length which gives this distance.

6.5.1 The optimal combinations for binary 3-SP DPM

The encoders examined were chosen according to the restrictions given in Section 6.2.1. Memory lengths between 1 and 3, and modulation indices between 0.05 and 1.20 in steps of 0.05, are studied. The mapping rule considered is the natural binary mapping rule given in Section 6.2.2.

The optimal combinations are given in Tables 6.3, 6.4 and, 6.5; these consist of the type of the encoder, the corresponding $d^2_{min}(h)$ and the OI length for which $d^2_{min,OI}(h) = d^2_{up}(h)$. For reasons of comparision, $d^2_{min}(h)$ values for binary uncoded 3-SP DPM are given in Table 6.6.

First $d^2_{min,OI}(h)$ corresponding to all combinations considered for v=1 case are found. These can be used to find the optimal combinations for a given modulation index. The found optimal combinations are shown in Table 6.3. It is found that the (1,2)-encoder is the optimal one for modulation indices $h \leq 0.70$. One exception is for h=0.55, for which the (2,3)-encoder combination is optimal. When the modulation index is greater than 0.75 the (2,1)-encoder is the best one. The largest d^2_{min} found for v=1 is 4.248, when h=1.20. The corresponding free Euclidean distance for the uncoded case is 1.912. The increase in d^2_{min} is more than two times. It is seen from Table 6.3 and Fig. 6.7 that the free Euclidean distances corresponding to all modulation indices are significantly increased, when com-

pared with uncoded cases.

For memory length v=2, the optimal combinations are shown in Table 6.4. It is clear from Table 6.4 that the (4,5)-encoder is the optimal one for modulation indices smaller than 0.80. For modulation indices larger than 0.80, the (4,3)-encoder is optimal; meanwhile the (1,6)-encoder is also as good as the (4,3)-encoder for some modulation indices between 0.80 and 1.20. The largest d^2_{min} found, for v=2, is 5.953 when h=1.10. It is increased from 4.248 (for v=1) to 5.953. If the memory length v=2 case is compared with the v=1 case it can be seen that all the $d^2_{min}(h)$ values for v=2 case are larger than the $d^2_{min}(h)$ values for the v=1 case. This shows that increasing the memory length from 1 to 2 increases the coding gain.

For memory length v=3, the search shows that the (11,15)-encoder is the optimal one for modulation indices $h \leq 0.40$. As it is seen in the Table 6.5 the (15,11)-encoder is the best one for modulation indices between $0.45 \leq h \leq 0.60$. The (13,11)-encoder is the example of best encoder for modulation indices in the interval $0.65 \leq h \leq 0.70$. For modulation indices between $0.75 - 1.10$ and $1.15 - 1.20$, the (8,3) and (10,7)-encoders are optimal respectively. The largest d^2_{min}, for v=3, is 6.632, when h=1.20.

It can be seen from Fig.6.7 and Tables 6.3, 6.4, and 6.5 that for memory length v=3, the $d^2_{min}(h)$ values are larger than the $d^2_{min}(h)$ values corresponding to memory lengths v=1 and v=2. This means 1/2 rate convolutional encoder with memory length equals to 3 when combined with binary 3-SP DPM modulator; this combination has the maximum $d^2_{min}(h)$ for every modulation index.

The numerical results show that increasing the memory length increases the coding gain for each modulation index considered in this study. As it is seen in Fig. 6.7, combining the modulator with rate 1/2 encoder having memory length of v=1 increases the optimal d^2_{min} significantly when compared with d^2_{min} for the uncoded case. Increasing the memory length from 1 to 2 increases the d^2_{min} significantly as well. Increasing v from 2 to 3 increases the free Euclidean distances but these increases are not significantly large. It means less gain when compared with the gain of increasing the memory length from 1 to 2.

Coded binary 3-SP DPM (v=1)			
h	Optimal encoder	d^2_{min}	OI Length
0.05	(1,2)	0.042	6
0.10	(1,2)	0.165	6
0.15	(1,2)	0.362	6
0.20	(1,2)	0.619	6
0.25	(1,2)	0.922	6
0.30	(1,2)	1.252	6
0.35	(1,2)	1.589	6
0.40	(1,2)	1.913	4
0.45	(1,2)	2.206	4
0.50	(1,2)	2.452	4
0.55	(2,3)	2.559	10
0.60	(1,2)	2.761	8
0.65	(1,2)	2.815	6
0.70	(1,2)	2.802	6
0.75	(2,1)	3.031	12
0.80	(2,1)	3.273	12
0.85	(2,1)	3.494	12
0.90	(2,1)	3.690	8
0.95	(2,1)	3.860	8
1.00	(2,1)	4.000	8
1.05	(2,1)	4.109	8
1.10	(2,1)	4.187	90
1.15	(2,1)	4.233	12
1.20	(2,1)	4.248	16

Table 6.3: Optimal combinations of 1/2 rate encoder and binary 3-SP DPM modulator (v=1)

Coded binary 3-SP DPM (v=2)			
h	Optimal encoder	d^2_{min}	OI Length
0.05	(4,5)	0.054	2
0.10	(4,5)	0.214	2
0.15	(4,5)	0.471	2
0.20	(4,5)	0.812	4
0.25	(4,5)	1.219	4
0.30	(4,5)	1.672	4
0.35	(4,5)	2.149	4
0.40	(4,5)	2.628	4
0.45	(4,5)	3.087	6
0.50	(4,5)	3.508	12
0.55	(4,5)	3.876	16
0.60	(4,5)	4.180	16
0.65	(4,5)	4.415	14
0.70	(4,5)	4.581	16
0.75	(4,5)	4.611	18
0.80	(4,3)	4.478	10
0.85	(4,3)	4.806	10
0.90	(6,1), (4,3)	5.106	12-10
0.95	(6,1), (4,3)	5.374	12-10
1.00	(6,1), (4,3)	5.606	12-12
1.05	(4,3)	5.800	12
1.10	(4,3)	5.953	14
1.15	(4,3)	5.870	16
1.20	(6,1)	5.898	24

Table 6.4: Optimal combinations of 1/2 rate encoder and binary 3-SP DPM modulator (v=2)

Coded binary 3-SP DPM (v=3)			
h	Optimal encoder	d^2_{min}	OI Length
0.05	(11,15)	0.069	2
0.10	(11,15)	0.270	2
0.15	(11,15)	0.593	4
0.20	(11,15)	1.018	4
0.25	(11,15)	1.520	6
0.30	(11,15)	2.071	6
0.35	(11,15)	2.640	6
0.40	(11,15)	3.196	8
0.45	(15,11)	3.718	10
0.50	(15,11)	4.266	10
0.55	(15,11)	4.759	10
0.60	(15,11)	5.089	14
0.65	(13,11)	5.316	18
0.70	(13,11)	5.575	34
0.75	(8,3)	4.751	12
0.80	(8,3)	5.123	12
0.85	(8,3)	5.461	12
0.90	(8,3)	5.758	12
0.95	(8,3)	6.009	12
1.00	(8,3)	6.211	12
1.05	(8,3)	6.362	14
1.10	(8,3)	6.459	16
1.15	(10,7)	6.529	14
1.20	(10,7)	6.632	16

Table 6.5: Optimal combinations of 1/2 rate encoder and binary 3-SP DPM modulator (v=3)

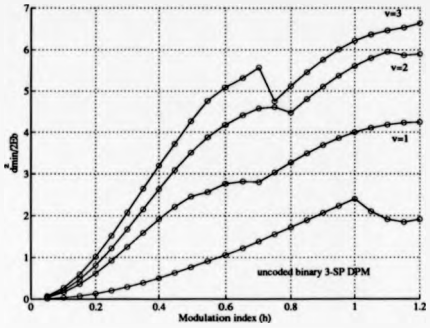

Figure 6.7: Optimum $d^2_{min}(h)$ for coded binary 3-SP DPM

6.5.2 The optimal combinations for 4-level 3-SP DPM

The encoders were chosen according to the restrictions given in Section 6.2.1. The memory length between 1 and 3, and modulation indices between 0.05 and 1.00 in steps of 0.05 are studied. The two mapping rules considered in this search are discussed in detail in Section 6.2.2.

The optimal combinations are given in Tables 6.7, 6.8, 6.9 and consist of the type of the encoder, the mapping rule, the corresponding $d^2_{min}(h)$, and the OI length for which $d^2_{min,OI}(h) = d^2_{sp}(h)$. For reasons of comparision, $d^2_{uncn}(h)$ values for 4-level uncoded 3-SP DPM are given in Table 6.6.

Firstly, $d^2_{min,OI}(h)$ values corresponding to all combinations considered for the v=1 case are found. These can be used to find the optimal combinations for a given modulation index. The optimal combinations found are shown in Table 6.7. For memory length v=1, as seen in Table 6.7, the (3,2)-encoder with map# 1 is the optimal combination for modulation indices smaller than 0.45, except for h=0.30 and 0.35, for which the (1,3) and (1,2)-encoders with map# 1 are optimal. When the modulation index is 0.45 or 0.50

the (1,3)-encoder with map# 2 is the best combination. The (1,2)-encoder with map# 1 is the optimal combination for modulation indices in the interval $0.55 \leq h \leq 0.75$, except for $h = 0.70$. For this h value, the (3,1)-encoder with map# 2 is the best one. Among the considered modulation indices the most convienent combination for h values equal to or larger than 0.80 is the (2,3)-encoder with mapping rule map# 1. The largest d^2_{min} found, for v=1, is 5.697, when h=0.95. It is increased from 0.920 to 5.697. If the $d^2_{min}(h)$ values for the v=1 case is compared with the uncoded case, it can be seen that all the $d^2_{min}(h)$ values are significantly increased for all modulation indices considered here.

For memory length v=2, the optimal combinations are shown in Table 6.8. It is clear from Table 6.8 that the (3,4)-encoder with map# 1 is optimal for most of the modulation indices smaller than or equal to 0.30, except for $h = 15$ and 0.20. For these modulation indices the (5,2)-encoder with map# 1 is optimal. For modulation index $h = 0.40$ two combinations ((1,6) and (4,3)-encoders with same mapping rule: map# 1) have the same d^2_{min} but different observation interval lengths. As the (1,6)-encoder with map# 1 has a smaller OI length , it can be considered as an optimal one. For modulation indices between 0.50 and 0.55, 0.60 and 0.65, 0.75 and 0.80, 0.85 and 0.95 the (4,1), (1,6)-encoders with map# 1, (2,5)-encoder with map# 2, and (4,7)-encoder with map# 1 are optimal combinations respectively. The largest d^2_{min} found, for v=2, is 7.557 when h=0.95. It is increased from 5.697 (for v=1) to 7.557. If the memory length v=2 case is compared with v=1 case it can be seen that all the $d^2_{min}(h)$ values for v=2 case are larger than the $d^2_{min}(h)$ values for the v=1 case. This shows that increasing the memory length from 1 to 2 increases the coding gain.

The optimal encoders have been found, for specific modulation index and for memory length v=3. The search shows that the (11,9)-encoder with map# 1 is the optimal one for modulation index $h = 0.05$. As it seen in Table 6.9 the (11,12)-encoder with map# 1 is the best combination for modulation indices between 0.10 and 0.25. The (11,2)-encoder with mapping rule map# 2 is an example of the best encoder for modulation indices in the interval $0.35 \leq h \leq 0.50$. For modulation indices between 0.55 and 0.60, 0.65 and 0.75,the (2,11)-encoder with map# 1, and (2,13)-encoder with map# 2, are optimal respectively. The largest d^2_{min} found, for v=3, is 7.943 when h=0.95. It is increased from 7.557 (for v=2) to 7.943.

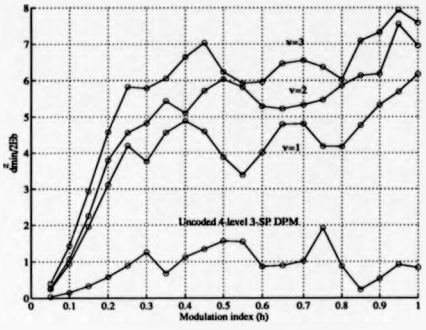

Figure 6.8: Optimum $d^2_{min}(h)$ for coded 4-level 3-SP DPM

It can be seen from Fig.6.8 and Tables 6.7, 6.8, and 6.9 that, for memory length v=3, the $d^2_{min}(h)$ values are larger than the $d^2_{min}(h)$ values corresponding to memory lengths v=1 and v=2. This means that a 1/2 rate convolutional encoder with memory length equal to 3, when combined with 4-level 3-SP DPM modulator, has the maximum $d^2_{min}(h)$ for every modulation index considered in this thesis.

The numerical results show that increasing the memory length increases the coding gain for each modulation index considered in this study. As seen in Fig. 6.8, combining the modulator with rate 1/2 encoder having memory length of v=1 increases the optimal d^2_{min} significantly when compared with d^2_{min} for the uncoded case. Increasing the memory length from 1 to 2 or from 2 to 3 increases the optimal free Euclidean distances also, but the increse is not significant. It mean less gain when compared with the gain going from the uncoded case to coded case, with the memory length equal to 1.

	$d^2_{min}(h)$ *for uncoded M-level 3-SP DPM*	
h	*Binary 3-SP DPM*	*4-level 3-SP DPM*
0.05	0.008	0.037
0.10	0.033	0.148
0.15	0.074	0.330
0.20	0.131	0.579
0.25	0.203	0.891
0.30	0.290	1.257
0.35	0.390	0.676
0.40	0.503	1.123
0.45	0.628	1.342
0.50	0.764	1.563
0.55	0.909	1.544
0.60	1.061	0.866
0.65	1.221	0.893
0.70	1.385	1.016
0.75	1.553	1.925
0.80	1.723	0.874
0.85	1.893	0.230
0.90	2.063	0.532
0.95	2.230	0.920
1.00	2.394	0.835
1.05	2.100	1.133
1.10	1.912	1.943
1.15	0.374	1.103
1.20	0.488	0.478

Table 6.6: $d^2_{min}(h)$ for uncoded binary and 4-level 3-SP DPM.

Coded 4-level 3-SP DPM (v=1)			
h	Optimal encoder and mapping rule	d^2_{min}	OI Length
0.05	(3,2), Map# 1	0.247	2
0.10	(3,2), Map# 1	0.941	2
0.15	(3,2), Map# 1	1.957	2
0.20	(3,2), Map# 1	3.110	4
0.25	(3,2), Map# 1	4.199	9
0.30	(1,3), Map# 1	3.760	11
0.35	(1,2), Map# 1	4.563	4
0.40	(3,2), Map# 1	4.885	12
0.45	(1,3), Map# 2	4.593	17
0.50	(1,3), Map# 2	3.882	7
0.55	(1,2), Map# 1	3.382	9
0.60	(1,2), Map# 1	4.015	10
0.65	(1,2), Map# 1	4.791	10
0.70	(3,1), Map# 2	4.807	11
0.75	(1,2), Map# 1	4.182	11
0.80	(2,3), Map# 1	4.173	63
0.85	(2,3), Map# 1	4.767	16
0.90	(2,3), Map# 1	5.336	26
0.95	(2,3), Map# 1	5.697	12
1.00	(2,3), Map# 1	5.256	11

Table 6.7: Optimal combinations of 1/2 rate encoder, mapping rule and 4-level 3-SP DPM modulator (v=1)

Coded 4-level 3-SP DPM (v=2)			
h	Optimal encoder and mapping rule	d^2_{min}	OI Length
0.05	(3,4), Map# 1	0.282	9
0.10	(3,4), Map# 1	1.067	8
0.15	(5,2), Map# 1	2.256	14
0.20	(5,2), Map# 1	3.797	16
0.25	(3,4), Map# 1	4.560	3
0.30	(3,4), Map# 1	4.827	7
0.35	(4,5), Map# 1	5.436	19
0.40	(1,6), Map# 1	5.099	17
	(4,3), Map# 1		34
0.45	(3,4), Map# 1	5.721	15
0.50	(4,1), Map# 1	6.035	19
0.55	(4,1), Map# 1	5.816	15
0.60	(1,6), Map# 1	5.294	17
0.65	(1,6), Map# 1	5.223	13
0.70	(2,5), Map# 1	5.336	38
0.75	(2,5), Map# 2	5.474	39
0.80	(2,5), Map# 2	5.869	32
0.85	(4,7), Map# 1	6.136	20
0.90	(4,7), Map# 1	6.185	21
0.95	(4,7), Map# 1	7.557	21
1.00	(3,7), Map# 1	6.964	26

Table 6.8: Optimal combinations of 1/2 rate encoder, mapping rule and 4-level 3-SP DPM modulator (v=2)

Coded 4-level 3-SP DPM (v=3)			
h	Optimal encoder and mapping rule	d^2_{min}	OI Length
0.05	(11,9), Map# 1	0.402	17
0.10	(11,12), Map# 1	1.430	11
0.15	(11,12), Map# 1	2.933	24
0.20	(11,12), Map# 1	4.578	33
0.25	(11,12), Map# 1	5.825	32
0.30	(11,4), Map# 1	5.787	18
0.35	(11,2), Map# 1	6.055	21
0.40	(11,2), Map# 1	6.642	22
0.45	(11,2), Map# 1	7.037	24
0.50	(11,2), Map# 1	6.235	16
0.55	(2,11), Map# 1	5.922	18
0.60	(2,11), Map# 1	5.936	14
0.65	(2,13), Map# 1	6.462	19
0.70	(2,13), Map# 1	6.552	26
0.75	(2,13), Map# 1	6.371	20
0.80	(2,11), Map# 1	6.030	65
0.85	(1,15), Map# 1	7.098	30
0.90	(6,13), Map# 1	7.327	20
0.95	(11,13), Map# 1	7.943	19
1.00	(2,11), Map# 1	7.592	20

Table 6.9: Optimal combinations of 1/2 rate encoder, mapping rule and 4-level 3-SP DPM modulator (v=3)

6.6 The minimum Euclidean distance growth with the observation interval length

In this section the normalized squared minimum Euclidean distance (NSMED) growth, $d^2_{min,OI}$, is presented as a function of the observation interval (OI) length. In the previous section the required OI lengths for optimal combinations are given for both coded binary and 4-level cases. These can be seen in Tables 6.3, 6.4, 6.5, 6.7, 6.8, and 6.9. In the following two subsections, the growth of $d^2_{min,OI}$ will be presented for some combination of encoder, mapping rule and modulator (binary and 4-level 3-SP DPM).

6.6.1 The minimum Euclidean distance growth for coded binary 3-SP DPM

Figs. 6.9, 6.10, 6.11 and 6.12 show the growth of Euclidean distances with the observation interval length for the combinations of (1,2), (1,3), (2,1) and (2,3)-encoders with binary 3-SP DPM modulator, respectively. These figures can be helpfull with finding the optimal encoder for desired modulation indices. These are for memory length v=1. For some modulation indices the upper bound can not be reached. The normalized squared minimum Euclidean distance growth, $d^2_{min,OI}(h)$, for the (1,2) and (2,1)-encoder, are given in Tables 6.10 and 6.11 as a function of OI length and given modulation indices. For some modulation indices the OI lengths which reach the free Euclidean distance are extremely large. An example to this is the combination of (2,1)-encoder with binary 3-SP DPM modulator, for h=1.10. The required OI length for this combination is 90.

For memory length v=2, Figs. 6.13, 6.14 and 6.15 show the growth of Euclidean distances with the observation interval length for some optimal combinations. These are (4,5), (6,1) and (4,3)-encoders combined with binary 3-SP DPM modulator, respectively. The memory length is 2. As is seen in Table 6.4, for modulation indices h=0.90, 0.95 and 1.00, two encoders have the same free Euclidean distance. But the OI lengths which give these distances are different. For the (6,1)-encoder, this length is 12 for all of them. For the (4,3)-encoder, these lengths are 10,10 and 12, respectively. The normalized squared minimum Euclidean distance growth for these combinations is given in Table 6.12, as a function of observation interval length. The growth of minimum Euclidean distance with the observation interval length is different for each combination. The combination of (4,3)-encoder with binary 3-SP DPM is seen to be better, because this combination can

reach the free Euclidean distance with smaller OI length, except for h=1.00. For this case both of them reach the free Euclidean distance with the same OI length. The normalized squared minimum Euclidean distance growth, $d^2_{min,OI}(h)$ for the (4,5)-encoder is given in Table 6.13 as a function of OI length and given modulation indices. As it is seen in this Table, the OI length is related to the amount of d^2_{min}. For a larger value of d^2_{min}, a larger OI length is required.

For memory length v=3, Fig. 6.16 and 6.17 show the growth of Euclidean distances with the observation interval length for some optimal combinations. These obtained combinations are (11,15) and (8,3)-encoders combined with binary 3-SP DPM modulator. The memory length is 3. The OI lengths which give the free Euclidean distances for optimal combinations are given in Table 6.5. The normalized squared minimum Euclidean distance growth, $d^2_{min,OI}(h)$ for the (11,15)-encoder is given in Table 6.14 as a function of OI length and given modulation indices.

The main conclusion concerning these results is that, for binary 3-SP DPM, increasing the observation interval length increases $d^2_{min,OI}$ except for weak modulation indices. Increasing the memory length also increases d^2_{min}. On the other hand, for some modulation indices, the required OI length increases, which has the effect of increasing the system's complexity. This can be seen from Tables 6.3, 6.4 and 6.5. It has been also shown that the increase in d^2_{min} depends on the combined system. For some combinations the increase of d^2_{min} with the OI length is slow e.g for the combination of (6,1)-encoder, and binary 3-SP DPM with h=0.90 and v=2, the required OI length to reach the d^2_{min} distance of 5.106 is a 12 symbol interval. On the other hand, for the combination of (4,3)-encoder, which has the same d^2_{min}, h and v, the required OI length is 10 symbol interval. This can be seen from Fig. 6.4 and Table 6.12.

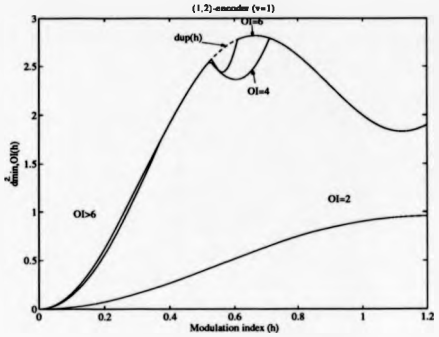

Figure 6.9: The NSMED growth with the observation interval length. For (1,2)-encoder combined with binary 3-SP DPM modulator

6.6.2 The minimum Euclidean distance growth for coded 4-level 3-SP DPM

Fig. 6.18 shows the growth of Euclidean distances with the observation interval for the combination of (3,2)-encoder, map# 1 and 4-level 3-SP DPM modulator, respectively. This is the optimal combination for $h \leq 0.25$ and memory length v equal to 1. The normalized squared minimum Euclidean distances growth, $d^2_{min,OI}(h)$, for the (3,2)-encoder combined with map# 1 is given in Table 6.15 as a function of OI length and modulation index.

For memory length v=2, Fig. 6.19 shows the growth of Euclidean distances with the observation interval for an optimal combination, namely (3,4)-encoder with map# 1 combined with 4-level 3-SP DPM modulator. The memory length is 2. As it is seen in Table 6.8, the required OI lengths -to reach the free Euclidean distances- are increased when compared with v=1 case. The normalized squared minimum Euclidean distances growth, $d^2_{min,OI}(h)$, for the (3,4)-encoder with map# 1 is given in Table 6.16 as a function of OI length and modulation index. As it is seen in this Table, the OI lengths do not grow with

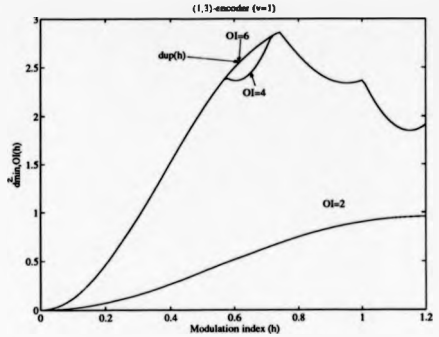

Figure 6.10: The NSMED growth with the observation interval length. For (1,3)-encoder combined with binary 3-SP DPM modulator

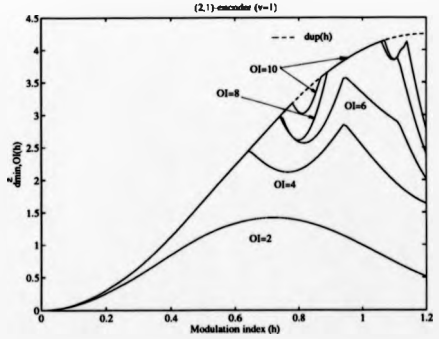

Figure 6.11: The NSMED growth with the observation interval length. For (2,1)-encoder combined with binary 3-SP DPM modulator

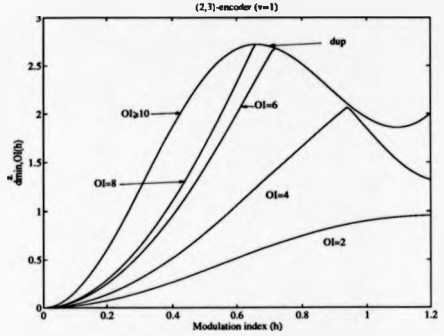

Figure 6.12: The NSMED growth with the observation interval length. For (2,3)-encoder combined with binary 3-SP DPM modulator

$d^2_{min,OI}(h)$ *for the (1,2)-encoder (v=1)*					
	h				
OI	0.10	0.15	0.40	0.45	0.60
2	0.019	0.041	0.265	0.326	0.516
4	0.144	0.320	1.913	2.206	2.365
6	0.165	0.362	–	–	2.652
8	–				2.761

Table 6.10: The NSMED growth with the observation interval length. For (1,2)-encoder combined with binary 3-SP DPM modulator (v=1)

$d^2_{min,OI}(h)$ for the (2,1)-encoder (v=1)							
	h						
OI	0.75	0.80	0.85	0.90	0.95	1.00	1.20
2	1.412	1.377	1.313	1.224	1.117	0.995	0.509
4	2.127	2.153	2.309	2.577	2.824	2.524	1.635
6	2.876	2.584	2.644	3.042	3.567	3.335	2.017
8	2.939	2.607	2.944	3.690	3.860	4.000	2.399
10	3.031	3.038	3.279	–	–	–	2.781
12	–	3.273	3.494	–	–	–	3.163
14		–	–				3.545
16							3.927
18							4.248

Table 6.11: The NSMED growth with the observation interval length. For (1,2)-encoder combined with binary 3-SP DPM modulator (v=1)

$d^2_{min,OI}(h)$ for the (6,1) and (4,3)-encoders (v=2)						
	h=0.90		h=0.95		h=1.00	
OI	(4,3)	(6,1)	(4,3)	(6,1)	(4,3)	(6,1)
2	0.407	0.407	0.473	0.473	0.518	0.518
4	0.871	1.861	1.216	1.706	1.329	1.518
6	2.947	2.285	3.239	2.451	3.511	2.400
8	4.400	4.395	4.473	4.473	4.511	4.518
10	5.106	4.819	5.374	5.216	5.511	5.329
12	–	5.106	–	5.374	5.606	5.606

Table 6.12: The NSMED growth with the observation interval length for (6,1) and (4,3)-encoders combined with binary 3-SP DPM modulator (v=2)

$d^2_{min,OI}(h)$ for the (4,5)-encoder (v=2)							
	h						
OI	0.15	0.35	0.45	0.50	0.65	0.70	0.75
2	0.471	0.474	0.603	0.793	0.721	0.446	0.210
4	–	2.149	1.811	1.136	1.835	2.341	2.042
6		–	3.087	2.773	2.341	2.870	3.496
8			–	3.231	3.093	3.280	3.558
10				3.459	3.469	3.712	4.048
12				3.508	3.845	4.143	4.213
14				–	4.415	4.554	4.275
16					–	4.581	4.306
18						–	4.611

Table 6.13: The NSMED growth with the observation interval length. For (4,5)-encoder combined with binary 3-SP DPM modulator (v=2)

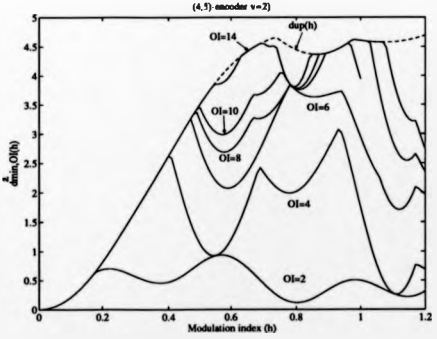

Figure 6.13: The NSMED growth with the observation interval length. For (4,5)-encoder combined with binary 3-SP DPM modulator

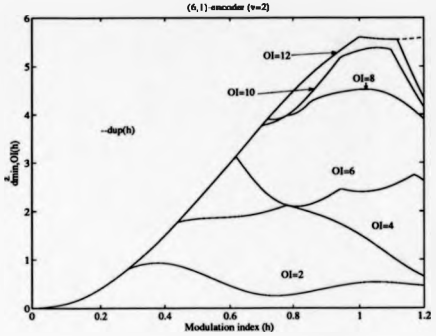

Figure 6.14: The NSMED growth with the observation interval length. For (6,1)-encoder combined with binary 3-SP DPM modulator

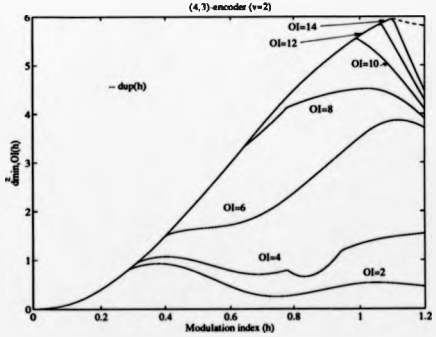

Figure 6.15: The NSMED growth with the observation interval length. For (4,3)-encoder combined with binary 3-SP DPM modulator

$d^2_{min,OI}(h)$ *for the (11,15)-encoder (v=3)*							
	h						
OI	**0.10**	**0.15**	**0.20**	**0.25**	**0.30**	**0.35**	**0.40**
2	0.270	0.551	0.690	0.683	0.575	0.474	0.475
4	–	0.593	1.018	1.359	1.503	1.667	1.933
6		–	–	1.520	2.071	2.640	2.910
8				–	–	–	3.196

Table 6.14: The NSMED growth with the observation interval length. For (11,15)-encoder combined with binary 3-SP DPM modulator (v=3)

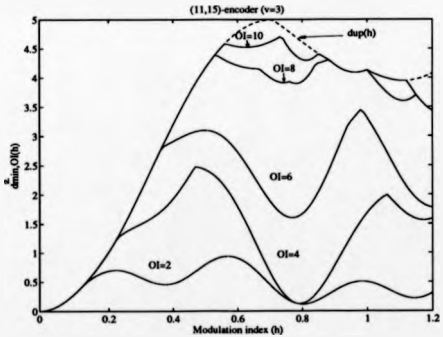

Figure 6.16: The NSMED growth with the observation interval length. For (11,5)-encoder combined with binary 3-SP DPM modulator

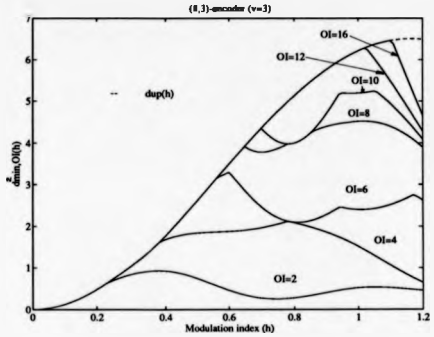

Figure 6.17: The NSMED growth with the observation interval length. For (8,3)-encoder combined with binary 3-SP DPM modulator

the increase of d^2_{min}. For small value of d^2_{min} the required OI length migth be larger as it is seen in Table 6.16.

For memory length v=3, Fig. 6.20 shows the Euclidean distances growth with the observation interval for the combination of (11,12)-encoder, map# 1 and 4-level 3-SP DPM modulator, which is an optimal combination for modulation indices between 0.10 and 0.25. The memory length is 3. The normalized squared minimum Euclidean distances growth, $d^2_{min,OI}(h)$, for the (11,12)-encoder with map# 1 is given in Table 6.17 as a function of OI length and some modulation indices. As it is seen in this Table the growth of minimum Euclidean distance with the OI length is very slow. Sometimes increasing the OI length does not increase $d^2_{min,OI}(h)$. For example increasing the OI length from 3 to 4, from 11 to 12, from 14 to 15, from 18 to 19 etc. does not increases the $d^2_{min,OI}(h)$.

The main conclusion concerning these results is that, for 4-level 3-SP DPM, increasing the observation interval length increases $d^2_{min,OI}$ except for weak modulation indices. Increasing the memory length also increases d^2_{min}. On the other hand, for some modulation indices, the required OI length increases, which has the effect of increasing the system's

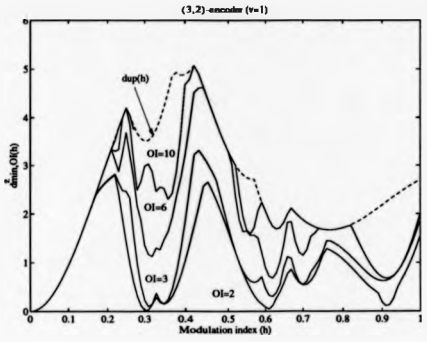

Figure 6.18: The NSMED growth with the observation interval length. For the combination of (3,2)-encoder, map# 1 and 4-level 3-SP DPM modulator

complexity. This can be seen from Tables 6.7, 6.8 and 6.9. It has been also shown that the increase in d^2_{min} depends on the combined system. For some combinations the increase of d^2_{min} with the OI length is very slow e.g for the combination of (11,12)-encoder, Map# 1, and 4-level 3-SP DPM with h=0.20 and v=3, the required OI length to reach the d^2_{min} distance of 4.578 is 33 symbol intervals (See Table 6.17). On the other hand for the combination of (2,11)-encoder, Map# 1 and 4-level 3-SP DPM with h=0.60 and v=3, which has greater d^2_{min} (5.936), the required OI length is 14 symbol intervals. This can be seen from Fig. 6.9 and Table 6.17.

6.7 Derivation of the power and bandwidth efficiency of the coded system

In this thesis, the encoders considered have a rate of 1/2. This means one bit coded into two bits. Because the coded scheme has one bit of information per symbol rather than two, the required bandwidth can be assessed to be twice the amount required for the uncoded scheme. Fig. 6.21 shows the power-bandwidth efficiencies of coded and uncoded binary and 4-level 3-SP DPM. The bandwidth defined here contains the 99 percent of the total

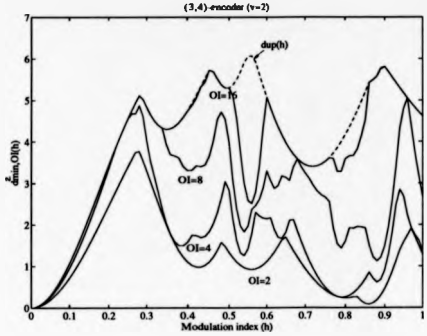

Figure 6.19: The NSMED growth with the observation interval length. For the combination of (3,4)-encoder, map# 1 and 4-level 3-SP DPM modulator

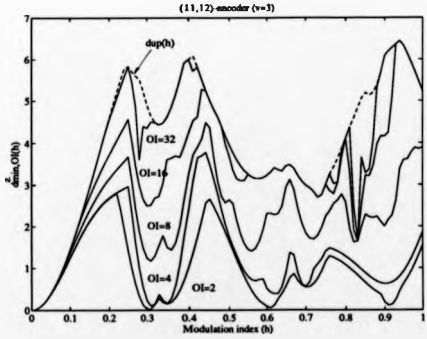

Figure 6.20: The NSMED growth with the observation interval length. For the combination of (11,12)-encoder, map# 1 and 4-level 3-SP DPM modulator

$d^2_{min,OI}(h)$ *for the (3,2)-encoder (v=1)*						
	h					
OI	0.05	0.10	0.15	0.20	0.25	0.40
2	0.247	0.941	1.957	2.675	1.421	1.048
3	–	–	–	2.688	2.463	1.857
4				3.110	2.525	2.015
5				–	3.346	3.115
6					3.689	3.219
7					3.751	3.271
8					3.864	3.414
9					4.199	3.890
10					–	4.680
11						4.857
12						4.885

Table 6.15: The NSMED growth with the observation interval length. For the combination of (3,2)-encoder, map# 1 and 4-level 3-SP DPM modulator (v=1)

$d^2_{min,OI}(h)$ *for the (3,4)-encoder (v=2)*					
	h				
OI	0.05	0.10	0.25	0.30	0.45
2	0.187	0.720	3.400	3.298	1.107
3	0.242	0.938	4.560	3.300	1.113
4	0.247	0.957	–	4.012	1.836
5	0.247	0.957		4.373	3.044
6	0.257	0.995		4.660	3.542
7	0.266	1.033		4.827	3.542
8	0.276	1.067		–	3.654
9	0.282	–			3.660
10	–				4.383
11					4.941
12					5.053
13					5.059
14					5.688
15					5.721

Table 6.16: The NSMED growth with the observation interval length. For the combination of (3,4)-encoder, map# 1 and 4-level 3-SP DPM modulator (v=2)

$d^2_{min,OI}(h)$ *for the (11,12)-encoder*				
	h			
OI	0.10	0.15	0.20	0.25
8	1.361	2.394	3.149	3.677
9	1.380	2.437	3.224	3.795
10	1.418	2.522	3.375	4.028
11	1.430	2.565	3.451	4.146
12	–	2.565	3.451	4.146
13		2.607	3.526	4.264
14		2.650	3.602	4.382
15		2.650	3.602	4.382
16		2.719	3.722	4.563
17		2.762	3.798	4.681
18		2.804	3.873	4.799
19		2.804	3.873	4.799
20		2.847	3.949	4.917
21		2.890	4.025	5.035
22		2.890	4.025	5.035
23		2.932	4.100	5.153
24		2.933	4.176	5.371
25		–	4.176	5.371
26			4.252	5.389
27			4.328	5.506
28			4.328	5.506
29			4.403	5.624
30			4.479	5.742
31			4.479	5.742
32			4.555	5.825
33			4.578	–

Table 6.17: The NSMED growth with the observation interval length. For the combination of (11,12)-encoder, map# 1 and 4-level 3-SP DPM modulator (v=3)

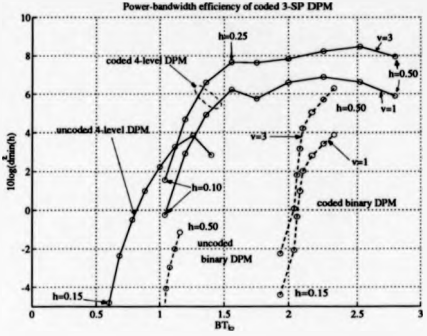

Figure 6.21: Power-bandwidth efficiency of coded and uncoded 3-SP DPM schemes (Binary and 4-level)

power.

It is obvious from Fig. 6.21 that the coded 3-SP DPM schemes are more power efficient than the uncoded shemes. Increasing the memory length increases the power efficiecny of the coded schemes. It is also shown that some coded schemes provide greater power-bandwidth efficiencies than uncoded ones. An example of such a scheme is the (11,12)-encoder combined with 4-level 3-SP DPM modulation and $h = 0.15$. This scheme has a 2.7 dB better performance and the bandwidth is only 85% of the uncoded 4-level 3-SP DPM scheme with $h = 0.50$. Another example, the uncoded 4-level 3-SP DPM scheme with h=0.5 has a squared free Euclidean distance of 1.563 (1.9 dB), whereas coded 4-level scheme with h=0.20 and v=3 having the same bandwidth has a squared free Euclidean distance of 4.578 (6.6 dB).

6.8 A receiver structure for coded 3-SP DPM signals in frequency selective mobile radio channel

In this section, a receiver structure is proposed for demodulating coded partial response DPM signals (See Fig. 6.24) in the presence of frequency selective Rayleigh channel.

The proposed receiver structure is similar to the receiver structure proposed for uncoded case, which is shown in Fig.5.8. It consists of two principal components:

1. The integration of the optimum coherent maximum likelihood sequence estimator (MLSE) which is called optimum Viterbi algorithm with a decision feedback equaliser
2. A channel estimator.

The task of the Viterbi algorithm is the same as for the uncoded DPM system, which is to remove the intersymbol interference caused by the modulator and, in addition to that for the coded case, to recover the coded data. After a certain symbol interval, which is called decision depth length, a decision maker in the Viterbi algorithm makes a hard decision on survived paths. The one having the smallest squared error is chosen, and the first symbol of this sequence is the estimated symbol. The constraint length of the receiver is, in fact, the OI length which gives d^2_{min}. As shown in Table 6.9, for (11,12)-encoder with Map#1 and $h = 0.20$, the required OI length is 33 symbol intervals. The number of states to be employed in Viterbi algorithm is seen to be $2^v.M^{L-1} = 128$ (when v=3, M=4 and L=3). As all the L symbol sequence outputs of the encoder do not occur, not all of the 128 states are encountered. If the starting states of the encoder and partial response 3-SP DPM modulator (see Fig.6.22) are [00011] then the following states are shown in Fig. 6.23. The total number of states is 32.

In the case of coded partial response DPM, The Viterbi algorithm works as follows:

As it is seen in Fig.6.23 to each state of the Viterbi algorithm , there are two braches which correspond to the existing two possible symbols. That makes it necessery to consider 64 sequences. The 32 paths with the relatively smaller squared errors are chosen and stored in the memory. The same computation is done for the next symbol interval. This procces is continued until the time instant is equal to the constraint length. At this time a hard

decision is made on one symbol. The first symbol of the surviving sequence having the smallest error distance is chosen as an estimated symbol. After that the data corresponding to this symbol are found. The newest three symbols of this survived sequence with smallest error are used as an input to the feedback equalizer, which helps with recovering the symbols from intersymbol interference introduced by the frequency selective mobile radio channel.

The following quantities have to be calculated and updated at $t = kT$ for each state:

$$f_1 = \Delta s_a, s_c(k) = cos(c_k^{a_a a_c} - r_k) + W_{sa}(k-1)$$
$$f_2 = \Delta s_b, s_c(k) = cos(c_k^{a_b a_c} - r_k) + W_{sb}(k-1)$$

where $c_k^{a_a a_c}$ and $c_k^{a_b a_c}$ represent the symbols corresponding to the transition from states a and b, to the state c, respectively and $W_{sa}(k-1)$ is the total accumulated error distance corresponding to the time instant $(k-1)$, and f_1 and f_2 are the two matrix corresponding to two different transitions and k is the current time interval.

the one with larger matrix is chosen, and stored as a total accumulated error corresponding to state c, i.e.

$$W_{sc(k)} = max(f_1, f_2).$$

At that time, the symbol is either $c_k^{a_a a_c}$ or $c_k^{a_b a_c}$. This symbol is stored in memory as well.

6.9 Performance studies of the scheme

The total coded 3-SP DPM transmission system, as has been simulated, is shown in Fig. 6.24, of which the receiver concept has already been described in the previous section.

The computer simulatation of the combination of (11,12)-encoder with Map# 1 and 4-level 3-SP DPM is performed for modulation indices equal to 0.15 and 0.20. The coefficients of the pulse shaping filter which are used in modulator are chosen according to Equation 2.27 given Chapter 2. For each different modulation index h, there are different coefficients. The oversampling ratio is assumed to be 1.

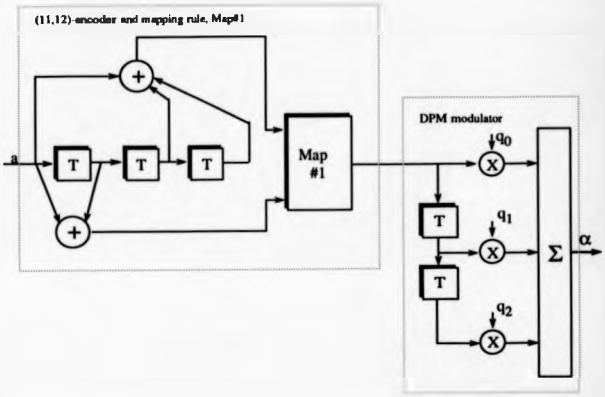

Figure 6.22: The block diagram of transmission section of coded partial response DPM signals

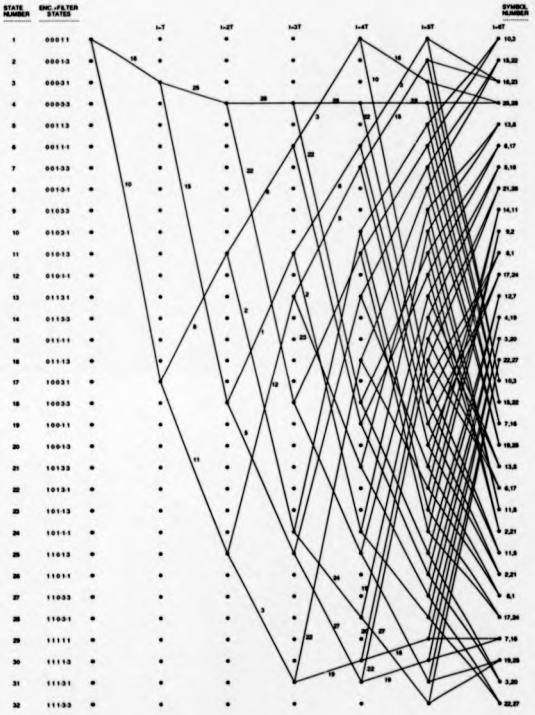

Figure 6.23: Trellis diagram of Viterbi decoding for 4-level coded 3-SP DPM

The fading channel in this study has a multipath spread T_M which spans four symbol intervals. The fading channel is modelled by a transversal filter with four taps and a memory of 3 symbols (see Fig.5.11). Each tap in the transversal filter has a Rayleigh distributed magnitude, and uniformly distributed phase. The output signal of this filter is then added to a white Gaussian noise. More details on the mobile channel can be found in chapter 3.

The decision depth length of the Viterbi algorithm depends on observation interval length of the combined system. For different combination of modulation index, encoder, mapping rule and M-level modulator, the observation interval length which gives d^2_{min} might be different. The OI lengths which give d^2_{min} for these combinations are shown in Table 6.9. For $h = 0.15$, the OI length is equal to 24, and for $h = 0.20$ it is 33 symbol intervals.

6.9.1 Bit error rate (BER) calculation

The minimum number of bits which must be sent to perform the BER of a system is provided from [75]. This number depends on the expected BER. In a particular simulation run, a total of 100 times the reciprocal of the error rate is required [75]. In other words, in order to measure an average probability of bit error as low as 10^{-3}, the number of transmitted bits must be at least as large as 10^5.

BER calculation for the combined system:
(11,12)-encoder, Map# 1 and 4-level 3-SP DPM

The variations of BER with S/N ratio under frequency selective Rayleigh fading channel, for 3-SP DPM schemes and with two different modulation indices, are shown in Fig. 6.25. The case of h=0.15 and 0.20 are considered. As can be seen from Table 6.9, d^2_{min} values for these modulation indices are 2.933 and 4.578 respectively. As is seen in Fig 6.25, increasing d^2_{min} decreases the BER of the system. An examination of the BER of 10^{-3}, which is the acceptable BER in speech transmission, shows that the scheme with modulation index h=0.20 is more power-efficient (about 2.5 dB) than the system with h=0.15.

The BER comparison between a coded and an uncoded 4-level 3-SP DPM scheme is shown in Fig. 6.26. Although both schemes have the same bandwidth, the coded scheme (the

Figure 6.24: The block diagram of the total simulated system for coded DPM

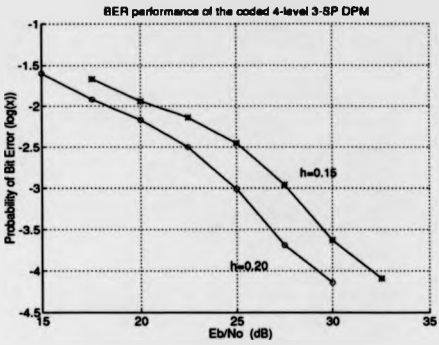

Figure 6.25: The BER performance of the combination system of (11,12)-encoder, Map# 1 and 4-level 3-SP DPM for the FSRF channel

combination of (11,12)-encoder, Map# 1 and 4-level 3-SP DPM modulator with h=0.20) is about 1 dB more power-efficient than the uncoded one (4-level 3-SP DPM scheme with $h = 0.50$), for bit error probabilities in the range of 10^{-3}.

6.10 Conclusion

In this chapter the free Euclidean distance and spectral properties of the coded partial response binary and 4-level 3-SP DPM signals have been analysed for given modulation indices. The power-bandwidth efficiencies of these systems are illustrated in Fig. 6.21.

The results show that considerable gain can be achieved by coding for both constant envelope binary and 4-level 3-SP DPM. It is shown that a significant increase in d^2_{min} can be obtained with coding. It has been also shown that increasing the memory length of the encoder increases d^2_{min} but the cost of this, for most of the modulation indices, is an increase in the observation interval length. It is shown that for some combination schemes, which have the same d^2_{min}, h,v and modulator, but different encoder, the required OI length to reach the free Euclidean distance is different. These are the combination of (4,3) and

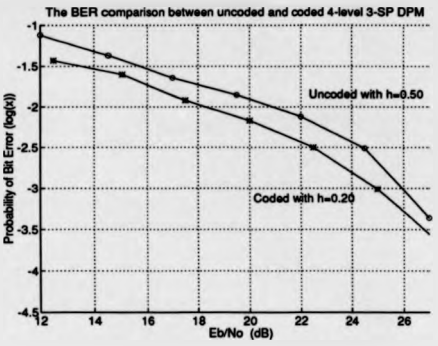

Figure 6.26: The BER comparison between the coded ((11,12)-encoder, Map# 1) and uncoded 4-level 3-SP DPM for the FSRF channel

(6,1)-encoders and binary 3-SP DPM modulator with h=0.90 and 0.95 (See Table 6.12). Finally, some coded schemes have been found which provide greater power and bandwidth efficiency than the uncoded ones. An example of such a scheme is the (11,12)-encoder combined with 4-level 3-SP DPM modulation and $h = 0.15$, $v = 3$. The d^2_{min} corresponding to this scheme is 2.933 (4.7 dB). This scheme has a 2.7 dB better performance and the bandwidth is only 85% of the uncoded 4-level 3-SP DPM scheme with $h = 0.50$. Another example can be seen from Tables Table 6.6 and 6.9. The uncoded 4-DPM with $h = 0.50$ has a squared minimum distance of 1.563 (1.9 dB), whereas coded 4-DPM with $h = 0.2$ and $v = 3$ having the same bandwidth has a squared minimum distance of 4.578 (6.6 dB). In order to decode these signals the Viterbi algorithm can be used effectively. However this algorithm is more complex than the algorithm used for uncoded cases. These two coded schemes with $h = 0.15$ and $h = 0.20$, when compared with d^2_{min} of 1.8 (2.5 dB) corresponding to GMSK (BT=0.3, h=0.5)[71], have approximately 2.2 - 4.1 dB better performance. On the other hand the required bandwidth of GMSK is 77% and 68% compared to the bandwidth required for coded two schemes, respectively. That means these coded DPM schemes need more bandwidth. As mentioned in Section 5.2, the required bandwidth for

DPM signal can be reduced by using larger values of η and K. It can also be shown that some coded 3-SP DPM schemes have greater power and bandwidth efficiency than some coded 3-RC CPM schemes found in [70]. For example, the coded 3-RC CPM, $h = 0.5$ and $v = 3$ has d^2_{min} of 5.26 (7.2 dB) whereas coded 3-SP DPM, $h = 0.30$ and $v = 3$ has d^2_{min} of 5.787 (7.6 dB). These two schemes have the same bandwidth.

These results show that convolutional codes when combined with 3-SP DPM can provide power and bandwidth efficiency relative to uncoded counterparts and to coded 3-RC CPM schemes.

A receiver structure to recover the trellis coded 4-level 3-SP DPM signals, corrupted by the frequency selective Rayleigh fading channel, has been proposed and presented. The VDFE (more detail of this is given in Chapter 4 and Section 6.8) with channel estimator (more detail can be found in Chapter 3) is employed in the receiver section. The Viterbi algorithm is used as a detector in the decision section of the VDFE. The bit error rate (BER) performances of two different combination schemes under the frequency selective Rayleigh fading channel have been presented. The simulation results show that increasing the free Euclidean distance of a coded 3-SP DPM system improves the BER performance of the system. The BER comparison between a coded and an uncoded 4-level 3-SP DPM scheme is shown in Fig. 6.26. Although both schemes have the same bandwidth, the coded scheme (the combination of (11,12)-encoder, Map# 1 and 4-level 3-SP DPM modulator with h=0.20) is about 1 dB more power-efficient than the uncoded one (4-level 3-SP DPM scheme with $h = 0.50$), for bit error probabilities in the range of 10^{-3}.

This confirm partly the results found for AWGN channels. Thus d^2_{min} can be considered as one criterion of power efficiency for 3-SP DPM even under the frequency selective Rayleigh fading channel.

CHAPTER 7

CONCLUSIONS AND FUTURE WORK

7.1 Conclusions

Three prevailing requirements in transmission systems are decreasing the power needed for reliable transmission, reducing the required bandwidth and using a modulation technique which is easy to implement. For spectrum conservation, the band occupancy of the chosen modulation scheme has to be small so that as many channels as possible can be transmitted in a given band. In addition to spectral efficiency, the modulation scheme should be power efficient as well. As the available transmitter power is limited, the system should be designed to use its power efficiently. Another criterion to be taken into account in choosing a modulation scheme for mobile systems is the implementation difficulty.

In recent years, efforts have been made in the search for power- and bandwidth-efficient modulation techniques. Over the last ten years two different classes of coding methods related to the bandwidth efficiency have been developed. One of them is trellis coding combined with PSK, pioneered by Ungerboeck. The other one is the combination of convolutional coding with continuous phase modulation (CPM).
The search for improving power efficiency has been addressed for some modulation schemes in the mobile radio environment.

The first modulation scheme examined in this thesis is the TCM scheme proposed by Ungerboeck. Ungerboeck showed that TCM schemes can provide coding gains of 3-6 dB relative to an uncoded scheme with the same spectral efficiency under AWGN channels. However, there are still open questions concerning coding gains under the time invariant intersymbol interference (ISI) and frequency selective Rayleigh fading channels. In this study, Ungerboeck's 4-state rate 2/3 8-PSK TCM scheme has been examined under time invariant ISI and frequency selective Rayleigh fading channels.

The second modulation scheme examined in this thesis is digital phase modulation (DPM). DPM has some advantages over most other forms of CPM. These are:

. It is well suited for VLSI implementation.

. It is relatively simple to implement.

. It uses phase modulation instead of frequency modulation. The shaped symbol pulses are applied directly to a phase modulation.

The modulator and the demodulator are easier to implement, because in the digital form of CPM which is called digital frequency modulation or in any similar modulation technique such as Gaussian minimum shift keying (GMSK), the carrier phase at any time instant is the accumulated phase of all the previous symbols. Consider the case of GMSK, filter bandwidth BT = 0.3 (which is used as an modulation technique in digital cellular mobile radio in Europe). Both DPM and GMSK employ a Viterbi processor in the receiver section. For GMSK, the number of states of the Viterbi processor is $4 * 2^L$. L can be considered as 3 for this GMSK scheme (in fact L=3.33). Then the required number of states in the Viterbi processor will be 32. On the other hand DPM requires the Viterbi processor to have M^{L-1} states. As mentioned in Chapter 5 this number is 4 for the binary 3-SP DPM case, and for the $M = 4$ case this number is 16. For both binary and 4-level DPM cases the required states in the Viterbi processor are smaller than the number required for this case of GMSK.

These advantages of DPM signals motivated a consideration of these signals in mobile radio environments. The effects of the coding in improving the power efficiency of partial response DPM signals are examined. The main interest is to investigate what improvements may be obtained by coding. The goal is to find the schemes which are both power and bandwidth efficient, in addition to having an implementation efficiency.

The first part of the project is the study of TCM signals in two environment, namely a time invariant ISI channel and a frequency selective Rayleigh fading channel.

For a channel with time invariant ISI, three types of algorithm have been examined. Two

of them are the known algorithms, namely the linear feedback equaliser, and the decision feedback equaliser. The third algorithm is an algorithm called the Viterbi decision feedback equaliser (VDFE). To evaluate and compare the performance of these three algorithms, computer simulations are carried out for a time invariant ISI channel, namely telephone channel 2. The results for LFE show that the coding gain for bit error probabilities in the range of 10^{-3}, which is important in digital speech transmission, is about 0.25 dB. The results for DFE show that the TCM 8-PSK scheme has little or no advantage over the uncoded counterpart (uncoded 4-PSK). Such disappointing results can be expected as the detector in the DFE makes hard decisions on the received signals, and hence the potential benefit offered by trellis coding is lost. The proposed algorithm, namely VDFE, was shown to be better than the other two algorithms. The results show that using this algorithm, a TCM 8-PSK signal can be received with 1.6 dB less S/N, than for an uncoded 4-PSK scheme, for the BER in the area of 10^{-3}. The VDFE shows superior performance when compared to conventional hard-decision demodulation. It has approximately 3 dB better performance at a bit error rate of 10^{-3} when compared with LFE, and 3.25 dB when compared with DFE.

The main conclusion concerning these results is that the TC 8-PSK scheme proposed for AWGN channels has also good performance under a time invariant ISI channel. The BER performance of this TCM scheme under a time invariant ISI channel is approximately the same as under AWGN channels. That means the criterion, which is used for forming good trellis coded schemes in AWGN channels, is also valid when the channel is a time invariant ISI channel.

Ungerboeck's 4-state rate 2/3 8-PSK TCM scheme has also been examined under a frequency selective Rayleigh fading (FSRF) channel. A receiver structure based on VDFE has been proposed. The complete transmission system has been simulated. The results of computer simulations for TC 8-PSK show that the coding gain of this scheme, for bit error probabilities in the area of 10^{-3} is about 0.5 dB. With high S/N ratios, a 1.5 dB coding gain is achievable. This gain is small when compared to the gain achieved under AWGN channels. This means the d^2_{min} is still a criterion, but not as effective as under AWGN channels. This can raise a question: Is there any other criterion than d^2_{min} which can be used for finding good trellis coded schemes?

Since the coding gain achieved in TC 8-PSK is low, searches have been conducted for improving this gain. A modulation scheme called Hybrid trellis-coded 8/4 PSK presented by Sundberg, which is the combination of the TC 8-PSK and the uncoded 4-PSK, has been studied under frequency selective Rayleigh fading. The results of computer simulation for hybrid TC 8/4-PSK show that the coding gain of this scheme, for bit error probabilities in the area of 10^{-3} is negligible. While the hybrid TC 8/4-PSK has better performance for the cases where BER is larger than $10^{-2.7}$, TC 8-PSK becomes better when the BER is smaller than $10^{-2.7}$. In the area of 10^{-3}, the TC 8-PSK scheme has approximately 0.4 dB better performance than the hybrid TC 8/4-PSK scheme. In conclusion, no significant advantage of hybrid TC 8/4-PSK over TC 8-PSK has been observed.

In the second part of the project, the effects of the coding in improving the power efficiency of partial response DPM signals have been examined. The main interest was to investigate what improvements may be obtained by coding. The goal of this research was to find the best combinations of 1/2 rate convolutional encoder, mapping rule and partial response DPM modulator (binary and 4-level) for given memory length and modulation index. The type of convolutional encoders which have been considered are of short constraint lengths. The constraint length (or memory length) v varies from 1 to 3. The binary mapping rule is used for the binary case, and two different mapping rules have been used for the 4-level case. The modulation indices between $0.05 \leq h \leq 1.20$ have been considered. The error probability of a system, in an additive white Gaussian noise channel, is a function of the free squared Euclidean distance. Since the error probability decreases with the increase of d^2_{min}, the combinations of encoder, mapping rule and modulator, which maximise d^2_{min} have been investigated for each memory length and modulation index. The results show that considerable gain can be achieved by coding for both constant envelope binary and 4-level 3-SP DPM. It has been shown that a significant increase in d^2_{min} can be obtained with coding. It has been also shown that increasing the memory length of the encoder increases d^2_{min} but the cost of this, for most of the modulation indices, is an increase in the observation interval length. Finally, some coded schemes have been introduced which provide greater power and bandwidth efficiency than the uncoded counterparts. An example of such a scheme is the (11,12)-encoder combined with 4-level 3-SP DPM modulation and $h = 0.15$, $v = 3$. The d^2_{min} corresponding to this scheme is 2.933 (4.7 dB). This scheme

has a 2.8 dB better performance and the bandwidth is only 86% compared to the uncoded 4-level 3-SP DPM scheme with $h = 0.50$. Another example, the uncoded 4-DPM with $h = 0.50$ has a squared minimum distance of 1.563 (1.9 dB), whereas coded 4-DPM with $h = 0.2$ and $v = 3$ having the same bandwidth has a squared minimum distance of 4.578 (6.6 dB). These two coded schemes with $h = 0.15$ and $h = 0.20$, when compared with d^2_{min} of 1.8 (2.5 dB) corresponding to GMSK (BT=0.3, h=0.5)[71], have approximately 2.2 - 4.1 dB better performance. On the other hand the required bandwidth of GMSK is 77% and 68% compared to the bandwidth required for the two coded schemes, respectively. That means these coded DPM schemes need more bandwidth. As mentioned in Section 5.2, the required bandwidth for DPM signal can be reduced by using larger values of η and K. It can also be shown that some coded 3-SP DPM schemes have greater power-bandwidth efficiency than some coded 3-RC CPM schemes found in [70]. For example, the coded 3-RC CPM, $h = 0.5$ and $v = 3$ has d^2_{min} of 5.26 (7.2 dB) whereas coded 3-SP DPM, $h = 0.30$ and $v = 3$ has d^2_{min} of 5.787 (7.6 dB). These two schemes have the same bandwidth.

These results show that convolutional codes when combined with 3-SP DPM can result in improved power and bandwidth efficiency relative to uncoded counterparts and to coded 3-RC CPM schemes.

In order to validate the outcomes of the analytic results, a computer simulation of the whole transmission system has been performed. Receiver structures have been proposed and presented to recover these coded signals under a frequency selective Rayleigh fading channel. The bit error rate (BER) performances of coded 4-level 3-SP DPM schemes under a frequency selective Rayleigh fading channel have been evaluated through the use of computer simulation. A receiver structure based on VDFE to recover the trellis coded 4-level 3-SP DPM signals, corrupted by the frequency selective Rayleigh fading channel, has been proposed and presented. Subsequently, the bit error rate (BER) performances of two different combination schemes under the frequency selective Rayleigh fading channel have been presented. The simulation results show that increasing the free Euclidean distance of a coded 3-SP DPM system improves the BER performance of the system. The BER comparison between a coded and an uncoded 4-level 3-SP DPM scheme with the same bandwidth is also accomplished. Although both schemes have the same bandwidth,

the coded scheme (the combination of (11,12)-encoder, Map# 1 and 4-level 3-SP DPM modulator with h=0.20) is about 1 dB more power-efficient than the uncoded one (4-level 3-SP DPM scheme with $h = 0.50$), for bit error probabilities in the range of 10^{-3}. This confirms partly the theoretical results found for AWGN channels.

Some of the results of the work are attached as an appendix.

7.2 Future work

It would be of interest to search for coded schemes with longer constraint length. Unfortunately the computation time for searching these schemes is long. DPM with a sine pulse (SP) of length $L = 3$ has been considered in this thesis [60]. For future work, DPM schemes with different pulse shape could also be considered. More efficient pulse shape, in terms of power and bandwidth efficiencies, could be used. Optimisation of the pulse-shaping filter for the minimisation of the signal bandwidth can be accomplished. Then these DPM signals with different pulse shaping filters could be analysed. Afterwards, the effects of the coding in improving the power efficiency of these DPM signals can be examined. The optimal combinations of convolutional encoder and this modulator can be found. In addition, all the coded schemes considered in this thesis can be used with interleaving. The only criterion used with finding good codes is the d_{min}^2. The other distance criteria such as Hamming distance and product distance can be considered.

APPENDIX

PUBLISHED PAPERS NOT FILMED FOR COPYRIGHT REASONS

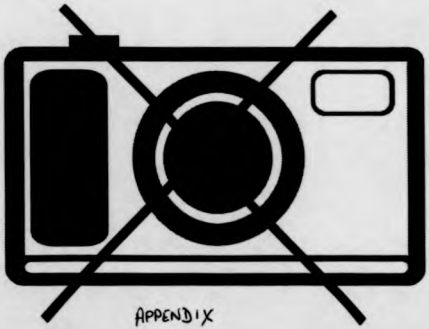

APPENDIX

BIBLIOGRAPHY

[1] JAKES, W.C., "Microwave mobile communications", New York, John Wiley & Sons, 1974.

[2] CALHOUN, G., "Digital cellular radio", Artech House, 1988.

[3] LIM, M.J., PARK, H.K., "The implementation of the mobile channel simulation in the basebans and its application to the quadrature type GMDSK modem design", IEEE Veh. Techn. Conf. Rec, pp. 496-500, 1990.

[4] MUNDRA, P.S., SINGAL, T.L., AND KAMAL, T.S., "A computer algorithm for prediction of service area in a mobile radio communication system", IEEE Veh. Techn. Conf. Rec., pp. 384-386, 1990.

[5] AGUSTE, R., ARGIMON, J., VILA, D., "Digital fading simulator for mobile radio", IEEE MELECON'85 Conf. Rec., pp.403-406, 1985.

[6] ARREDENDO, G.A., CHRISS, W., WALKER, E.H., "A multipath fading simulator for mobile radio", IEEE Trans. Veh. Tech., vol. VT-22, No.4, pp.241-244, Nov. 1973.

[7] UEDA, T., AND SUZUKI, H., "Frequency-selective fading simulator for mobile radio communications", Proc. of ISAP'89, pp. 865-868, Tokyo 1989.

[8] HASHEMI, H., "Simulation of the urban radio propagation channel", IEEE Trans. Veh. Tech. vol. VT-28, No.3, August 1979.

[9] COMROE, R.A., "All-digital Rayleigh fading simulator"

[10] LEE, W.C.Y., "Mobile communications engineering", McGraw-Hill Book company, 1982.

[11] HIRADE, K., "Mobile-radio communications", Englewood Cliffs: Prentice-Hall In., 1987.

[12] PARSONS, J.D., "The mobile radio propagation channel", Pentach, London, 1992.

[13] STEELE, R., "Mobile radio communications", Pentach, London, 1992.

[14] MOGENSEN, P.E., ANDERSON, B.L., MADSEN, B., ANDERSON, J.B., "Short-term variations of the mobile channel and the GSM signal", IEEE Veh. Tech. Conf. Rec, pp. 443-448, 1990.

[15] LOO, C., "A statistical model for a land mobile satellite link" IEEE Trans. Veh. Tech., vol. VT-34, No3, pp.122-127, Agust 1985.

[16] LOO, C., "A statistical model for a land mobile satellite link", IEEE Conf. Rec., ICC'84, pp. 588-594, Holland, 1984.

[17] LOO, C., MATT, E.E, BUTTERWORTH, J.I, AND DUFOUR, M., "Measurements and modelling of land-mobile satellite signal statistics", IEEE Veh. Tech. Conf. Rec., Dallas, May 1986.

[18] LO, N.W.K., FALCONER, D.D, SHEIKH, A.U.H., "Channel interpolation for digital mobile radio channels", IEEE ICC'91 Conf. Rec., pp. 25.3.1-25.3.5, 1991.

[19] LEE, W.C.Y., "Mobile communications design fundamentals", John Wiley & Sons, Inc., Second edition, 1993.

[20] GANS, M.J., "A power-spectral theory of propagation in the mobile-radio environment", IEEE Trans. Veh. Tech., vol. VT-21, No.1, Feb. 1972.

[21] KOFMAN, W. AND SILVENT, A., "Adaptive estimator of a filter and its inverse", IEEE Tran. commun., vol. COM-33, No.12, Dec. 1985.

[22] SATORIUS, E.H., PACK, J.D., "Application of least squares Lattice algorithms for adaptive equalization", IEEE Trans. Commun. Technol., vol. COM-29, No.2, pp.136-142, Feb. 1987.

[23] PAHLAVAN, K., MATTHEWS, J.W., "Performance of adaptive matched filter receivers over fading multipath channels", IEEE Trans. Commun. Technol., vol. COM-38, No.12, pp.2106-2113, Dec. 1990.

[24] CLARK, A.P., HARUN, R., "Assesiment of Kalman filter channel estimator for an HF radio link" IEEE proceedings, vol.133, part.F, No.6, pp.513-521, Oct. 1986.

[25] WIDROW, B. and STEARNS, S.D., "Adaptive signal processing", Prentice-Hall, Inc., 1985.

[26] BIGLIERI, E., DIVSALAR, D., McLANE, P.J., SIMON, M. K., "Introduction to trellis-coded modulation with applications", Macmillan, 1991.

[27] UNGERBOECK, G., "Channel coding with multilevel/phase signals" IEEE Trans. Inf. theo., Vol. IT-28, pp 55-67, Jan. 1982.

[28] UNGERBOECK, G., " Trellis coded modulation with redundant signal sets part I: Introduction ", IEEE commun. Mag., vol. 25, pp. 5-11, Feb, 1987.

[29] UNGERBOECK, G., " Trellis coded modulation with redundant signal sets part II: State of the art ", IEEE commun. Mag., vol. 25, pp. 12-21, Feb, 1987.

[30] JAMALI, S.H., LE-NGEC, T., "A new 4-state 8-PSK TCM scheme for fast fading, shadowed mobile radio channels" IEEE Trans. Veh. Tech., vol. VT-40, No. 1, pp.216-222, Feb. 1991.

[31] WILSON, S.G., LEUNG, Y.S., " Trellis-coded phase modulation on Rayleigh channels" in ICC'87 Conf. Rec., Seattle, WA, June 1987, pp. 21.3.1-21.3.5.

[32] WILSON, S.G., "Bandwidth-efficient modulation and coding: A survey of recent results" in ICC'86 Conf. Rec., Toronto, Ontario, Canada, June 1986.

[33] CALDERBANK, R., MAZO, J.E., " A new description of trellis codes" IEEE Trans. Inf. Theo., Vol. IT-30, No. 6, pp.784-791, Nov. 1984.

[34] RAMSIER, S., "Bandwidth-efficient trellis coded modulation schemes" in ICC'90 Conf. Rec., 1990, pp.340.3.1-340.3.4.

[35] ELNOUBI, S., FAHMEY, E. and EL-BADAWY, E.S., "Performance of Trellis coded QPSK in mobile radio channels" in ICC'90 Conf. Rec., 1990.

[36] LODGE, J.H., and MOHER, M.L., "Time diversity for mobile satellite channels using trellis coded modulation" In GLOBECOM'87 Conf. Rec., pp 8.7.1-8.7.5, 1987.

[37] KAMIO, Y., "Performance of trellis coded modulation using multi-frequency channels in land mobile communications" in ICC'90 Conf. Rec., 1990.

[38] DIVSALAR, D., and SIMON, M.K., "The design of trellis coded MPSK for fading channels: Performance criteria" IEEE Trans. Commun. Technol., vol. COM-36, No. 9, pp.1004-1011, Sept. 1988.

[39] WONG, L.N., McLANE, P.J., "Performance of trellis codes for a class of equalized ISI channels" IEEE Trans. Commun. Technol., vol. COM-36, No. 12, pp.1330-1336, Dec. 1988.

[40] MAKRAKIS, D., MATHIOPOULAS, P., "Trellis coded noncoherent QAM: A new bandwidth and power efficient scheme" in IEEE ICC'89 Conf. Rec., Boston, MA, June 1989.

[41] HO, P., AND FUNG, D., "Error performance of interleaved trellis coded PSK modulation in correlated Rayleigh-fading channels" IEEE Trans. Commun. Technol., vol. COM-40, No. 12, pp.1800-1809, Dec. 1992.

[42] CHAN. K., and BATEMAN, A., "The performance of reference-based M-ary PSK with trellis coded modulation in Rayleigh fading" IEEE Trans. Veh. Technol., Vol. VT-41, No. 2, pp.190-198, May 1992.

[43] ZEHAVI, E., "8-PSK trellis codes for Rayleigh channel" IEEE Trans. Commun. Technol., vol. COM-40, No. 5, pp.873-884, May 1992.

[44] SUNDBERG, C-E.W., "Hybrid trellis-coded 8/4-PSK modulation" IEEE Trans. Commun. Technol., vol. COM-38, No. 5, pp.602-614, May 1990.

[45] VITERBI, A.J., "Convolutional codes and their performance in communication systems" IEEE Trans. Commun. Technol., vol. COM-19, No.5, Oct. 1971.

[46] GORDEN, G., "System simulation" 2nd ed., Prentice-Hall, 1978.

[47] CLARK, A.P., "Advanced data transmission systems", Pentech press, 1977.

[48] CLARK, A.P., "Equalizers for digital modems", Pentech press, 1985.

[49] CLARK, A.P., ABDULLAH, S.N., AMEEN, S.Y., "A comparison of decision feedback equalizer for a 9600 bits/s modem", Journal of the IERE, Vol. 58, No. 2, pp., March/April 1988.

[50] CLARK, A.P.,FAIRFIELD M.J., "Detection processes for a 9600 bits/s modem", Journal of the IERE, Vol. 51, pp. 143-154, Sept. 1981.

[51] DRISCOLL, J.P., KARIA, N., "Detection process for V32 modems using trellis coding", IEE Proceedings, part F, vol. 135, No.2, April 1988.

[52] LIU, C-L., FEHER, K., "Noncoherent detection of $\pi/4$-QPSK systems in a CCI-AWGN combined interference environment", in Proc. of the IEEE Veh. Technol. Conf., San Francisco, 1989.

[53] LIU, C-L., FEHER, K., "Performance of non-coherent $\pi/4$-QPSK in a frequency selective fast Rayleigh fading channel", in Proc. of the IEEE Veh. Tech. Conf., Orlando, Florida, 1990.

[54] FUNG, V., AND RAPPAPORT, T.S., "Bit-error simulation of $\pi/4$ DQPSK in Flat and frequency-selective fading mobile radio channels with real time applications", in IEEE ICC'91 Conf. Rec., Orlando, 1991.

[55] BUNE, P.A.M., "Effective low-effort adaptive equalizers for digital mobilophone systems", IEEE 39th Vehicular Tech. Conf. Rec., San Francisco, 1989.

[56] BUNE, P.A.M., "A low-effort DSP equalization algorithm for wideband digital TDMA mobile radio receivers", IEEE ICC'91 Conf. Rec., pp. 25.1.1-25.1.5, 1991.

[57] GITLEN, R.D., and WEINSTEIN, S.B., "Fractionally-spaced equualization: An improved digital transversal equalizer", The Bell Sys. Tech. Journal, Vol. 60, No. 2, pp., Feb. 1981.

[58] QURESHI, S. U. H., "Adaptive equalization", Proc. of the IEEE, Vol. 73, No. 9, pp. 1349-1385, Sept. 1985.

[59] SUNDBERG, C.-E. W. and HAGENAUER, J., "Hybrid trellis-coded 8/4-PSK modulation systems", IEEE Trans. Commun. Technol., vol. COM-38, No. 5, pp. 602-614, May. 1990.

[60] MASENG, T., "Digitally phase modulated (DPM) signals ", IEEE Trans. commun.,vol. COM-33, pp 911-918, Sep. 1985.

[61] TRANDEM, O., "Implementation of a modem for digital phase modulation using Viterbi decoding", IEEE GLOBECOM'86 Conf. Rec., 1986.

[62] DZUNG, D., "Generalized CPM and DPM: 'Digital angle modulation schemes with improved bandwidth efficiency' IEEE Trans. Commun. Technol., vol. COM-38, No. 11, pp. 1971-1979, Nov. 1990.

[63] ANDERSON, J. B., AULIN, T., SUNDBERG, C.-E.W, and RYDBECK, N.,"Power-bandwidth performance of smoothed phase modulation codes", IEEE Trans. Commun. Technol., vol. COM-29, pp. 187-195, March.1981.

[64] AULIN, T., SUNDBERG, C.-E.W, " Continous phase modulation- part I: full response signaling ", IEEE Trans. Commun. Technol., vol. COM-29, pp. 196-209, March.1981.

[65] AULIN, T., RYDBEC, N., SUNDBERG, C.-E.W., "Continuous phase modulation part II:Partial response signaling ", IEEE Trans. Commun. Technol., vol. COM-29, pp. 210-225, March.1981.

[66] LINDELL, G., SUNDBERG, C.-E.W., AULIN, T.,"Minimum Euclidean distance for combinations of short rate 1/2 convolutional codes and CPFSK modulation", IEEE Trans. Infor. Theo., vol. IT-30, pp. 509-519, May 1984

[67] LINDELL, G., "On coded continuous phase modulation", Ph.D. Dissertation, University of Lund, Lund, Sweden, 1985.

[68] ANDERSON, J.B., AULIN, T., and SUNDBERG, C.-E.W., " Digital phase modulation", New York: Plenum Press, 1986.

[69] MAKRASIS, D., MATHIOPOULOS, P., " Performance evaluation of a fading estimation/cancellation receiver for Trellis coded CPM signals ", IEEE San Francisco'89 Telecommunication Conf., pp. 95-100, 1989.

[70] PIZZI, S.V., WILSON, S.G., "Convolutional coding combined with continuous phase modulation ", IEEE Trans. Commun. Technol., vol. COM-33, pp. 20-29, Jan.,1985.

[71] MUROTA, K., and HIRADE, K., "GMSK modulation for digital mobile radio telephony", IEEE Trans. Commun. Technol., vol. COM-29, pp. 1044-1050, July,1981.

[72] VITERBI, A.J., OMURA, J.K., " Principles of digital communications and coding ", McGraw-Hill, 1979.

[73] CLARK, G.C., CAIN, J.B., "Error correction coding for digital communications", Plenum Publishing Co., 1981.

[74] PROAKIS, J.G., " Digital communications ", McGraw-Hill, 1983.

[75] HAYKIN, S., " Digital communications ", John Wiley & Sons, 1988.

[76] WOZENCRAFT, J.M., and JACOBS, I.M., "Principles of communication engineering", John Wiley & Sons, Inc., 1965.

[77] ANDERSON, J.B., and TAYLOR, D.P., " Channel coding with multilevel/phase signals ", IEEE Trans. on Info. Theory, IT-24, No 6, pp 703-712, Nov., 1979.

[78] MULLIGAN, M.G., and WILSON, S.G., "An improved algorithm for evaluating trellis phase codes" IEEE Tran. Inf. Theo., Vol. IT-30, No.6, pp. 846-850, Nov., 1984,

[79] WILSON, S.G., SLEEPER, H.A., SCHOTTER, P.J., LYONS, M.T., "Rate 3/4 convolutional coding of 16-PSK: Code design and performance study" , IEEE Trans. Commun. Technol., vol. COM-32, No. 12, Dec. 1984.

[80] YILMAZ, R., POON, F.S.F., and DENBIGH, P.N., "Optimal combination of convolutional codes and partial response M-level digitally phase modulated (DPM) signals", In IEEE SICON/ICIE'93 Conf. Rec., Singapore, 1993.

[81] YILMAZ, R., POON, F.S.F., and DENBIGH, P.N., "Performance of coded partial response M-level digitally phase modulated (DPM) signals in a frequency selective Rayleigh fading channel", To be published in IEEE MELECON'94 Conf. Rec., Antalya, Turkey, April 1994.